CERN
CH-1211 Geneva 23
Switzerland

EDMS NO.	REV.	VALIDITY
0000000	0.0	DRAFT

REFERENCE
XXXXXX

Date: 201X-XX-XX

TRANSLATION OF MASTER THESIS

EVALUATION, OPTIMIZATION AND TEST OF PULSED HIGH VOLTAGE COAXIAL CABLES AND CONNECTORS FOR KICKER MAGNETS AT CERN

ABSTRACT:

This work is about my final thesis for the master's diploma in electrical engineering for the National Technical University of Athens, Greece. It has been entirely done at CERN in the framework of my technical studentship which had a duration of twelve months, (1/9/2017 – 31/8/2018). It is about high voltage measurements and tests of coaxial cables and connectors used for kicker magnets and introducing ways for optimizing and producing new models of cables using new materials, in an effort to replace old cables.

DOCUMENT PREPARED BY:	DOCUMENT CHECKED BY:	
Dimitrios Kontelis	Tobias Stadlbauer Thomas Kramer	

ΕΘΝΙΚΟ ΜΕΤΣΟΒΙΟ ΠΟΛΥΤΕΧΝΕΙΟ
ΣΧΟΛΗ ΗΛΕΚΤΡΟΛΟΓΩΝ ΜΗΧΑΝΙΚΩΝ
ΚΑΙ ΜΗΧΑΝΙΚΩΝ ΥΠΟΛΟΓΙΣΤΩΝ
ΤΟΜΕΑΣ ΗΛΕΚΤΡΙΚΩΝ ΒΙΟΜΗΧΑΝΙΚΩΝ
ΔΙΑΤΑΞΕΩΝ ΚΑΙ ΣΥΣΤΗΜΑΤΩΝ ΑΠΟΦΑΣΕΩΝ

ΔΙΠΛΩΜΑΤΙΚΗ ΕΡΓΑΣΙΑ

ΔΗΜΗΤΡΙΟΣ Γ. ΚΟΝΤΕΛΗΣ

Αξιολόγηση, Βελτιστοποίηση και Έλεγχος Ομοαξονικών Καλωδίων και Συνδέσμων Παλμικής Υψηλής Τάσης για Μαγνήτες Kicker στο CERN

Επιβλέπων:
Ιωάννης Φ. Γκόνος
Επίκουρος Καθηγητής Ε.Μ.Π.

Αθήνα, Οκτώβριος 2018

HISTORY OF CHANGES

REV. NO.	DATE	PAGES	DESCRIPTIONS OF THE CHANGES
1.0	2017-10-11	5	Beginning of introduction
1.1	2017-10-13	12	Continue of intro
1.2	2017-10-16	12	Corrections, references
1.3	2017-10-17	12	Captions, table of figures, bibliography
1.4	2017-10-20	13	Corrections, change of style to IEEE
2.0	2018-04-19	35	Added: Chapters – Structure – Photographic Material
2.1	2018-06-04	36	Writing: text for simulation procedures/difficulties
3.0	2018-06-19	36	Writing: formulas for intro
3.1	2018-06-20	37	Writing
3.2	2018-06-21	39	Formulas, changing fonts, writing chapter 3: Measurements Procedure
3.3	2018-06-24	40	Extending the introductory part about coax cables theory
3.3	2018-06-25	43	->>-
3.4	2018-07-02	38	Writing, corrections in chapt. 2,3
3.4.10	2018-07-22	49	writing chapt.3,4
4	2018-07-23	53	writing
4.1	2018-07-26	61	writing
4.2	2018-07-26	57	correcting/writing
4.3.1	2018-07-30	61	writing
4.3.3	2018-07-31	62	processing Mathcad files
5	2018-08-29	77	Annex
5.1	2018-08-31	81	Tables

TABLE OF CONTENTS

1. INTRODUCTION

1.1 ABOUT THE THESIS

1.1.1 Description

This work is about high voltage measurements and tests of various existing and new models of coaxial cables and connectors used for kicker magnets and also developing new ways and methods for optimizing and ultimately producing new, more efficient and more technologically upgraded cables using new materials, and replacing outdated old ones. First, there is a look on the current situation today regarding cables, connectors, conclusions are drawn, and current problems are outlined. What is discussed is the possible replacement of HV coaxial cables, which use a mixture of pressurized SF_6 (Sulphur hexafluoride) gas with polyethylene as insulation, with new ones much friendlier to the environment. New designs of cables are proposed, set up, and built as prototypes, which use silicon oils as dielectric. Afterwards there is an attempt to simulate the performance and behaviour of the test subjects under high voltage with the help of finite element method software. In this direction, computer simulation methods are being used for designing and optimizing.

A complete list of the equipment needed and the measurement set up inside the lab is being documented. Subsequently, old samples of cables and connectors used at CERN, as well as the new oil-filled ones, are put under examination, and the experiments take place: the work that is being done in the laboratory involves:

(a) the setting up of a HV cable test stand and

(b) the actual measuring and testing of the existing cable samples and connectors, as well as the optimized designs.

A simpler and easy-to-use method regarding the accuracy of the results and ways to improve it, is introduced. Results are then being processed with the help of computer software and conclusions are drawn. Then, the results of the computer simulations are being confirmed and compared to the results from the lab. Finally, the total contribution of the experiment is being assessed and questions are posed about the next day. An outlook is given on the feasibility of oil-filled cables as replacement for SF_6 gas pressurized cables and the foreseen future developments.

1.1.2 Chapters

In chapter **(1)**, there is a short introduction about the institution of CERN and the work which is being conducted currently. A brief description on kicker magnets and pulse forming lines. Subsequently, in chapter **(2)**, the principles around high voltage coaxial cables are outlined and the basics of transmission line theory are explained. Chapter **(3)** is about partial discharges theory. In chapter **(4)**, there is the description and methodology of the measurements procedure. Chapter **(5)** is a short presentation and theoretical evaluation of the cable samples under examination. In chapter **(6)**, there is the presentation of the measurements and the tests conducted in the laboratory, along with their results. Chapter **(7)** describes the numerical simulations conducted and shows the results. Finally, in chapter **(8)** there are the conclusions and analysis of all the results, and the assessment of the total project. **(0)**, **(10)**, **(11)** and **(12)** are annex, table of figures, references and bibliography, respectively.

1.2 GENERAL OUTLINE

Fig. 1. The LHC tunnel and aerial layout [2]

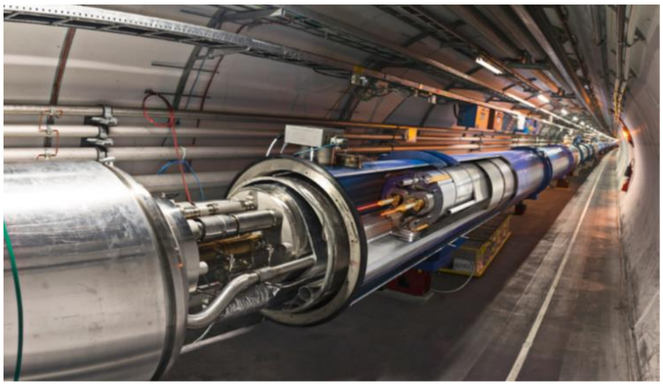

Fig. 2. The Large Hadron Collider (LHC) [2]

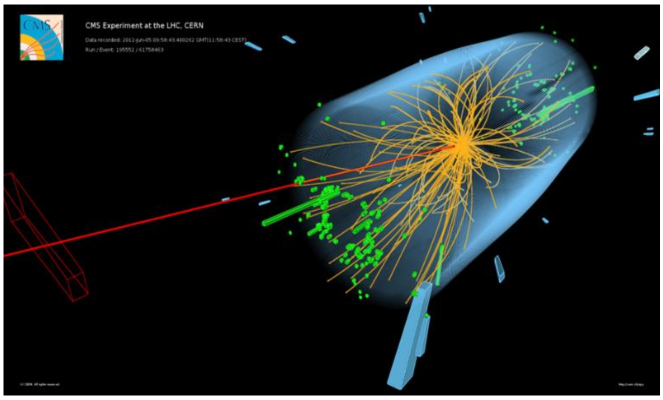

Fig. 3. Collision events recorded with the CMS detector in 2012 at a proton-proton centre-of-mass energy of 8 TeV [25]

1.2.1 WHAT IS CERN – BRIEF HISTORY

C.E.R.N. stands for “Conseil Européen pour la Recherche Nucléaire”, which in French means European Council for Nuclear Research, as it was named in its original form in 1952. Since then the name changed to European Organization for Nuclear Research, but the acronym CERN remained.

CERN is the world-class organization based in the heart of Europe, whose purpose is the research in the field of Physics, and more accurately, of Particle Physics, that is the science which studies the structure of matter. It is a joint venture from European member states which was founded in 1954, and its establishments are located in the wider area in the outskirts of the city of Geneva in Switzerland, on the Franco-Swiss border.

It is the largest particle physics laboratory in the world and the best of its kind, in which physicists and engineers from around the globe, work together in order to discover the tiniest components of matter and the laws of nature that hold them together. In order to do that, the scientists are trying to simulate the circumstances which existed during the first moments of the birth of our universe, fractions of a second after the Big Bang. This is when the building blocks of our world, the particles of matter were forming for the first time. [1]

1.2.2 PARTICLE COLLISIONS

The basic idea behind this venture is extremely high-energy collisions of particles. Through many series of collisions, new particles will be created and this in turn will lead to the deeper understanding of the most fundamental structure of matter and energy, and also of the laws of physics that govern them.

In order to achieve these collisions, large amounts of energy are required (TeV). Particles like heavy ions, such as protons and lead ions, form in groups called "beams" and will have to be accelerated to speeds close to speed of light. Then these beams are directed to each other and collide with each other. From the collisions, thousands of particles are emerging, and with the help of huge detectors, they are recorded and studied. [1]

1.2.3 ACCELERATORS

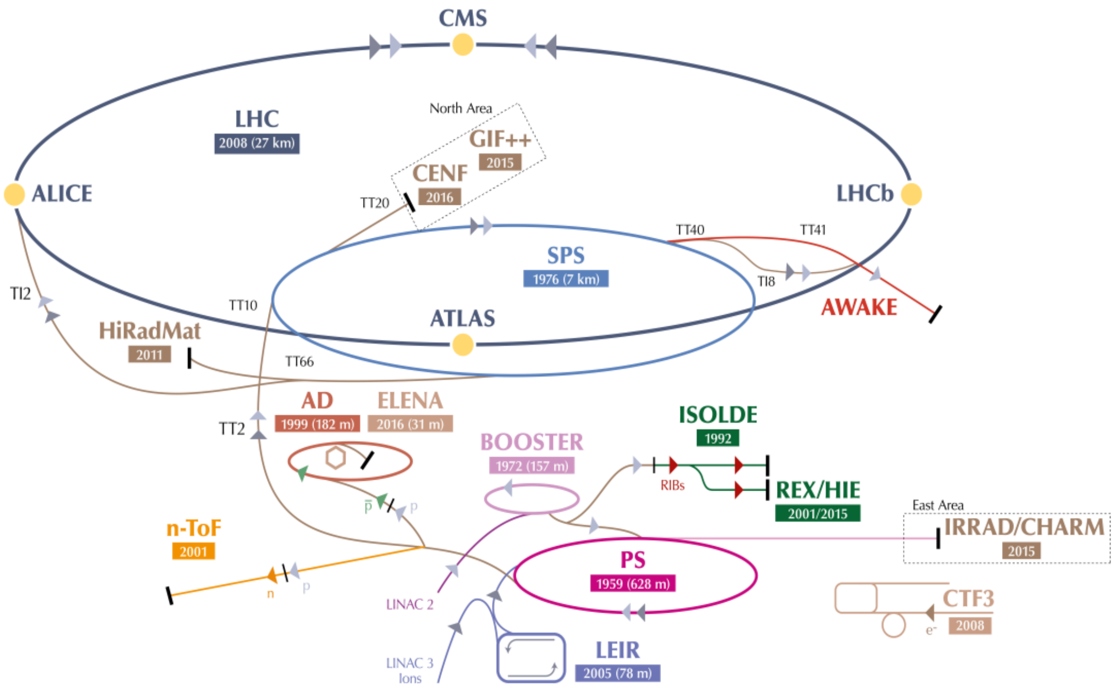

Fig. 4. The CERN accelerator complex [27]

As the main instrument for the conduction of this impressive experiment, CERN uses powerful and large machines of circular shape called Accelerators (or Colliders), in which the particles are accelerated with the use of electromagnets. The accelerators are situated in huge underground tunnels, with the largest one, the Large Hadron Collider, LHC, having a 27km circumference. Firstly, the particles are charged in order to be controlled by the magnets. Then they are injected into the accelerator which consists of a high vacuum tube,

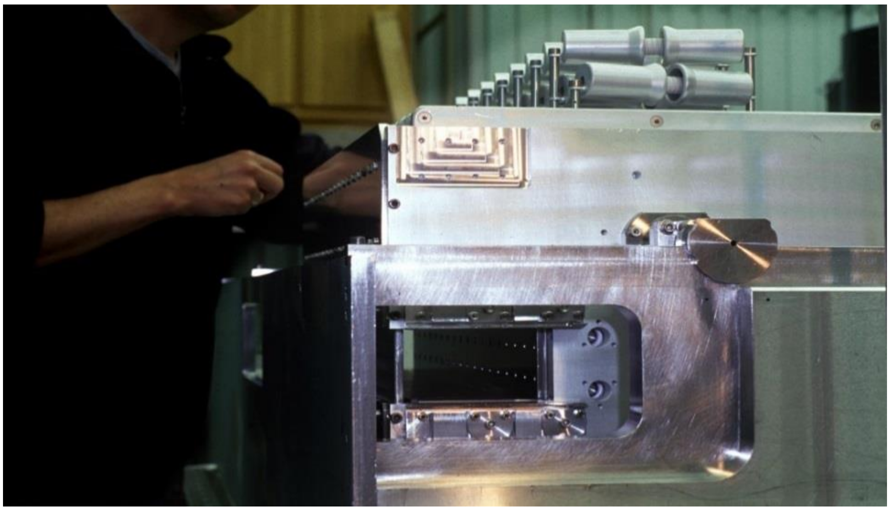

Fig. 5. One of the kicker magnets used to kick an injected beam onto the SPS circulating orbit [26]

and in there, different kinds of magnets are used to manipulate them in many ways. For example, the particles are accelerated with the use of accelerating cavities and electromagnetic resonators while they are kept at a constant energy level to balance the losses of energy. Dipole and quadrupole magnets are widely used for keeping the particles in orbit and focusing the beam. There is a quite large variety of magnets used in the accelerators. [2]

1.2.4 KICKER MAGNETS – PULSE FORMING LINES

In order to reach the high energies required for the collisions of the beam particles, there must be a whole system of accelerators, with multiple levels of energy, gradually raising from one stage to the other. First the beam is injected to a booster, and then from smaller to larger accelerators, that work together to accelerate the particles to velocities close to the speed of light. All this means that beams have to be transferred from one machine to another in a fast, accurate and efficient way. The special kind of magnets that are used to inject, extract and generally transfer beams from one stage to another, are called Septa and Kicker magnets and often the combination of the two is used. The kicker magnets (Fig. 5) have very fast rise/fall times of rectangular field pulses with low field strength, and the electromagnetic septa are DC or slow pulsed but provide a strong field strength.

A Kicker system, as shown in Fig. 6, consists of many components like: the Pulse Forming Line or Network (PFL or PFN), the kicker magnet, fast high power switches, the Resonant Charging Power Supply (RCPS), the transmission line(s), and the terminating resistors. [3]

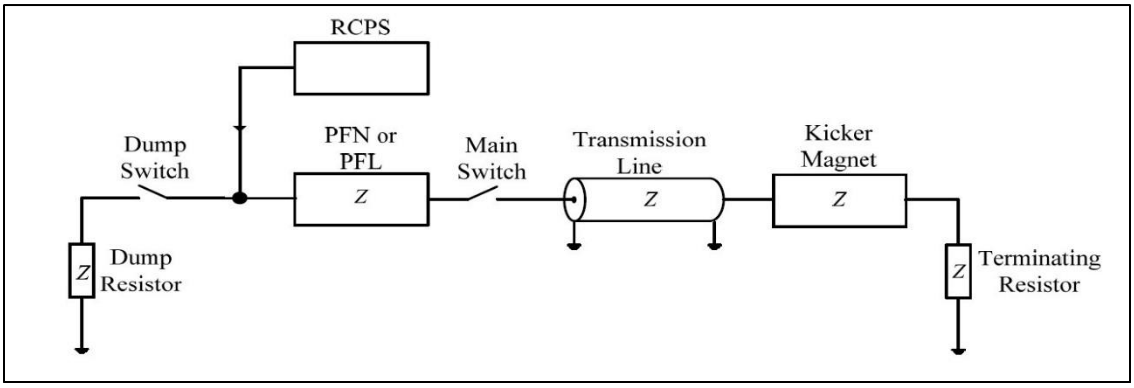

Fig. 6. Simplified schematic of a kicker system [3]

More specifically, the **pulsed high voltage coaxial cable** is the main component of the forming circuit in which the pulse is being generated. [3]

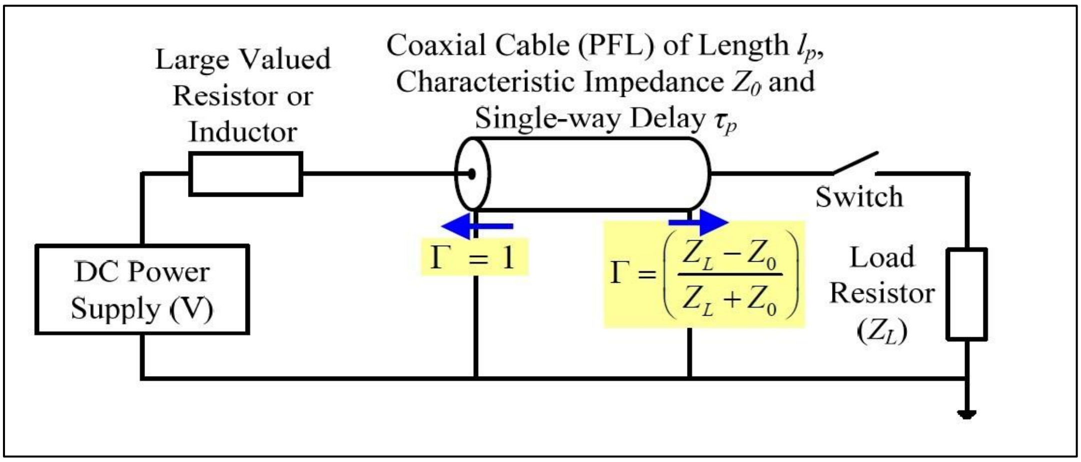

Fig. 7. Simplified schematic of a pulse-forming circuit [3]

2. HIGH VOLTAGE COAXIAL CABLES AND CONNECTORS

Fig. 8. 20Ω, 40Ω Coaxial Cables [28]

Fig. 9. 20Ω Cables and Connectors [28]

Fig. 10. HV coaxial cables [36]

2.1 DEFINITION

A coaxial cable is a type of transmission line that consists of mainly three different parts: (i) The inner conductor, which is a conductive tube or solid cylinder, (ii) the outer conductor surrounding the inner, which can be a solid tube (plate or corrugated) or a woven braid and (iii) the insulation, which is the dielectric material between the two conductors, and can be either solid, liquid or gas. The dimensions of the diameters of the two conductors (D_2 for the outer and D_1 for the inner conductor) as well as the value of the dielectric constant (ε_r) of the insulation, play a great role for the cable, as they determine its characteristic impedance and other important parameters. The most common type of material for these metallic conductors is copper (Cu), and for the insulation, what is often used low-density polyethylene (PE).

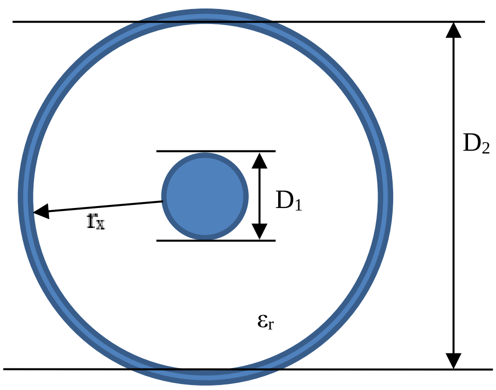

Fig. 11. Cross-section of a coax cable

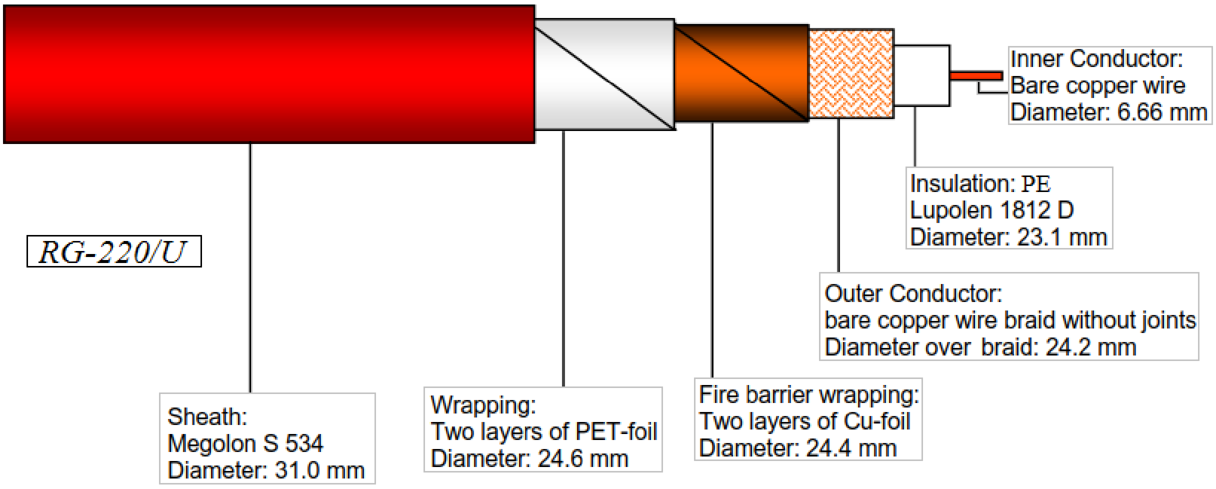

Fig. 12. Structure of coaxial cable type *RG-220/U*, showing its different layers of material [29]

2.2 PRINCIPLE CHARACTERISTIC ELEMENTS

Coaxial lines and cables are commonly used for forming and transmitting high voltage pulses [4]. According to the Transmission Line Theory [5], from the corresponding bibliography, a transmission line consists of two conductors - one live and one ground – and in between them the appropriate insulation made of a dielectric material. The two conductors have a constant cross-section area. Together with the dielectric, they can be represented in an equivalent circuit, whose discreet components are evenly distributed along its length. A schematic representation of the elements of a transmission line is shown in Fig. 13.

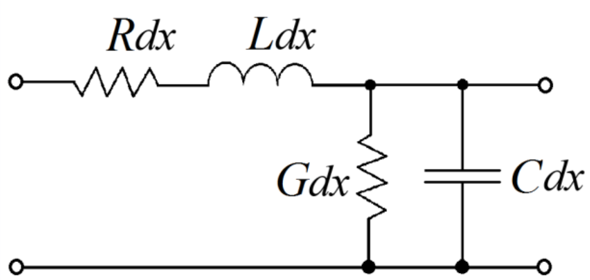

Fig. 13. A coaxial cable with its elements per unit length

The principle characteristic elements per unit length of the line are:

- h: the length of the cable
- R/h: The loop series resistance of the inner and outer conductor, in Ω/m
- G/h: The shunt conductance G, in S/m, which represents the leakage current flowing in the insulation between the two conductors
- C/h: The shunt capacitance C of the cable in F/m, that is formed from the dielectric and the two conductors
- L/h: The series inductance L, in H/m, which is depended on the cross-sectional area of the cable.

From these four basic components, we can derive the formula of the input impedance of a transmission line which is its characteristic impedance Z_0 in Ω at any frequency:

$$Z_0 = \sqrt{\frac{R + j\omega L}{G + j\omega C}} \tag{1}$$

For high frequencies (above several MHz), the above formula can be simplified to:

$$Z_0 = \sqrt{\frac{L}{C}} \tag{2}$$

The wave propagation constant is:

$$\gamma = \alpha + j\beta = \sqrt{(R + j\omega L)(G + j\omega C)} \tag{3}$$

where α is the attenuation in nepers/km (or in dB/km if multiplied by 8.686) and β is the phase change coefficient.

These formulas give the two basic parametres for coaxial cables: the characteristic impedance Z_0 and the attenuation α. However, as mentioned before, these parametres can result from the geometrical and electrical specifications of the cable, meaning its dimensions and the relative permittivity of the insulation.

According to the corresponding bibliography [5], we find that the equations for the principle characteristic elements per unit length of the line, L, C, R, and G are depended on the diameters of the inner and outer conductors, the frequency and other material properties, as shown below. Also on the dielectric constant $\varepsilon = \varepsilon_0 (\varepsilon_r' - j\cdot\varepsilon_r'')$, where $\varepsilon' = \varepsilon'_r\cdot\varepsilon_0$, is the real part of the complex permittivity $\varepsilon = \varepsilon' - j\cdot\varepsilon'' = \varepsilon' \cdot (1 - j\tan\delta)$, $\tan\delta = (\omega\cdot\varepsilon'' + \sigma) / (\omega\cdot\varepsilon')$ is the tangent of losses and ε_0 the permittivity of vacuum, $\varepsilon_0 = 8.85\cdot10^{-12}$ F/m.

From Fig.11:

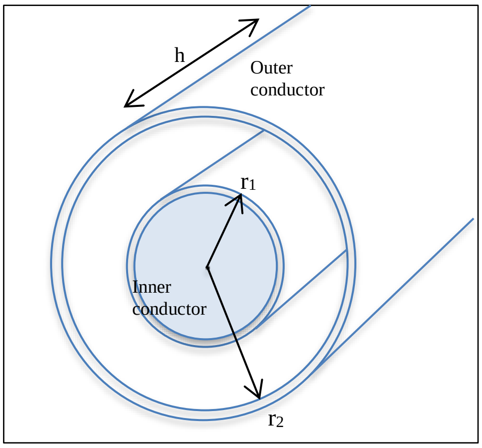

Fig. 14 Cross-section of a coax cable

$$\frac{L}{h} = \frac{\mu}{2\pi}\ln\left(\frac{D_2}{D_1}\right), \quad (H/m) \tag{4}$$

where $\mu = \mu_0\cdot\mu_r$ is the permeability of the material of the conductor.

$$\frac{C}{h} = \frac{2\pi\varepsilon_r'}{\ln\left(\frac{D_2}{D_1}\right)}, \quad (F/m) \tag{5}$$

From Fig. 14:

$$\frac{R_{total}}{h} = \left[R_{DC_{inner}} + R_{DC_{outer}}\right] + \left[R_{AC_{inner}}(f) + R_{AC_{outer}}(f)\right] =$$

$$= \left[\frac{1}{\Delta_{inner}\cdot\sigma_{CU}} + \frac{1}{\Delta_{outer}\cdot\sigma_{CU}}\right] + \left[\frac{1}{\Delta_{eff_{inner}}\cdot\sigma_{CU}} + \frac{1}{\Delta_{eff_{outer}}\cdot\sigma_{CU}}\right], (\Omega/\text{m}) \qquad (6), [5]$$

where Δ_{inner} and Δ_{outer} are the surfaces of the cross section of the two conductors respectively, $\Delta_{eff_{inner}}$ = 2·π·r_1·δ_s, where r_1 is the outer radius of the inner conductor, and $\Delta_{eff_{outer}}$ = 2·π·r_2·δ_s is the inner radius of the outer conductor, δ_s is the skin depth, $\delta_s = \frac{1}{\sqrt{(\mu_0 \cdot f \cdot \pi \cdot \sigma_{CU})}}$, and σ_{CU} the conductivity of the copper.

$$\frac{G}{h} = \frac{4\pi^2 \varepsilon_0 \varepsilon_r' \tan(\delta)}{\ln\left(\frac{D_2}{D_1}\right)} \cdot f \ , \quad (S/m) \tag{7}$$

Using these formulas, another way to express the cable impedance Z_0, in Ω, from the cable dimensions is:

$$Z_0 = \sqrt{\frac{\mu}{\varepsilon}} \left(\ln\left(\frac{D_2}{D_1}\right)\right) \frac{1}{2\pi} \tag{8}$$

and the attenuation constant, in dB/km:

$$\alpha = \frac{1}{2} \cdot \left(\frac{R}{Z_0} + G \cdot Z_0\right) \cdot 8.686. \tag{9}$$

where G = G(f) and R = R_{total} = R_{DC} + R_{AC}(f), calculated for both inner and outer conductor, $D_2 = r_2$, $D_1 = r_1$.

2.3 HIGH VOLTAGES AND DIELECTRICS

2.3.1 THE ROLE OF THE DIELECTRIC CONSTANT ε_r

A high voltage coaxial cable uses different kind of insulating materials as dielectric media between the two conductors. These can be either solid (like in the case of polyethylene), liquid (e.g. mineral/silicon oil), gas (i.e. air, SF_6) or vacuum. The dielectric constant (or relative permittivity) sets the correct impedance needed for each application, and also plays a great role in the attenuation of the signal and the losses of the pulse in the cable. The most common types of dielectric materials used as insulators are shown in table I.

Under certain conditions, this insulation maybe damaged and fail, partially or fully, which leads to the destruction of the cable. There are many different mechanisms considering the dielectric medium, in which this phenomenon may occur, during the lifetime of a cable, and the procedure depends on many variables. These factors are the thermal stresses, the electrical stresses, the radiation, the mechanical stresses, the environmental conditions and also the time period under which the cable is subjected to each kind of stress. Therefore, the important factors, responsible for the deterioration of the insulation, are: the voltage, the temperature, the pressure, the moisture, the radiation; moreover and more importantly, the existence of impurities in the dielectric and imperfections of the cable, i.e. in the form of contaminants and voids and also sharp edges, and the type and shape of the conductors.

Table I. Dielectric Constants for different materials at 20°C

Material	Dielectric Constant
Vacuum	1
Air (1 Atm)	1.00059
SF_6 gas	1.00204
Air (100 Atm)	1.0548
Fluorinert™ liquid FC-40	1.9
Teflon	2.1
Various Silicon Oils	2.18 - 2.8
Polyethylene	2.2 - 2.3
Polypropylene	2.2 - 2.3
Polystyrene	2.55
Bluesil™ Fluid oil 47 V 20	2.7
Plexiglas	2.7 - 3.7
Mica	3 - 6
Polyvinyl Chloride	3.18
Paper	3.3 - 3.5
Bakelite	3.5 - 5
Epoxy Resin	3.6 - 6
Glass	5 - 10
Porcelain	6 - 8
Neoprene Rubber	6.7
Silicon	11.9
Germanium	16
Water (distilled)	80.4
Strontium Titanate	310

2.3.2 THE BREAKDOWN VOLTAGE AND PEAK VOLTAGE

The most significant and permanent damage that can occur to the insulation of a cable is called an electrical breakdown (BD). It is this kind of dielectric failure where the applied voltage over the two conductors exceeds the breakdown voltage (BDV), the electric fields exceed the electric strength of the material and therefore the two conductors are bridged and thus the insulation becomes conductive as well. Another way to express this, is that the dielectric strength of a material is the maximum electric field stress it can withstand before it breaks down.

The variety of the factors that can lead to a BD is wide and complex and sometimes it is a combination of several breakdown mechanisms acting simultaneously, and other times there is one accepted theory, like the avalanche theories for example in the case of liquids and gases. Under low electric stress, in a dielectric gas there is no current flowing unless there are enough free ions or electrons inside the gas. If the electric stress is high enough then it can cause an electron to ionize a gas molecule by collision, from which two electrons and an ion will be produced. Then these two electrons will ionize in turn two more ions producing four electrons and two ions and so on. This whole process, which is called “electron avalanche”, will eventually lead to a conductive path of electrons, thus to failing the insulation and causing the breakdown. The voltage right before this phenomenon starts to occur, is called peak voltage of the cable and is the maximum permissible operating voltage (nominal) voltage under which the cable is permitted to operate safely [5] [6].

Table II. Dielectric Strength for different materials at 20°C

Material	Dielectric Strength (kV/mm)
Epoxy Resin	0.5 - 2
Air	3
Paper	6 – 12
Strontium Titanate	8
SF_6 gas	9.018
Germanium	10
Bakelite	12 - 28
Bluesil™ Fluid oil 47 V 20	14
Various Silicon Oils	14 - 18
Glass	17-30
Fluorinert™ liquid FC-40	18.11
Neoprene Rubber	18 -25
Polyethylene	18.9 - 160
Polystyrene	19.7
Vacuum	20 - 40
Plexiglas	30
Silicon	30
Polyvinyl Chloride	40
Porcelain	40 - 50
Teflon	60
Water (distilled)	65 - 70
Mica	200
Polypropylene	230 - 250

2.3.3 IMPORTANT PARAMETERS OF A COAXIAL CABLE

The factors that play a great role in the quality and performance of a coaxial cable, in accordance to the needs of the CERN kicker systems, are those electrical data and properties that are mentioned in the data sheet of each cable that is being ordered from the manufacturing cable companies. These properties are:

- The characteristic impedance (Z_0) of the cable, in Ω
- The attenuation (losses) of the transmitted signal along the length of the cable, in dB/km
- The maximum magnitude of the partial discharges in the insulating dielectric of the cable, in pC
- The peak voltage in AC and DC, plus the breakdown voltage (BDV) of the cable.

These electrical properties are of great concern to CERN, and engineers are always obliged to test and confirm whether or not the cables comply with the CERN standards and whether they are manufactured according to the specific requirements of each application. For this reason there are frequent tests and measurements on cable samples and connectors, in order to test the reliability of these products. Another important parameter that must be taken into consideration is relevant with the circumstances under which the specific coaxial cables will be used. These cables must be radiation hard in order to withstand the radiation dose they will receive over their lifetime. Radiation is proved to lead to mechanical failure or to a change of dielectric properties. [7]

2.3.4 WHERE AND WHY WE USE COAXIAL CABLES

Kicker magnets are used throughout the CERN accelerator complex for transferring particle beams between accelerators and for dumping beams. They need to achieve fast magnetic field rise/fall times in order to deflect, for example, one bunch of the injected beam without affecting the already circulating beam. For this application, fast pulse forming circuits are required. Coaxial high voltage cables are widely used at CERN for kicker pulse generation and transmission. The magnetic field of the kicker must rise and fall very fast, from tens to hundreds of nanoseconds. The simplest configuration is a PFL (Pulse Forming Line, coaxial cable). For such fast transient events, according to wave propagation theory, different requirements and conditions must be achieved to ensure smooth operation. The most important properties of coaxial cables for use in pulsed systems are a matched and homogeneous characteristic impedance to avoid reflections along the line and loss in kick strength, while achieving a low attenuation, to avoid current droop and pulse distortion, and a high dielectric strength to withstand the high voltages required to drive the current.

In a nutshell, the important properties of coaxial cables are:

- ✓ matched and homogeneous characteristic impedance, to avoid reflections along the line and loss in kick strength
- ✓ low attenuation, to avoid current droop and pulse distortion
- ✓ high dielectric strength to withstand the high voltages required to drive the current

2.3.5 CERN USES SPECIALIZED SF_6 GAS FILLED HIGH VOLTAGE COAXIAL CABLES

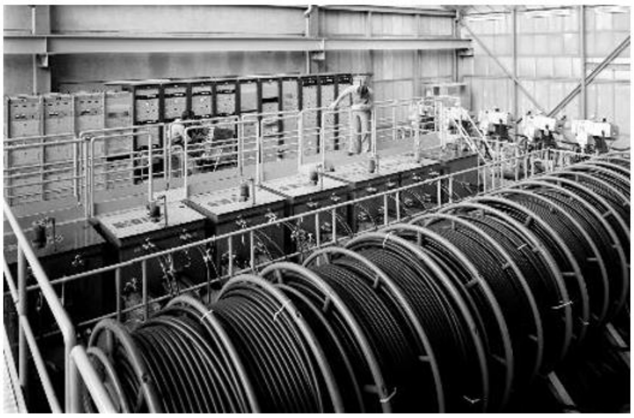

Fig. 15. SF_6 Coaxial cable pulse forming lines [19]

It is crucial for kicker applications that the field pulse has an ideally rectangular form. Thus, not only the rise and fall time needs to be fast but also the droop during discharge has to be low and the so called “flat top” needs to be ripple free: this requires a low loss cable with very low attenuation (<2.9 dB/km) and homogeneous impedance to minimize the pulse distortion. As a result the usage of semi-conducting layers which normally smoothens the electric field strength at the transition of conductor to insulator is not possible. Such layers normally allow for construction of compact extruded cables for high voltage applications. At CERN, the maximum voltage amplitude is given by the magnet kick strength requirement and goes up to 80 kV. To avoid reflections the cable impedance needs to be matched and is defined by the magnet. Usually impedances between 2 and 25 Ohms are used. Already basic calculations show that for such impedances, attenuation and voltage requirements, the insulation thickness for a polyethylene (PE) extruded cable plays a great role and hence the cable diameter is large. This causes production issues in terms of a precise extrusion process.

CERN took advantage of the excellent properties of SF_6 gas in the past and introduced a design where the cable consists of a hollow inner copper conductor pressurized with SF_6 gas and perforated in such a way that the gas can penetrate into the dielectric. The dielectric itself consists of many layers of wrapped PE tape and SF_6 gas. The wrapping (with overlapping and alternate directions) of the PE tape is done in such a way that the SF_6 gas can penetrate throughout the whole dielectric and fill all voids. The outer conductor is extruded aluminium or parallel corrugated copper (two designs exist) and protected by a Low Smoke Zero Halogen outer sheath (LSZH jacket). CERN currently operates approximately 15 km of SF_6 gas filled cables, manufactured by Les Câbles de Lyon (extruded aluminium coaxial cable) in the 1970’s and Brugg (corrugated, copper) in the 1990’s. [8]

There is an increasing need for replacement not only because of system aging but also because of more restrictive SF_6 gas handling procedures. Sulphur hexafluoride is an efficient absorber of infrared radiation and is estimated to have a global warming potential that is 25.000 times greater than that of CO_2 [9]. On top of all this, the specific coaxial cable is not available because it is not produced anymore. CERN is therefore intensively searching for an alternative.

2.3.6 REPLACEMENTS OF THE SF_6 CABLES ARE INVESTIGATED

In this framework, potential candidates for the replacement of the SF_6 gas cables have been identified. A first option would be the use of improved polyethylene extruded cables with large diameter and without semiconducting layer. Other promising solutions include new pulse generator technologies such as the Inductive Adder [10] and the Marx-Generator [11]. Another option, which is also examined in this thesis, is the adaptation of an off-the-shelf (OTS), low-loss, air-dielectric cable, the HCA118-50J "Heliflex" manufactured by Radio Frequency Systems, RFS [12], by replacing the air dielectric with electrical insulating oil. The increase in dielectric strength should allow achieving higher peak voltages, reducing corona and increasing the partial discharge inception voltage.

2.3.7 CONNECTORS FOR HV COAXIAL CABLES

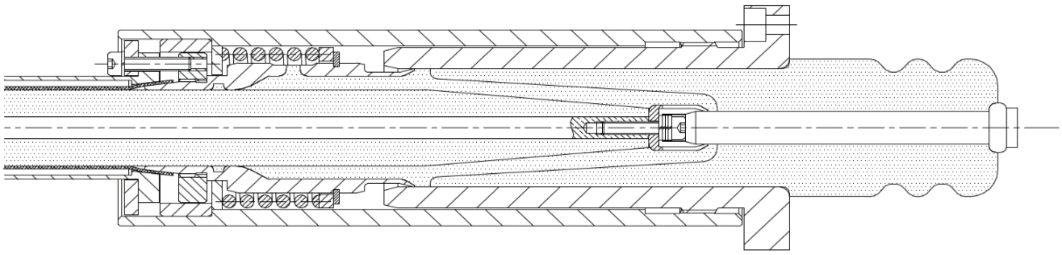

Fig. 16. RG 220/U cable connector assembly design [13]

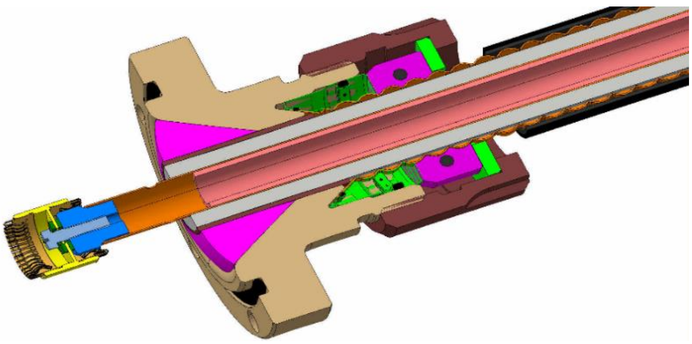

Fig. 17. SF_6 gas filled coax cable connector (CAD cross section) [37]

High voltage coaxial cable connectors play a crucial role in the performance and the electrical behaviour of the cables themselves. They must meet certain criteria including: leak-tight connector socket, specific characteristic impedance, radiation resistance, safe design for fast pulses of tens of kV amplitude, and other mechanical requirements, suitable for during installation and manipulation. [13]

However, probably the most important part of installing these connectors at cable ends, is the fact that they ensure that no partial discharges, corona, arching or other kind of malfunction will occur. Cable ends are possible weak points of a cable due to the fact that the electric field lines there are not homogeneous and smoothly distributed, because of the sharp edges at those ends. This is why connectors must be designed in such a way as to fit perfectly the cable insulation, leaving no air gaps or other voids, and most importantly have such a shape that forms a smooth electric field surrounding the conductors. As a consequence in many cases round, spherical or more likely cylindrical geometrical shapes are preferred, or also conical ones (deflectors, fig.20).

Fig. 18. M30311h (Spinner) connector for RFS HCA118-50J Heliflex coaxial cable [30]

Following the criteria mentioned above, the connectors must be designed and manufactured accordingly, since very often these components are not available on the market. Therefore, extensive testing in the laboratory and simulating beforehand is required.

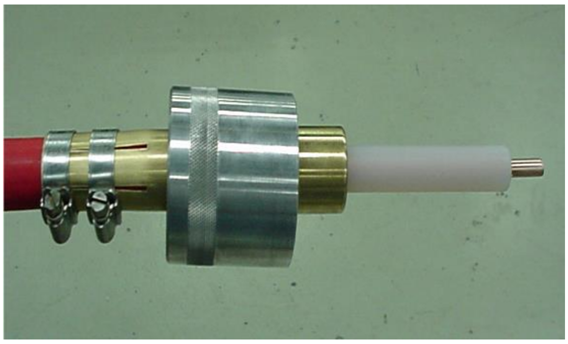

Fig. 19. 40 Ω coaxial cable end [31]

Fig. 20. Deflector

Fig. 21. LEMO HT50 connector, in use for system voltages up to 40kV [19]

3. PARTIAL DISCHARGES - IEC 60270

3.1 DEFINITION

IEEE and the IEC 60270, the international standard on "High-voltage test techniques – Partial discharge measurements", define the term "partial discharge" (PD) as the phenomenon of an electrical discharge which is not fully bridging the insulation between the two conductors that are under high voltage, but rather happens, for example, along a certain width (part) of the insulation, or in the medium surrounding the conductor, or inside a void (i.e. in an air gap, Fig.22). More specifically, PDs are the discharges that occur inside or in the surface of the insulation because of 'local electrical stress concentrations' in it, they usually last under 1 μs, and therefore they are considered as pulses. They make a characteristic sound which is easily heard, they sometimes emit light and heat and also ionize the air molecules surrounding the conductor or inside the gap. This leads to the production of ozone, which is toxic when is present at the lower levels of the atmosphere. "Corona" is a form of partial discharge but differs from other forms of PDs. It is luminous, as it emits a faint glow while ionizing the air or other gaseous media surrounding the conductor which is not close to solid or liquid insulation, whereas not all PDs are necessarily luminous. [14], [6]

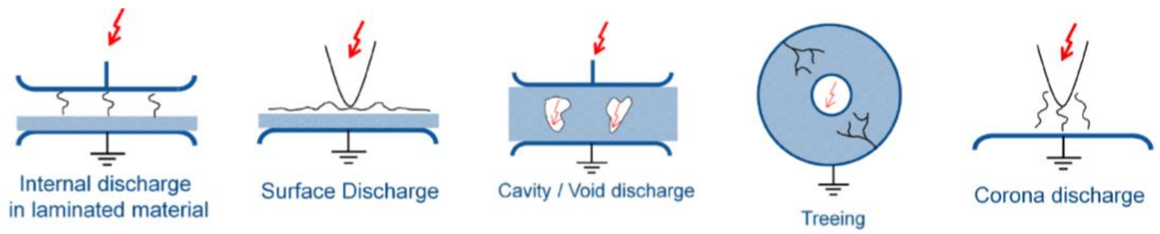

Fig. 22. Forms of discharges [16]

3.2 THE PARTIAL DISCHARGE PULSE – APPARENT CHARGE Q – INCEPTION / EXTINCTION VOLTAGE

The PD pulse is the current or the voltage that is produced during a PD, and is measured with the help of appropriate detector circuits and equipment. That means that a PD produces a current pulse of a specific charge and then the detector produces a proportional signal of a current or a voltage. What is being measured is the apparent charge q of a PD charge. The international standard IEC 60270 defines the apparent charge q (pC) as the charge that 'if was injected between the terminals of a test object in a specified test circuit, it would give the same reading on the measuring instrument as the PD current pulse itself, and it is not equal to the amount of charge locally involved at the site of the discharge, which cannot be measured directly'. This is the quantity which is measured during the test with the help of the appropriate test circuit and measuring system. Each of these systems need calibration and have different operating principles and requirements that have to be met. In a nutshell, what interests us more, when measuring PDs, is the largest repeatedly occurring PD magnitude. [14]

The partial discharge inception voltage U_i is defined as "the applied voltage at which repetitive partial discharges are first observed in the test object, when the voltage applied to the object is gradually increased from a lower value at which no partial discharges are observed. In practice, the inception voltage U_i is the lowest applied voltage at which the magnitude of a PD pulse quantity becomes equal to or exceeds a specified low value". As for the extinction voltage U_e, this is defined as "the applied voltage at which repetitive partial discharges cease to occur in the test object, when the voltage applied to the object is gradually decreased from a higher value at which PD pulse quantities are observed", and "in practice, it is the lowest applied voltage at which the magnitude of a chosen PD pulse quantity becomes equal to, or less than, a specified low value". [14]

3.3 IMPORTANCE OF PDs

The presence of partial discharges in a high voltage transmission line, such as a coaxial cable with solid insulation, will lead with great certainty, in time, to the progressive and complete destruction of the insulation of the cable, rendering it useless. Due to very good insulating materials nowadays, when a lot of sparks accumulate in one point (i.e. because of a sharp edge), the cable may eventually break down. Because of PDs the dielectric is constantly degrading and gradually what follows is breakdown. The mechanism behind this is the produced ozone, which is a highly reactive form of oxygen, attacks the insulation, together with the stray electrons which are being produced by ionization. The phenomenon of the PDs takes place in a lot of forms and in many ways. It can occur in the gaseous media surrounding an HV conductor (corona discharge), in a gap inside the insulation (cavity / void discharge), i.e. when the electric field inside the gap exceeds the electric strength of the medium inside the gap. In the other forms, we have internal discharges in laminated materials, surface discharges and also electrical treeing, as shown in Fig. [22].

We might say that a partial discharge creates excess energy which is released in parts of the cable that were not planned for this by the constructor. As a result, the surrounding materials decompose. This in turn is what finally triggers the initiation of the breakdown and consequently the lifetime of the cable is reduced. [15]

3.4 PARTIAL DISCHARGES IN HV COAXIAL CABLES

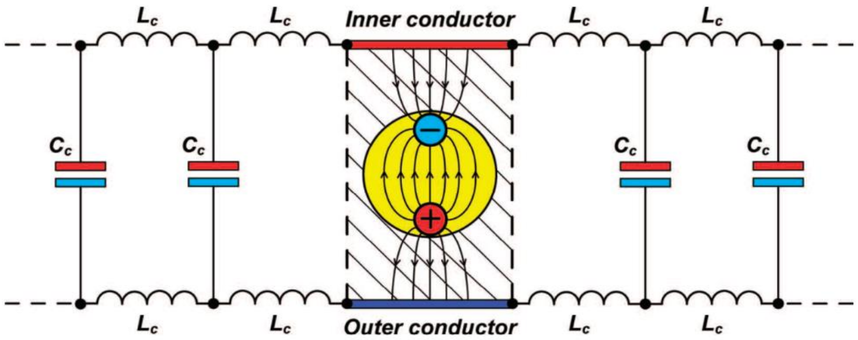

Fig. 23. Equivalent circuit of a power cable with a void (cavity) inside which there is a discharge [35]

3.4.1 DAMAGES TO THE INSULATION

The unit of the magnitude of a PD is its charge, measured in coulombs (more often, pC). The appearance of the first partial discharges during an HV test, happens with the gradual raise of the voltage between the two conductors. The specific (lowest) voltage at which continuous partial discharges or corona of specified pulse amplitude occurs is called "(Corona) Inception Voltage". The higher the voltage stress, the more partial discharges are detected and with higher magnitudes, and they are observed both in AC and DC systems. In AC, the damage they cause to the insulation increases with the increase of frequency of the current. Because of the ionization, the damages suffered by the insulation and the insulation surface are very intense, even in the most common solid insulating materials, like polyethylene (PE), polypropylene and PTFE (Teflon): some saturated polymers which have high resistance to oxidation but low resistance to ionization. Other materials like silicon rubber, which is considered to be the best flexible insulation, have better resistance in ionization and ozone in high temperatures (over 130 ºC), and other polymers, like ethylene-propylene copolymer, butyl rubber, nylon and chlorinated polyolefins, have better resistance at lower temperatures. Last but not least, other well protected cables against both ionization and oxidation, are paper-oil insulated ones. [6]

It is very important to measure PDs as a way of preventive maintenance, as the continuous evaluation of the insulation condition, ageing and quality, e.g., in cables, connectors and mounting, potting and transformers. In this direction measuring PDs can help us improve the design of the devices under high voltage, detect any developing faults in them, extend their lifetime and reduce their downtime. [15]

Concerning HV lines, one of the most important factors of quality and good performance of a coaxial cable is the maximum partial discharge magnitude. It is mentioned in every manufacturer's cable data sheet and often it should not exceed a few picocoulombs (pC). It is very important to do partial discharge measurements because it is a good indicator and useful advanced diagnostics for the lifetime and the assurance of the quality of the cable.

3.4.2 WHAT IS BEING MEASURED

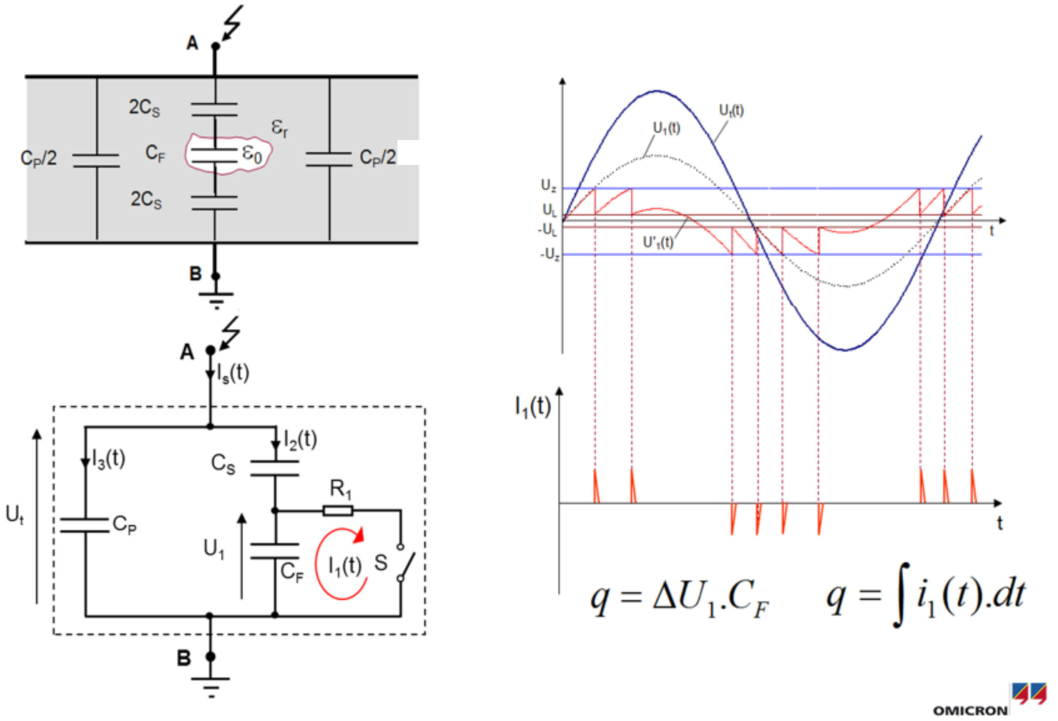

Fig. 24. Equivalent circuit diagram [16]

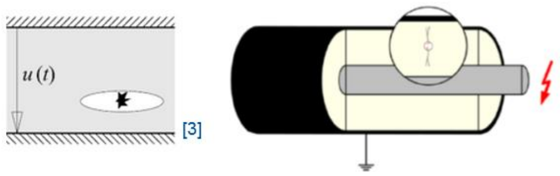

Fig. 25. Gas void inside the insulation of the cable [32], [33]

The gas void inside the insulation of the cable in figure 25, is being represented with the equivalent circuit diagram of figure 24. A capacitor C_F with its own dielectric strength, much smaller than this of the rest of the dielectric of the insulation has a lower voltage drop U_1 than that of the applied voltage U_t, since the capacitors C_S and C_F behave like a capacitive divider. As the sinusoidal voltage raises, the electric field inside the cavity surpasses the strength of the air gap, and it breaks down (U_1 reaches its max value U_z). Then the switch S closes, the C_F is discharged and U_1 becomes zero. As the U_t continues to raise, the C_F charges, U_1 raises again, until the gap breaks down again, and it discharges again. Then the polarity changes and we have the same procedure from the negative direction. The current that flows during that partial breakdowns is the PD we measure. [16]

3.4.3 PD PATTERNS – FINGERPRINTS

Another important case concerning partial discharges, is the source that produces them. This can be easily identified by the PD patterns they follow, according to the phase at which they occur. This procedure is called 'phase resolved PD'. As a result, depending on the phase that the PDs occur when observed on our measuring system, we can determine whether they originate, for example, from surface discharges, from corona, from scratches and cuts or from internal voids and cavities inside an XLPE cable, or as we will later realize, from air bubbles in oil.

The next figure (26) shows some of these examples. [17]

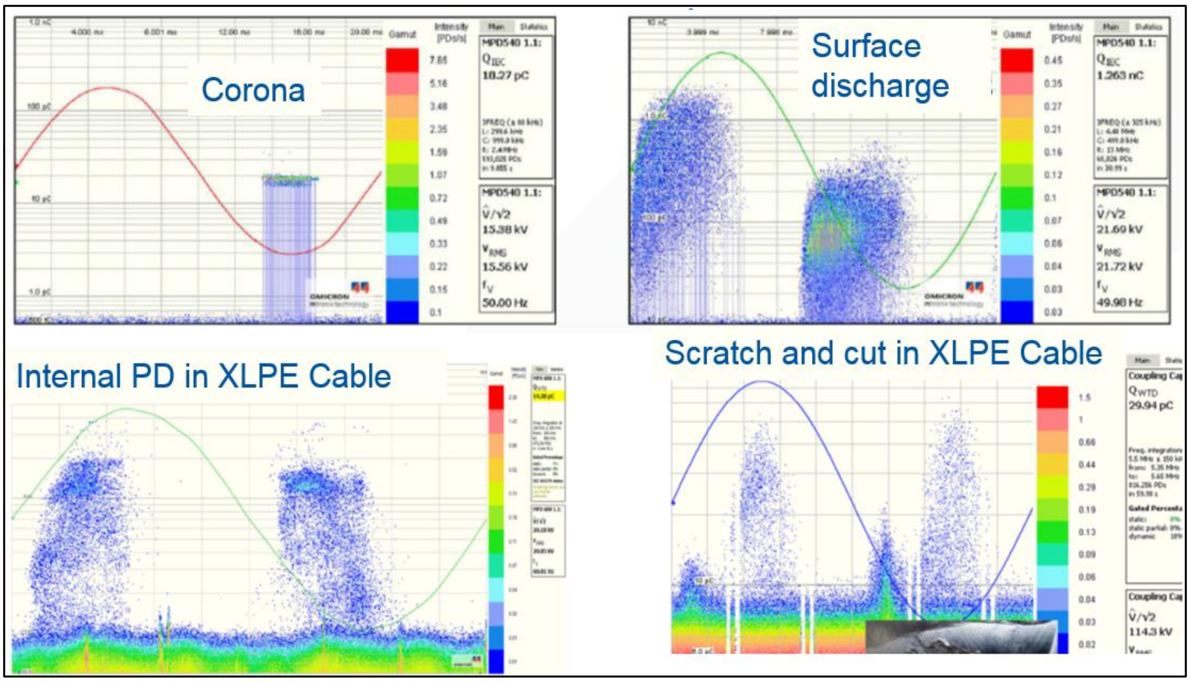

Fig. 26. Different PD sources produce different PD patterns [17]

3.5 TEST CIRCUITS FOR PARTIAL DISCHARGE MEASUREMENTS

3.5.1 THE COUPLING CAPACITOR

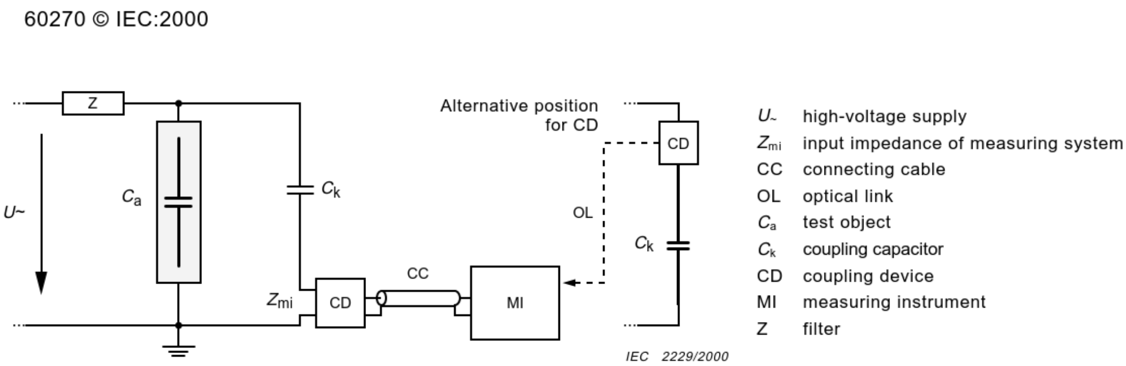

Fig. 27. Coupling device CD in series with the coupling capacitor [14]

According to the IEC 60270 standard the test circuits for PD measurements mainly consist of the test object, which is basically a capacitor C_a, a coupling capacitor C_k, which is of low inductance, the measuring system with its input impedance, the HV power supply with low background noise, HV connections with low background noise, and an impedance or filter for the background noise. PD measuring systems can be divided to three subsystems, which are the coupling device, the transmission system, and the measuring device. The coupling device is the "integral part of the measuring system and test circuit" and its task is to convert the input current signals to output voltage signals that are then transmitted to the measuring instrument by a transmission system.

In principle, when discharges occur in the test object C_a, there is a sudden voltage drop across it (which is basically the apparent charge we want to measure) and a small current will then be induced to the test object to balance the voltage difference because of the discharge. The coupling capacitor C_k and the coupling device (has an input impedance Z_{mi}), which they are connected in series, will form an RC filter ($f_C = \frac{1}{2\pi RC}$) that blocks the low frequencies and will allow to pass the high frequencies from the partial discharges due to its low impedance of the capacitor at high frequencies, $X_c = \frac{1}{j\omega C}$. Moreover, the coupling capacitor must have a much larger capacitance than the test object in order for the system to have accurate measurements. This is because we only want small voltage changes of the supply voltage when PDs occur. Plus, it must be a high voltage rated capacitor in order to block the HV excitation.

3.5.2 INDUCTIVE CURRENT TRANSFORMER

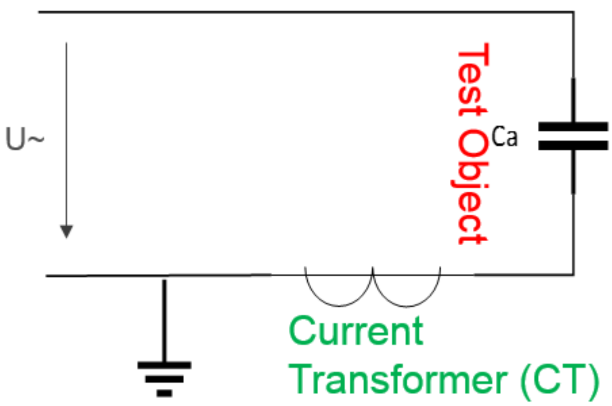

Fig. 28. Test circuit of the inductive current transformer method [15]

Another method of measuring partial discharges is with the help of the Inductive Current Transformer (CT). It is quite simple in its function and principle, and it was for this that it was used during our PD tests. Its use is simply by placing the transformer on the return cable (ground) of the test circuit, and without interrupting it, it measures the current flowing. Its operating principle is that, as current flows in the cable, it passes through the windings, creates a magnetic field which in turn produces current to the output of the CT. The measured current is then represented as a voltage waveform which is the output signal of the transformer and can be visualized by an oscilloscope. Depending on the ratio of the CT which is defined by the manufacturer, the current measured translates then into a voltage. [15]

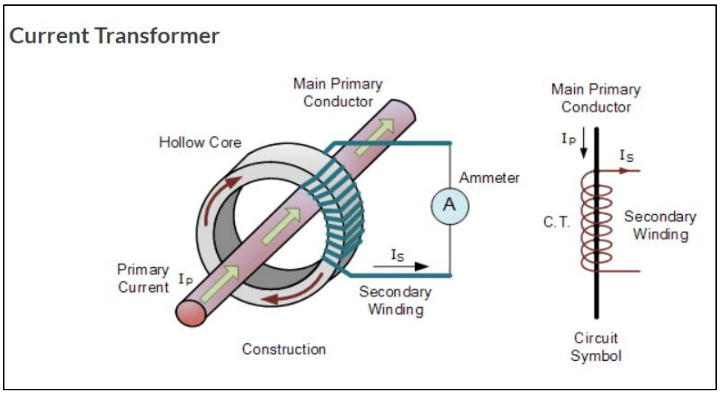

Fig. 29. The current transformer [34]

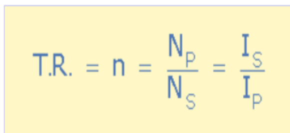

$$T.R. = n = \frac{N_P}{N_S} = \frac{I_S}{I_P}$$

Fig. 30. Induction formula of the CT [34]

This allows us to measure the current flowing from the inner conductor of the test subject - through the insulation - to the outer conductor, by observing its waveform on the oscilloscope. As the voltage was being raised gradually, when it reached the inception voltage, the first partial discharges appeared as irregular “spikes”, as shown in fig. 31, on the waveform of the current. The procedure of the extracting the values of the current from the waveform and finally calculating the PD charge magnitudes is to be described later on.

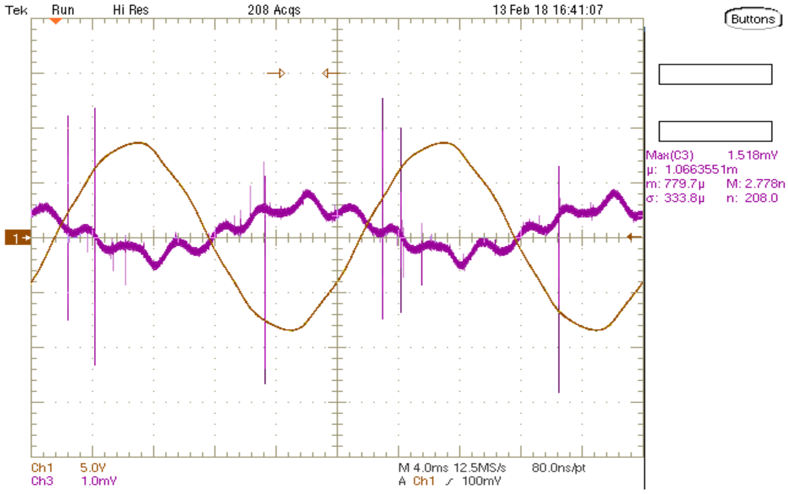

Fig. 31. Oscilloscope screenshot example of the PDs depicted as "spikes" on the waveform of the current (purple colour), represented as the output signal from the CT

4. MEASUREMENTS SETUP AND PROCEDURE

4.1 DEVELOPMENT OF THE PARTIAL DISCHARGE MEASUREMENT SYSTEM - METHODOLOGY

As to assure that the system measures the specified PD magnitude correctly, the PD measuring system needs to be calibrated before any measuring takes place. The goal is to measure the apparent charge q, which is injected to the terminals of the test object. A generator produces step voltage pulses of amplitude U_0 in series with a known capacitor C_0 (often 10 or 100 pF), so that the charge is then $q_0 = U_0 \cdot C_0$. Afterwards, using the measuring system, we measure the current, which we will integrate over time, and calculate the charge Q. Finally, we compare the two charges and, because there is going to be an attenuation of the signal, we can use the results of the comparison in order to calibrate our system. (For more detailed information and the corresponding calibration circuits, see IEC 60270, [14]).

Another important factor that must be taken into account is the background noise which originates from signals not arising from the device under test, or it could just be white noise from the measuring system, a radio broadcast, and ultimately any kind of continuous or impulsive systems. We can use two ways in accomplishing the noise cancellation: one is by visually detecting which parts of our signal are noise and set a threshold to cut them off. The other method would be to perform tests at zero voltage and when measuring peak-to-peak, detect the noise of the background.

Lastly, the procedures mentioned above prove not suitable for DC voltage. Although the same set up can be used as for AC, nonetheless there isn't a generally accepted way of measuring of PDs in DC. However, there is detection of PDs when the polarity of the current changes, but it is difficult to measure inception and extinction voltages. [14]

As mentioned the main device of measuring PDs during the tests was the CT. The integral parts of the test system are the ones described in the IEC 60270 standard. Before listing the various equipment that was used, it is wise to outline the development, methodology and preparations that took place before commencing the tests. A complete monitoring of the experimental equipment needed and the measurement set up inside the lab was recorded.

4.1.1 The scope

The main purpose of the tests and measurements was to set up an HV test stand with the use of the right equipment available in the lab, calibrate it, and then start the evaluation of coaxial cables and connectors: Samples that had already been used in various applications, as well as new samples, that had to be tested, modified and then tested again. The main value to be measured was the current and consequently the partial discharges in the cable.

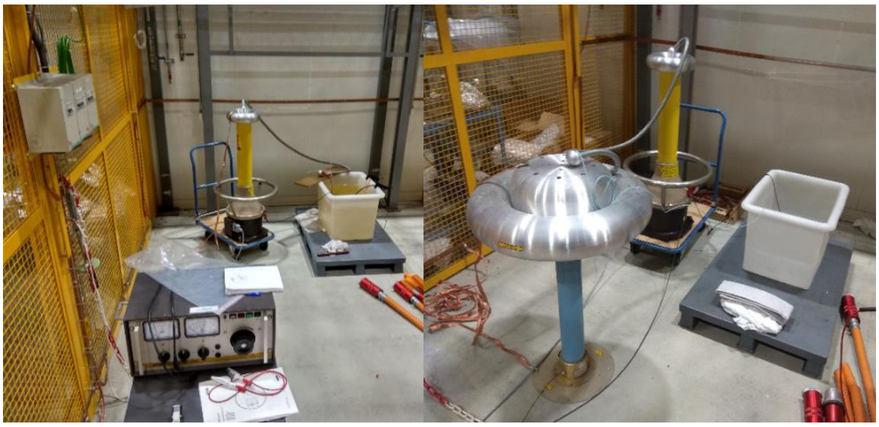

Fig. 32. “Jura 2”, the test-cage where the first tests took place

4.1.2 The Setup (Experimental Equipment, Place - Lab - Electrical Safety Lockout Steps)

In the first phase of tests, the test-cage that was used was the “Jura 2”, a 3x4m cage in the laboratory b.867, in the Prévessin CERN site. The room had to be prepared. That means that measurements of distances, which would be considered safe for the use of high voltage, were done, before arranging the HV equipment in the cage. In addition, along with the equipment needed, which was already available, there had to be some purchases according to the needs. The second phase of the experiments took place in a bigger test-cage, the “Saleve 6”, for higher voltage tests up to 96 kV.

Fig. 33. The ‘Saleve 6’ HV test cage in b.867

The instrument used as the AC high voltage power supply was the BAUR PGK 110 HB High Voltage testing set. It has the capability of reaching up to 94/126kV AC/DC. It consists of two main parts: (a) the operating unit (Fig. 34) with the indicating and operating elements, as well as the power supply and the safety devices and (b) the High Voltage unit (Fig. 35.), an oil filled housing with an HV transformer which transforms and the delivers the high voltage.

Fig. 35. BAUR PGK 110 operating unit

Fig. 34. The High Voltage unit

1.3 Technical Data

	PGK 70 HB	PGK 70 - 2,5 HB	PGK 110 HB	PGK 150 HB	PGK 260 HB	unit
Mains voltage	see type plate					V ~
Mains frequency	45 to 60	45 to 60	45 to 60	45 to 60	45 to 60	Hz
Power consumption at nominal working point	640	3200	1380	1380	2600	VA
Max. power consumption (in short-circuit operation)	1200	6500	2650	2650	5000	VA
Power output at nominal working point AC/DC	330/190	2750/1260	1260/495	990/530	1665/1000	VA/W
Max. output voltage ACeff/DC in no-load	56/78	56/78	94/126	110/160	185/260	kV
Output voltage ACeff/DC at nominal working point	47/66	55/62	90/108	110/137	185/250	kV
Max. output current ACeff/DC at short-circuit	20/12	117/84	30/17	23/20	20/20	mA
Accuracy of kV-meter	2,5	2,5	2,5	2,5	2,5	%
Accuracy of mA-meter	2,5	2,5	2,5	2,5	2,5	%
Dimensions of operating unit housing (W x H x D)	502 x 242 x 290	502x 242 x 290	502 x 242 x 290	502 x 242 x 290	502 x 242 x 290	mm
Dimensions of H.V. unit (height / diameter)	810/385	1130/455	1130/455	1450/455	2050/1270	mm
Weight of operating unit	13,5	22	17	17	19	kg
Weight of H.V. unit	27	93	75	85	260	kg
Relative humidity	not condensing					
Ambient temperature	working: 0...+45° C storage: -20...+60° C					

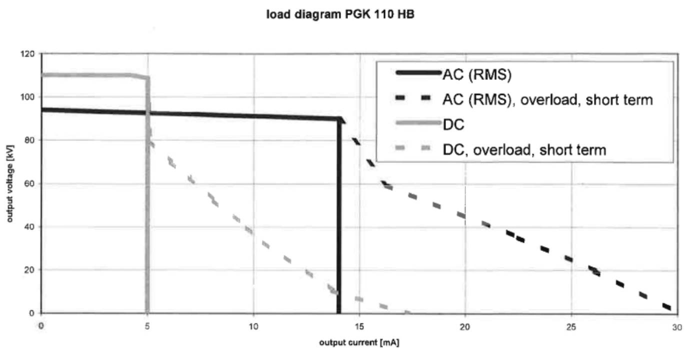

Fig. 36. Data sheet of the Baur PGK 110 HV test set. The load diagram shows that the maximum output current (AC) is 14mA.

For the DC tests up to 30 kV, the 30 kV Non-Destructive Insulation Tester Type JP 30 A by Danbridge Denmark was used (Fig.37).

Fig. 38. 30 kV Non-Destructive Insulation Tester

Fig. 37. 160 kV DC Power Supply

For test with voltages higher than 30 kV DC, a 160 kV power supply from the laboratory in b.867 was used (Fig. 38)

Fig. 39. The CT that was used during the experiments

The specific CT that was used, had a V/A ratio of 0.5 for 50 Ω termination, meaning that, e.g. when connected to a measuring device (i.e. an oscilloscope) and shows 1 millivolt, that corresponds to 2 milliampere. Nevertheless, in order to increase the sensitivity of the measurement we made several loops of the cable to be measured (primary winding of the CT), which meant that we had to divide the result by the number of the loops. For example, if we use 10 loops, as shown in fig. 39, then the measured value of the voltage at the oscilloscope has to be divided by 10.

It is manufactured by Bergoz Instrumentation, model number CT- F1.0 B, with a BNC termination connection for connecting it to the oscilloscope. The current model can measure 11 A RMS and 1 kA peak, and has lower cutoff frequency of 200 Hz and high cutoff 500 MHz.

The BNC cable that connected it to the scope had a 50 Ω impedance and for that it was terminated with a 50 Ω termination. As a measure of protection of the CT and the oscilloscope from high currents due to possible breakdown or other equipment failure, an extra grounding cable was added to the termination of the CT. Plus, for over-voltage protection of the scope a Spark gap of 90 Volts was added in parallel.

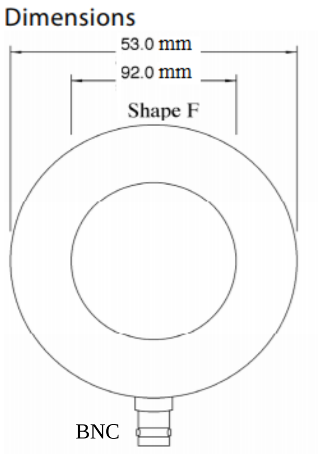

Fig. 40. Outline diagram of the CT

Fig. 41. The HV divider, with the toroidal conductor placed on top

The next device is the voltage divider (Fig. 41). Made by Ross Engineering Corp., it has a ratio of 1000:1 voltage division, a max input voltage of 240 kV DC (or peak AC), and it consists of a tube filled with pressurized SF_6 gas. It allows high accuracy measurements of very low PDs/corona for oscilloscopes and other sensitive electronic devices. On top of it, we specially adjusted a metallic toroidal. Placing it serves as a means of making the electric field more evenly distributed and homogeneous around the conductors of high voltage. Because of its round shape, it prevents the event of concentrating high electrical fields close to possible sharp edges, and thus helps avoiding electric arcs and unwanted breakdowns, PDs/corona.

Fig. 42. Specifications of the device

Because at CERN, safety comes always first, a specific operating procedure in which the experiments were conducted was followed. This procedure consists of six "electrical safety lock-out steps" that have to be followed every time an experiment has been carried out, and the cage door opens, to allow us to work with the equipment. These are:

1. Electrical separation of the installation from power supply sources
2. Locking in open position of disconnecting components – place warning sign
3. Identification of the installation concerned – consult the electrical diagram
4. Checking there is no voltage (VAT) – use voltage detector, check every conductor including neutral
5. Earthing and short-circuiting (HV-side) with equipment adapted to the voltage level
6. Additional measures: screens, marking out, etc.

There are also other specific requirements when operating HV equipment, like the distances one has to keep from the live parts of the equipment (Fig. 43). These are defined by the standard NF C 18-5 10, which sets the safety limits and zones around uninsulated parts, depending on the voltage range.

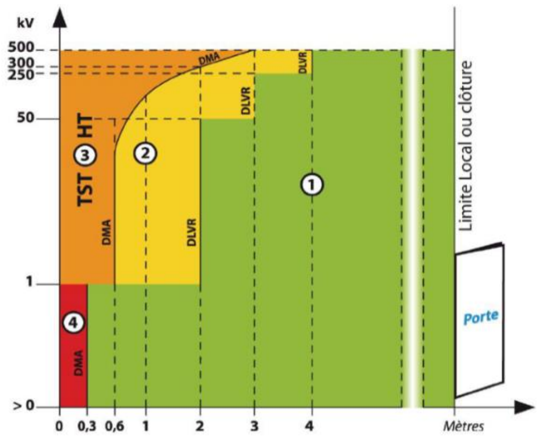

Légende :

Zone 1	zone de voisinage simple
Zone 2	zone de voisinage renforcé en haute tension
Zone 3	zone des travaux sous tension en haute tension
Zone 4	zone de voisinage renforcé en basse tension

NOTE La valeur 0 Volt est exclue de la figure.

Fig. 43. Safe working distances / vicinity area

Other parts of equipment that are needed for the proper function of the test cage were: The plastic tank where the cable samples and the conductors were submerged in insulating oil, connecting cables, signs with the electrical safety lock-out steps and the vicinity area, grounding braid cables, clips and pins, crocodiles, banana cables, gloves, cable ties, big clams, semi conductive and isolating tape, cable jacket stripping tool, saw, pence, pliers, grounding clips, and a grounding rod that would be used after every experiment for discharging the test subjects, which, after all, behave quite like capacitors.

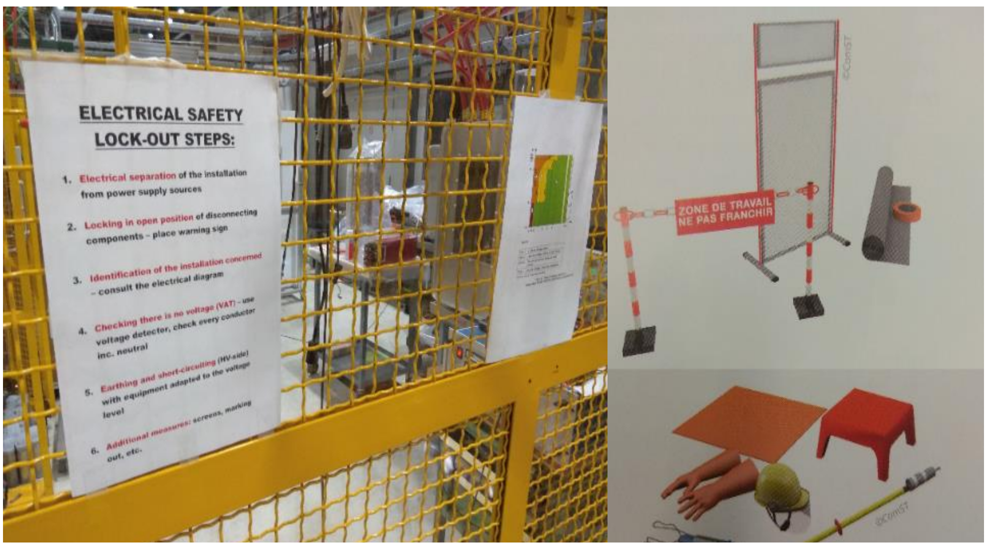

Fig. 44. Electrical safety measures

The electronic measuring device was the Tektronix TDS5054B Digital Phosphor Oscilloscope. It has a sampling rate of 2.5 MS/s. While taking precautions and making preparations for the tests, one aspect that had be taken into account was the magnitude of the voltage that the respective oscilloscope could measure without being damaged. A parallel resistance should be added each time according to the level of voltage to be measured. Moreover, a spark gap was a necessary option to insure that no excess voltage would destroy the device in case of overload or breakdown of the sample. On channel 1, the BNC cable coming from the voltage divider was connected, measuring the applied voltage. Then an appropriately designed resistance (voltage divider) was added in parallel to limit the incoming signal as to not exceed the limit of the channel of the scope. Also, on channel 3, there was the signal from the CT, measuring the current and subsequently showing the PDs when present. There, the 90 volts spark-gap was added as a protective device.

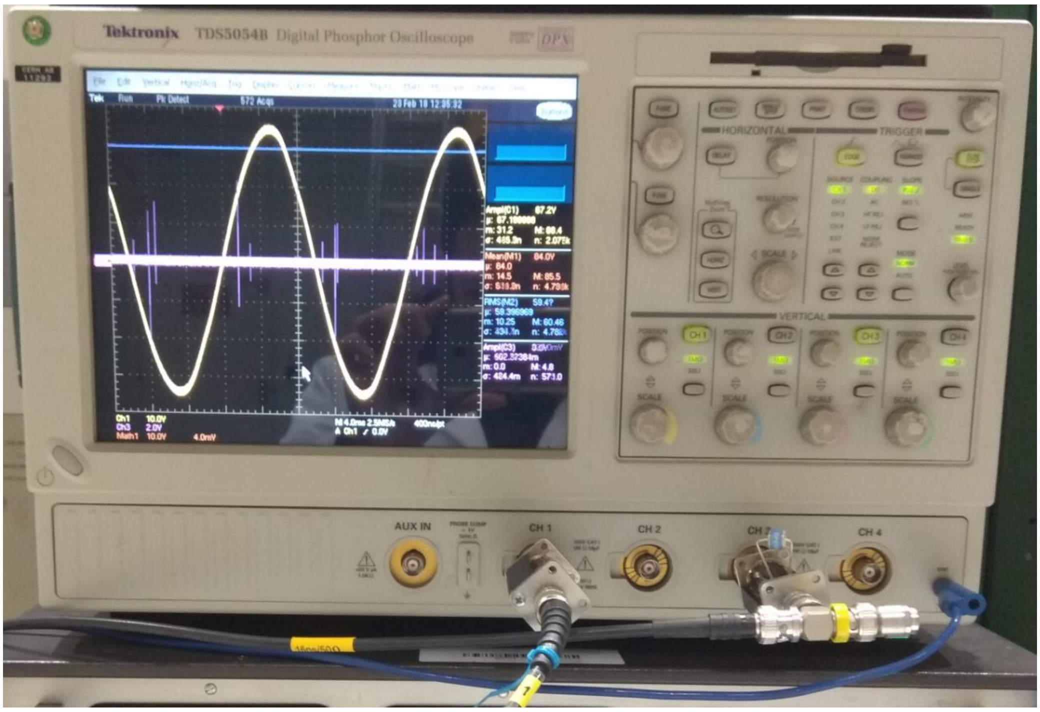

Fig. 45. The Tektronix oscilloscope

Another important figure that had to be calculated before the beginning of the tests was the maximum length (in meters) of the respective cable sample according to the maximum current that the HV power supply could deliver. According to the data sheets, from the load curve of the specific instrument, the maximum output current is 14mA (fig. 36). Due to the fact that we would have partial discharges during the tests, we had to reduce this value by 10%, so this means we should consider the max current to be 12.6mA. Therefore, for example, for an RG-220/U cable, which is of 93 pF capacitance per meter, at 90kV, 50Hz, the maximum length of the cable that could be tested without damaging the instrument, would be below 4.792m (fig. 46).

Max length of cable

$\omega := 2\cdot\pi\cdot(50Hz)$

$Imax := 12.6mA$

$U := 90kV$

$Cmax := \frac{Imax}{\omega\cdot U}$ $\quad Cmax = 445.634\cdot pF$

RG220 (2003) $\quad Co := 93\frac{pF}{m}$

$Lengthmax := \frac{Cmax}{Co}$ $\quad Lengthmax = 4.792\,m$

Fig. 46. Necessary calculations for determining the maximum length of the cable

4.1.3 The Procedure / Method / Model

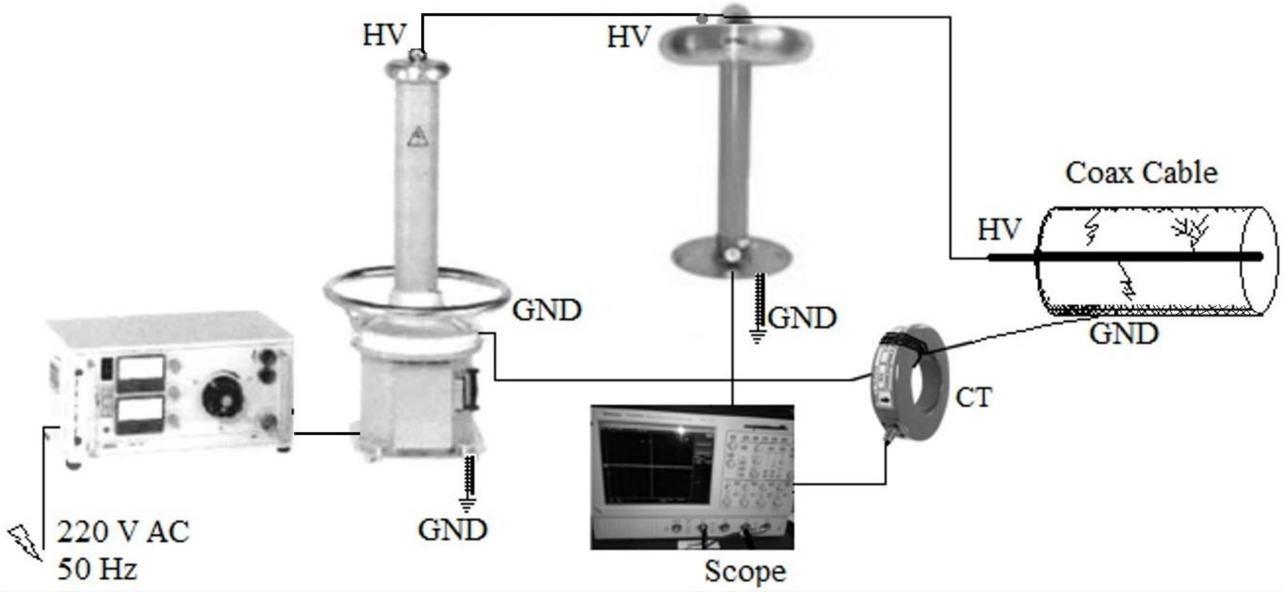

Fig. 47. Schematic diagram of the AC test circuit used for measuring partial discharges in the laboratory

The above figure (47) shows exactly the connectivity between the different electrical and electronic devices that were for measuring PDs in AC. Likewise, almost the same circuit was used for DC, replacing the AC HV power supply with the DC one.

The inducted current from the CT was transmitted as voltage via BNC cable to the oscilloscope, which represented the waveform of current. Similarly, the divided voltage from the voltage divider was transmitted to the scope which served in this case as an accurate voltmeter, and also provided the measurement for the voltage waveform.

With the gradual raise of the voltage, we were able to: measure the PD inception voltage, as well as the extinction, determine the breakdown voltage, and most importantly, measure the total PD charge, the PD count and the highest PD magnitude, with the help of the computer software ‘MATHCAD’ [18], where the results from the oscilloscope where processed.

Example of an AC test measurement processed with Mathcad and extraction of results:

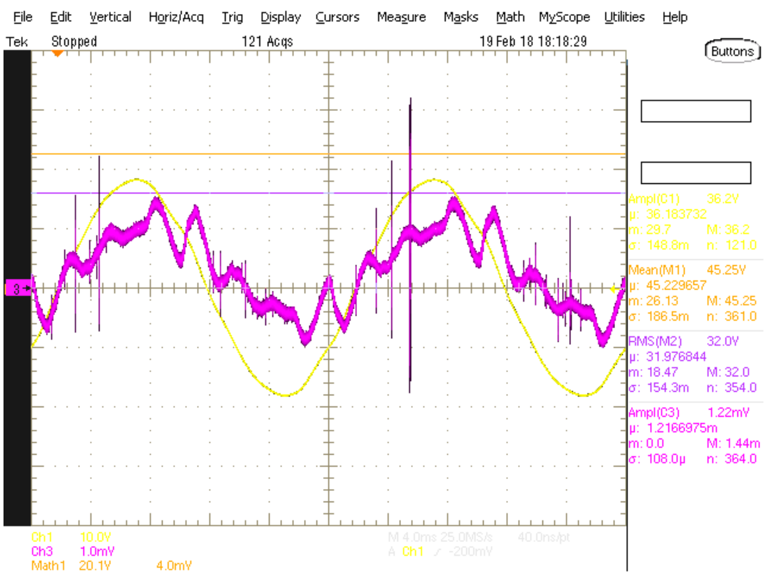

- This is an oscilloscope screenshot of the Heliflex cable with oil as dielectric.
- The yellow colour is the voltage (here = 45.25 kV peak).
- The purple waveform is the current.
- The ‘spikes’ (peaks) are the partial discharges in oil.

Calculate the PDs – with the help of Mathcad:

- Export the waveform of the current, from the oscilloscope, to a .csv file, then import it into Mathcad.
- The developed code uses the smoothing function and keeps only the peaks of the signal, while removing the rest of the waveform, along with the noise.
- Then it counts the number of spikes = #PDs
- And it integrates each peak (I) over time (t) to give the magnitude of each discharge (Q) and sums it to calculate the total charge of the PDs in one period.

So, from the scope, with a use of a USB stick, we import data to Mathcad. The waveforms of the current and voltage are represented in blue and red colour respectively:

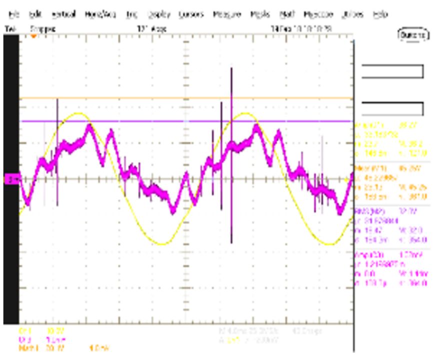

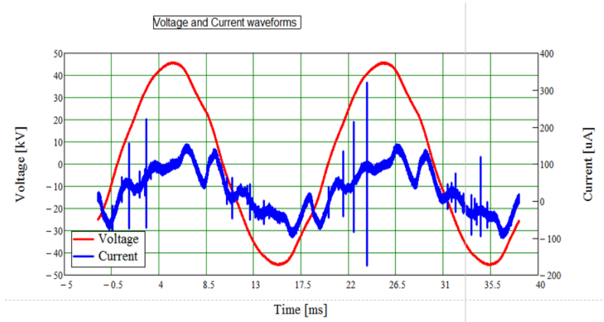

By using the smoothing function from Mathcad, and subtracting it from initial signal of the current, we can remove the low frequencies and leave only the peaks which represent the PDs:

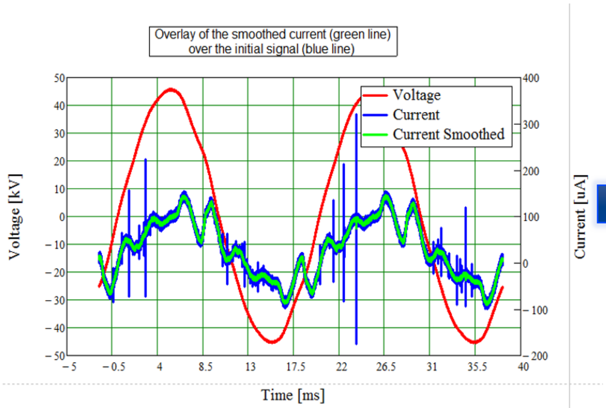

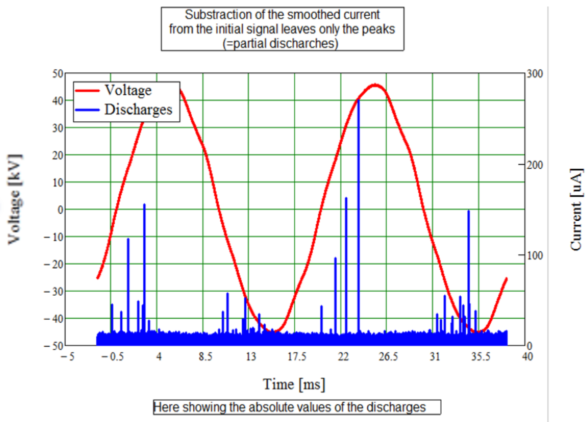

Note: Because different PD sources bring different PD patterns: Our pattern confirms indeed that the PDs originate from voids (gas bubbles – trapped air) in the dielectric.

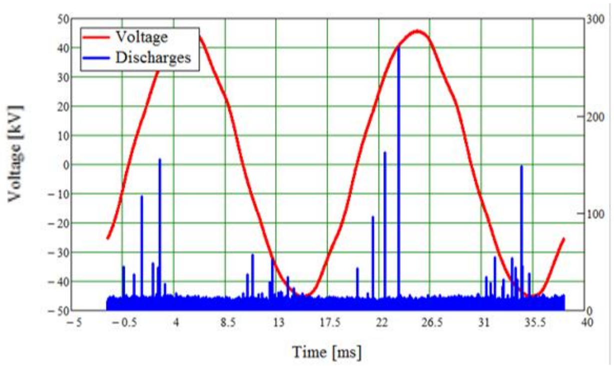

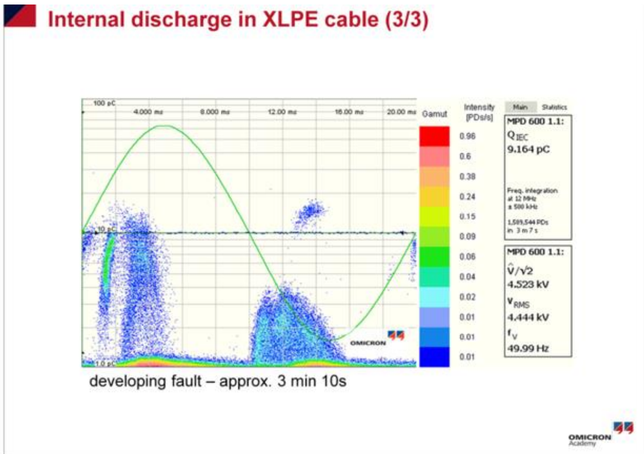

Omicron Academy, Training Material

If we zoom in to the Y axis, we can see that approximately below 15µA, is just noise. So we can set the threshold to that level. The program will cut off any signal is below that level.

$PD_{threshold} := 15 \cdot 10^{-6} A$

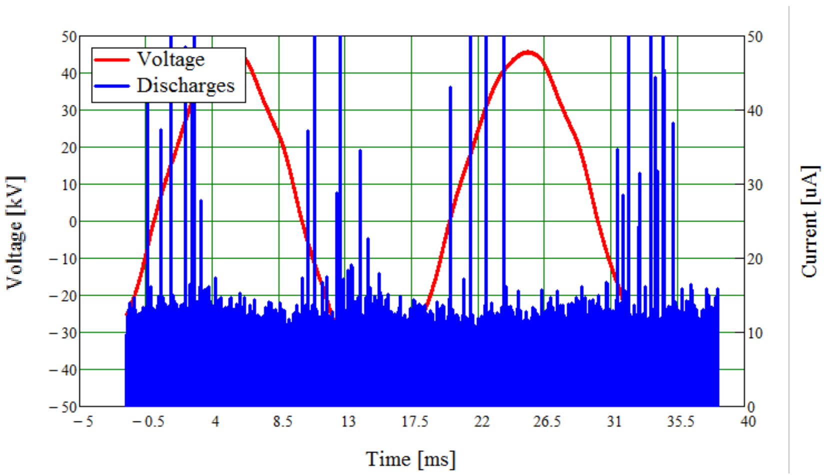

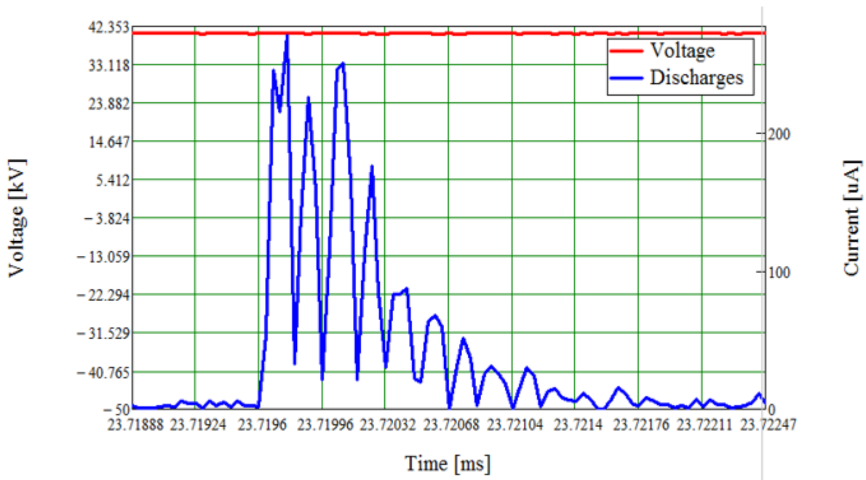

Finally, what is left from the initial signal is only the partial discharges. These are peaks of current. The program first counts the number of those peaks in one period and gives the PD count. Then it integrates the current I over time t, for each peak separately, and gives the charge q for each discharge. It can also state the value of the highest discharge, and finally sums all the discharges to give the total charge Q of the PDs in one period.

Results:

- Number of PDs: 125
- Total charge: 547.82 pC
- Highest discharge: 122.67 pC

Number of discharges:

$PD_{count} = 125$

Total charge:

$$Qpartialdischarges := \sum_{i=0}^{length(Q)-1} Q_i = 547.817 \cdot pC$$

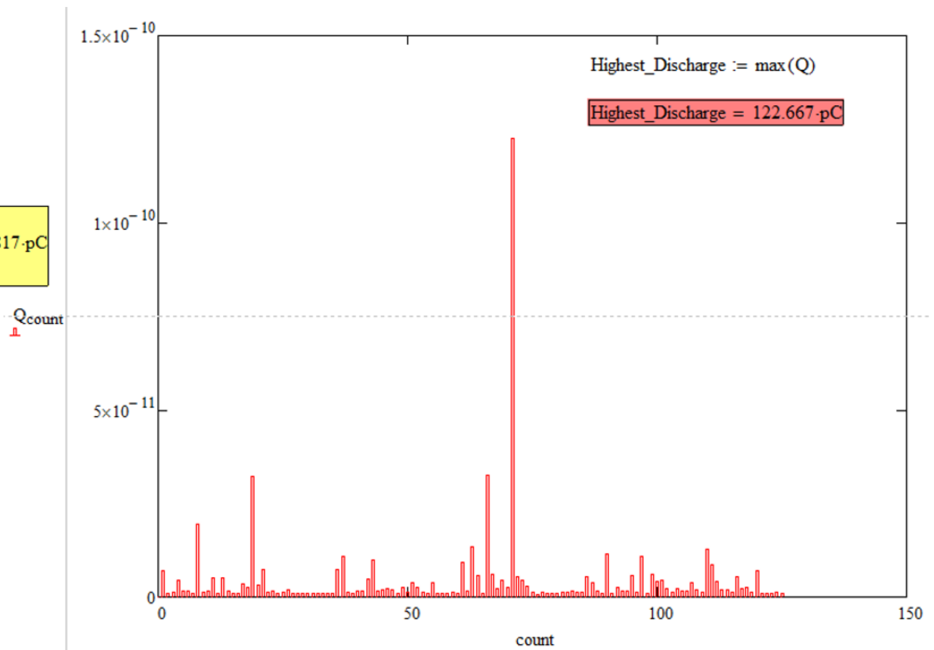

Note: Even though this particular example was for 2 periods, which means we should divide all values by 2, still it gives a good idea for future improvements, as to average over many periods for better results.

Correct values:
63 PDs, 273.91 pC, 61.34 pC

4.2 THE IMPEDANCE / ATTENUATION MEASUREMENTS EQUIPMENT

The device that was used for the measurements of the impedance and attenuation of the cable samples was the Agilent E5071C Vector Network Analyzer.

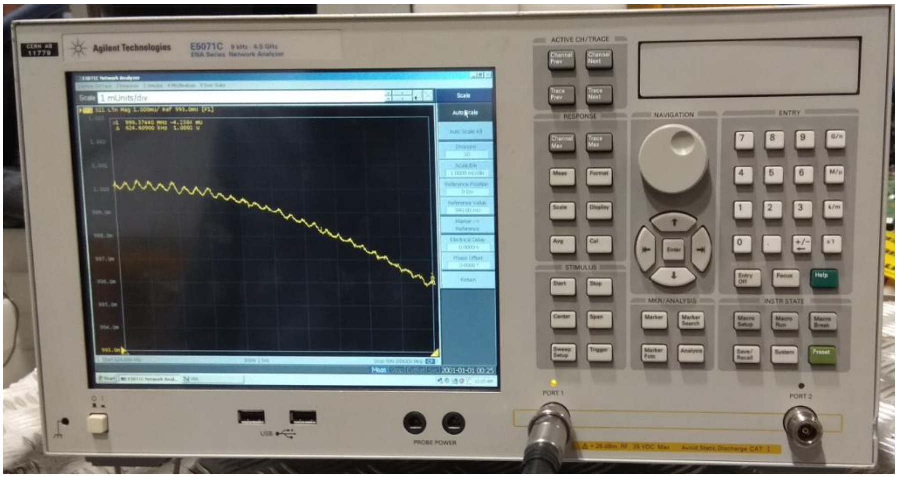

Fig. 48. Agilent E5071C Vector Network Analyzer

It is an instrument that measures the scatter parameters (S-parametres) of electrical networks. Out of the scatter parameters, transmission line attenuation can be derived. In addition, by using a Discrete Fourier Transformation of the S-parametres, information about the impedance and the length of the transmission line can be measured.

5. THEORETICALLY EVALUATED HIGH VOLTAGE COAXIAL CABLES

5.1 EVALUATION PROCESS OF THE CABLES

The cable samples under examination were varying from cables that have already been used at CERN for many years, to new prototypes, as well as new optimized models which were taken of the shelf (OTS) and were modified. More specifically, the cables were: (i) the specialized SF_6 (Sulphur hexafluoride) gas filled coaxial high voltage cable (Kabelwerke Brugg), (ii) the standard coaxial cable HCA118-50J Heliflex (RFS), (iii) the CLP50 (RG220/U) and (iv) the CLP30 new prototype (DRAKA), figures 49, 50, 51 and 52.

- *SF_6 cable*

The already mentioned Kabelwerke Brugg SF_6 coax cable: build in 1994, this cable has a corrugated copper outer conductor, and uses thin PE foils wrapped around the inner conductor, which they are pressurized with SF_6 gas. This has the major advantage that the gas fills all the voids inside the insulation, which means it provides superior dielectric strength. Also the cable has a lower velocity factor due to low density PE core. There have been no issues with surface discharge of spacers, usually used in large diameter air insulated coax cables. It is characterized by low attenuation/losses (~3dB/km at 10 MHz) due to large its large inner diameter and because it has no semiconducting layers. This cable has been in use at CERN since the 1990’s and there have been no issues so far.

It operates at nominal voltages up to 80 kV. It comes in many impedances, while in this study, the 26.3 Ω was

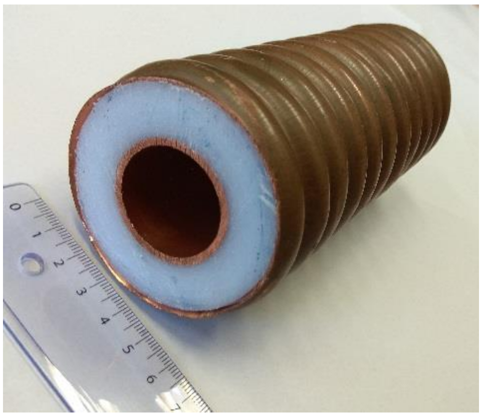

Fig. 49. The Kabelwerke Brugg SF_6 gas filled cable

examined. Its main disadvantages are: the fact that vacuum and SF_6 gas systems are needed; also special gas tight connectors (in house production) with slow disconnect. It is a relatively stiff and heavy cable (one pulse forming line weighs 2.6 tons) and most importantly, it not produced anymore [19], [20].

- *HCA118-50J Heliflex*

The main cable under test was the HCA118-50J HELIFLEX® 1-1/8", low loss air dielectric cable by RFS, Radio Frequency Systems, in 2012. It has a 12 mm diameter inner conductor, a corrugated copper outer conductor of 30.2 mm mean diameter, and in between a helical polyethylene spacer with a diameter of 27.2 mm. The RF peak voltage is quoted with 3.7 kV and the nominal impedance Z is 50 Ω. Due to the air dielectric, it has of course low attenuation benefits, however lower voltage strength and thus no direct use in our HV applications. The main idea of modifying it, will be extensively discussed later on here.

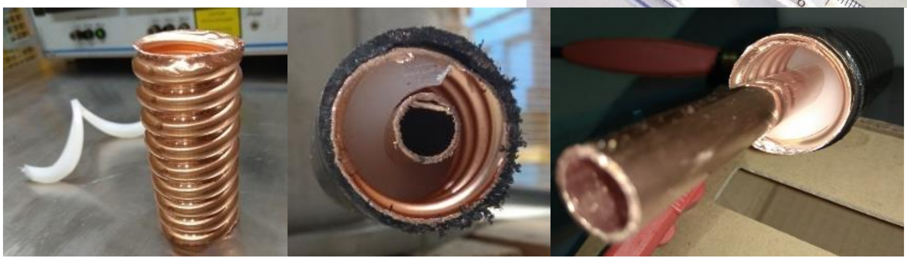

Fig. 50. The RFS HCA118-50J Heliflex

- *CLP50*

The “workhorse” at CERN. It is an improved RG-220/U coaxial cable by DRAKA Cable Company. It has a 50 Ω impedance and has no semiconductor layer. It is compliant with CERN IS23, and factory tested, at 35kV RMS. At CERN it is used for operational voltages up to 40kV pulsed, and more than 32 km of it are in use. It can be used with LEMO and in house made connectors. It has a “regular” consumption due to the often exchange of irradiated cables in critical systems. [19]

- *CLP30*

The new CLP30 prototype from Draka has an impedance of 30 Ω, also no semiconducting layer, low attenuation and a good BDV (48 kV RMS) with respect to the RG220 type cables. It has a potential for future optimization towards higher operational voltages. CERN could profit from its low attenuation and higher BDV, as an SF_6 cable replacement solution.

Fig. 51. The DRAKA CLP50

Fig. 52. The DRAKA new CLP30

TABLE III: Structure properties of the four cables under examination

		Material, ø:diameter, (width)		
Cable / Data Specs	***manufacturer***	***inner conductor***	***insulation***	***outer conductor***
SF_6	Brugg	copper tube, ø: 30/34 mm (2mm)	LDPE-tape, ø: 34/61.2 mm (13.6mm)	corrugated copper, ø: 61.35/68.47mm (1.15mm)
Heliflex	RFS	copper tube, ø: 12 mm (0.8mm)	helical PE spacer, ø: 27.2 mm	corrugated copper, ø: 33.2mm
CLP50	DRAKA	bare copper wire, ø: 6.66 ± 0.02 mm	PE, ø: 23.1 ± 0.2 mm	bare copper braid, ø: 24.2 ± 0.4 mm
CLP30	DRAKA	bare copper tube, ø: 15mm (1.5 mm)	PE, ø: 32.0 ± 0.2 mm	bare copper braid, ø: 33.1 ± 0.4 mm

5.2 PLANNING THE EXPERIMENTS

The main task at hand was replacing the air-dielectric of the Heliflex with electrical insulating oil, in order to introduce it as a substitute of the SF_6 gas filled cable. The upgraded cable was expected to reach a higher peak voltage whilst having also less partial discharges.

The strategy was to confirm the feasibility of this approach by a quick and efficient evaluation of the cable with standard equipment. Therefore, a small-scale model to reduce the required voltage and ease the handling was established. This model was characterized by measurements of partial discharge inception voltage, break down voltage (AC and DC) and the impedance both in air and in oil. These results together with simulations and analytic calculations allowed to initially decide if the basic requirements for a possible replacement of the 80 kV SF_6 cables are fulfilled.

A simple, user-friendly and cost effective method to measure partial discharges was set up. It consists of a high voltage generator, a voltage divider, a current transformer, an oscilloscope and a tank of oil where the cable sample was tested.

The first tests were made to evaluate the prototype cable as delivered, without any modifications, hence with air as dielectric. Measurements were taken in AC and DC, PD inception was determined, and the impedance was verified. The same tests were then repeated using electrical insulating oil as dielectric.

In addition, numerical simulations of the different cables and options have been performed using OPERA v18R2 [20]. Finally, the measurements of the impedance of the cable, along a certain length of it, were carried out.

5.3 THE OIL USED

The oil used for subsequent tests was BLUESIL™ FLUID 47 V 20 [21], a type of silicone oil which is commonly used as an electrical insulator. It is a low viscosity polydimethylsiloxanic fluid, whose relative dielectric constant (ε_r) is 2.7 and the nominal dielectric strength is 14.0 kV/mm.

5.4 ANALYTIC CALCULATIONS – THEORETICAL PREDICTIONS

5.4.1 Characteristic impedance Z_0 calculations

From (8), using the dimensions of the cable and the relative permittivity ε_r of the insulation we can calculate the impedance Z_0 of each cable. The values of the constants are $\mu = 4\pi \cdot 10^{-7}$ H/m (copper), and $\varepsilon_0 = 8.85 \cdot 10^{-12}$ F/m for vacuum.

- *Kabelwerke Brugg SF_6 Cable*

The relative dielectric constant ε_r of the combined media (PE with pressurized SF_6) is given in the cable datasheet at ~2.2 [22]. Using (8), we obtain:

$Z_0 = 26.146\ \Omega$

- *Heliflex HCA118-50J*

The datasheet does not provide the ε_r of the combination or air and the PE spacer. However, it mentions: $L_0 = 0.183$ µH/m and $C_0 = 73$ pF/m. By using (2), we obtain:

$Z_0 = 50.068\ \Omega$

If we use (8), we can then calculate the ε_r of the Heliflex cable:

$\varepsilon_r = 1.222$

- *CLP50*

We have the specific dimensions of the cable and the ε_r of the insulation. The common RG-220/U cables use as insulation material the LE6006, low loss LDPE compound for coaxial cables, which has a dielectric constant of 2.29 (at 1 MHz). From (8), we get:

$Z_0 = 51.133\ \Omega$

- *CLP30*

Again, knowing the dimensions and the $\varepsilon_r = 2.29$, we obtain:

$Z_0 = 31.367\ \Omega$

5.4.2 Electric field *E* calculations

One very important aspect of coaxial cable transmission lines is the voltage holding which they can undergo. High electric field quantities are obviously observed close to the inner conductor. These high fields usually create the “unwanted” PDs and corona, hence the need to keep them as low as possible. But high voltage is not the only one responsible for these high fields. As mentioned earlier, the shape of the conductors, the sharp edges and, most importantly, the cracks and voids in the insulation or even between the insulation and the conductor, are also factors.

All of the above can and will be referred to from now on as the “weak points” of the cable, that is, points (small areas around them) that can potentially create such high fields that can cause PDs or even total breakdowns. However, one special category of weak points inside a coaxial cable are the so-called “triple points” of the cable. They are not referring to water. A ‘triple point’ is called the junction of metal, dielectric and vacuum. These spots inside a cable, and the area surrounding them, give exceptionally high electric field values, and, together with the sharp edges of the conductors, they are absolute candidate spots for creating partial discharges, flashovers and breakdowns. In the case of our cables we have air instead of vacuum, or oil, and SF_6 gas. So, the triple points may give possibly the highest electric fields, according to analytical calculations, which will later be confirmed by FEM simulations.

As shown in (2), when h_1 goes to zero, E_1 acquires its highest value:

$$E_1(h_1) = \frac{V}{(h_1 + h_2)\cdot\left(\frac{\varepsilon_1}{\varepsilon_2} + 1\right)} \tag{10}$$

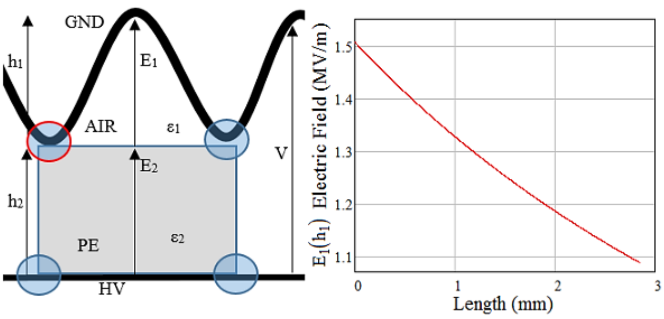

Fig. 53. (Left) Illustration of ‘triple points’ and (right) the graph of the electric field around the area of one point

where $E_1(h_1)$ is the electric strength in air, V the applied voltage, while h_1, ε_1 and h_2, ε_2 are distances and dielectric constants inside the air gap and the PE, respectively, as shown in Fig. 53.

- *Simple cylindrical coaxial geometries*

The electric strength E_x is depended on the applied voltage and the dimensions of the coaxial line. When located at a distance r_x, ($D_1/2 < r_x < D_2/2$), from the cable axis, it is given by [4]:

$$E_x = \frac{V}{r_x \ln\frac{D_2}{D_1}}, \tag{11}$$

where V is the voltage between the conductors.

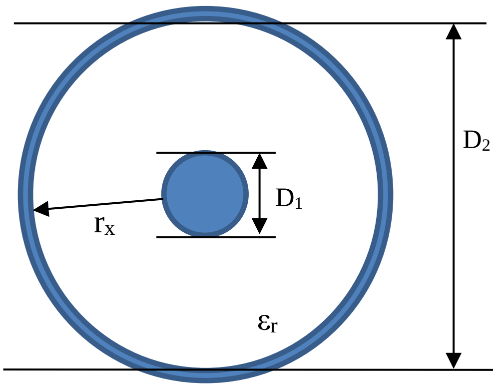

Fig. 54. Cross-section of the cable

As expected, the highest value of E_x is when $r_x = D_1/2$ and the lowest is when $r_x = D_2/2$.

- *CLP50*

Using (11), for the simple coaxial geometry of the CLP50 cable, and for the operating voltage of the 40 kV, we get:

E_{max} = 9.31 kV/mm

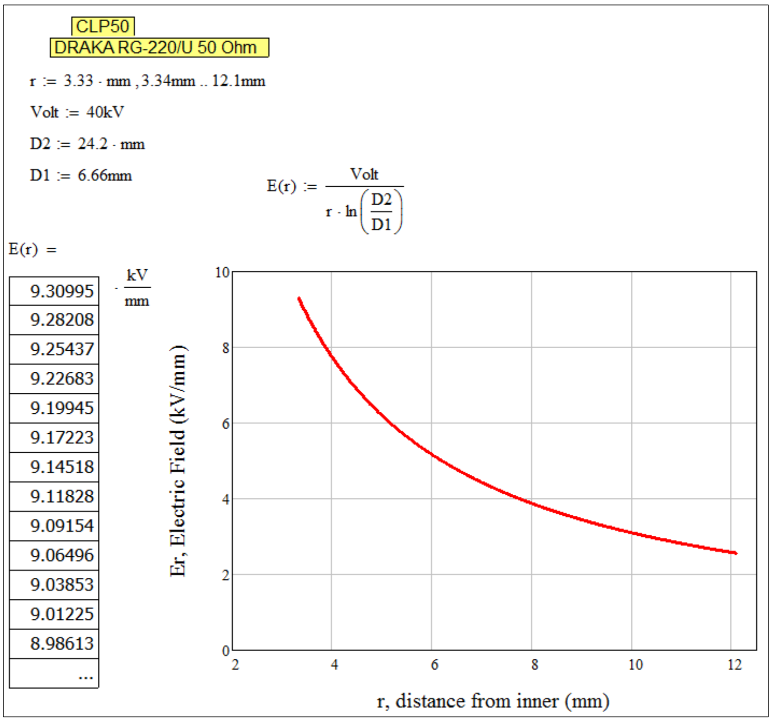

Fig. 55. Mathcad calculations and graph of the electric field inside the CLP50 cable

- *CLP30*

Using (11), for the CLP30 cable, at 40 kV, we obtain:

E_{max} = 6.74 kV/mm

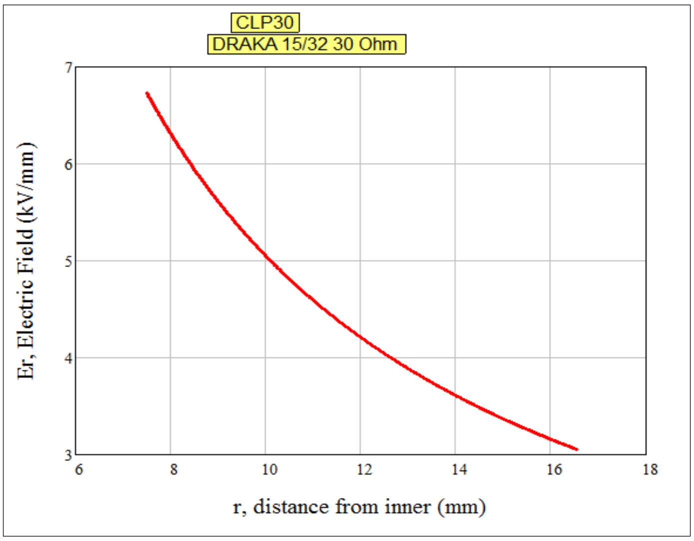

Fig. 56. Mathcad calculations and graph of the electric field inside the CLP30 cable

- *More complex coaxial geometries*

The geometrical shapes of both the Brugg SF_6 and the RFS Heliflex are more compound in their structure, especially due to the fact that the outer conductor is corrugated in both of the cables. The corrugation (although needed for such bulky structures) is useful for the flexibility of the cables, but not for the voltage holding. It is needed when bending a cable of that size, in order not to deform the copper. However, because of it, the PE does not fit smoothly to the copper in both cables, leaving areas surrounding the triple points that create high fields, subsequently showing PDs and lower BDV.

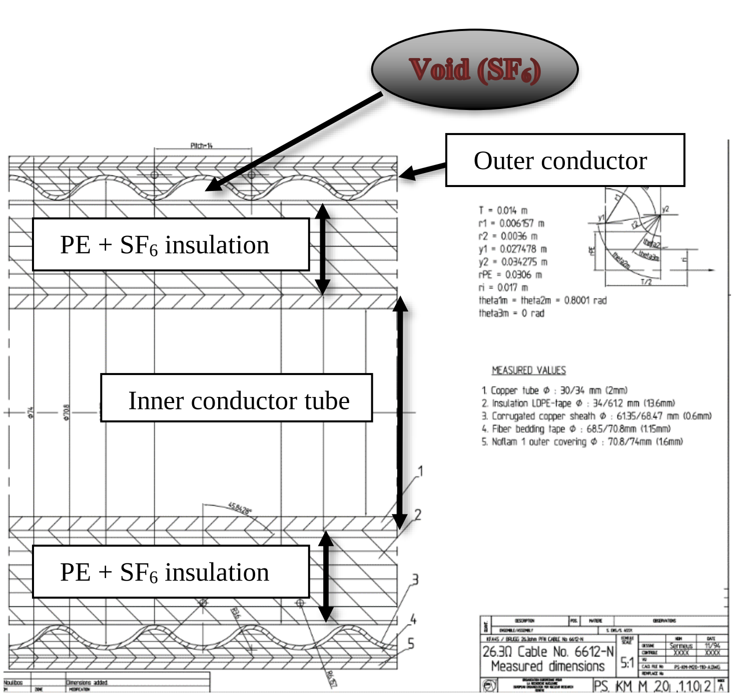

Fig. 57. Design printout of the 26.3 Ω Brugg SF_6 cable

- *SF_6 cable*

In fig. 57 it is clearly shown that the geometry of the cable allows the existence of triple points, because of the presence of voids filled with SF_6, between the insulation and the outer conductor. This is exhibited more vividly in the next figure (58). With its help, we will try to explain why electric field strength acquires such high values around triple points, two of which are depicted in blue circles.

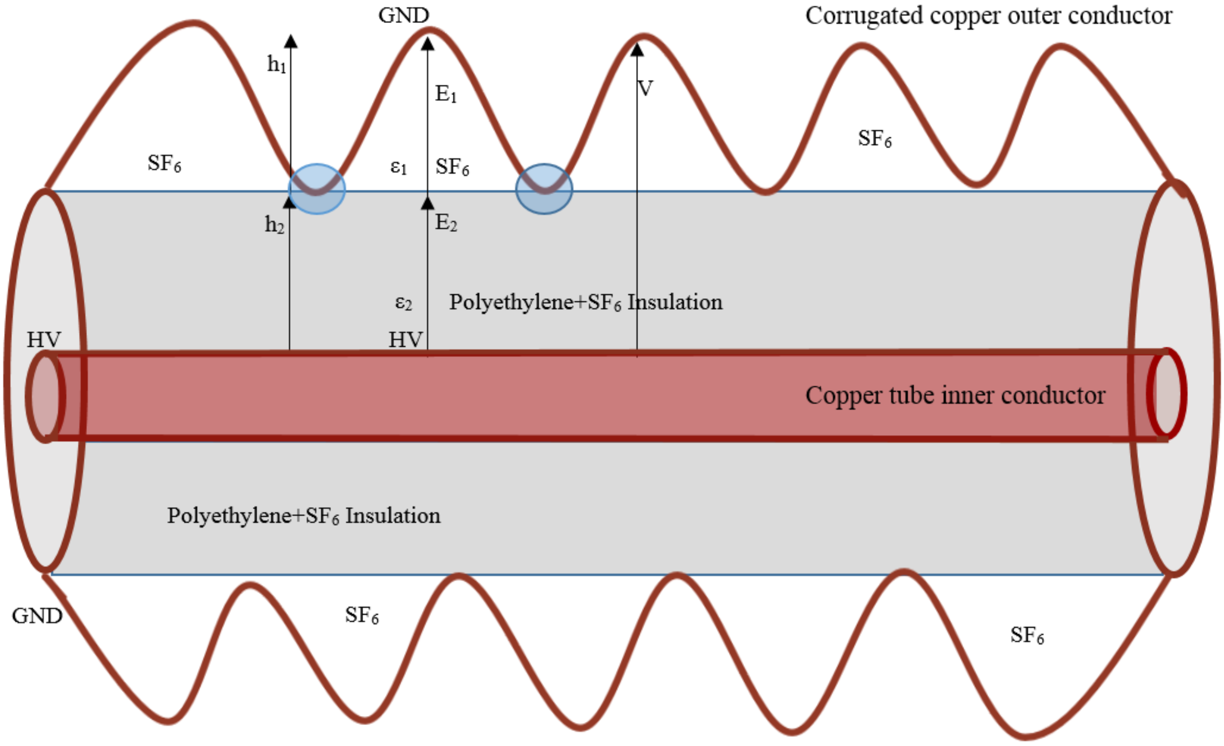

Fig. 58. Schematic representation of the inside of an SF_6 gas filled coax cable (not in scale)

Here, the triple point consists of three different materials with dielectric constants: $\varepsilon_1 = 1.00204$ for SF_6 gas, $\varepsilon_2 = 2.17$ from the mixture of polyethylene pressurized with SF_6, and finally the outer conductor which is made of copper. Since it was not possible to calculate the exact value of the E-field close to the triple point, we calculate it in the middle of the 'arc' of the void. From the simplified schematic in fig. 59, given that the applied voltage is 80 kV, we can derive the following:

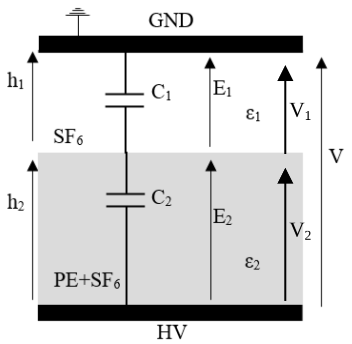

Fig. 59. The above schematic, simplified

From the schematic we get:

$$\frac{C_1}{C_2} = \frac{V_2}{V_1}$$

$$C_1 = \varepsilon_0 \cdot \varepsilon_1 \cdot \frac{A}{h_1} \quad , \quad C_2 = \varepsilon_0 \cdot \varepsilon_2 \cdot \frac{A}{h_2}$$

Turns out: $V_1 = 15.189$ kV, $V_2 = 64.811$ kV

Hence, $E_1 = V_1 / (h_1 \cdot \ln(D_2/D_1)) = 7{,}520{,}172.9$ V/m = 7.52 MV/m

And $E_2 = 3{,}472{,}815.8$ V/m = 3.47 MV/m

$\mathbf{E_{total} = 10.99}$ **MV/m**

- *Heliflex*

The exact equivalent phenomenon is observed in the Heliflex cable. Here, instead of SF_6 gas, we have air as a dielectric with $\varepsilon_r \approx 1$. The polyethylene helical spacer creates triple points (fig. 60) where it touches the corrugated outer copper conductor.

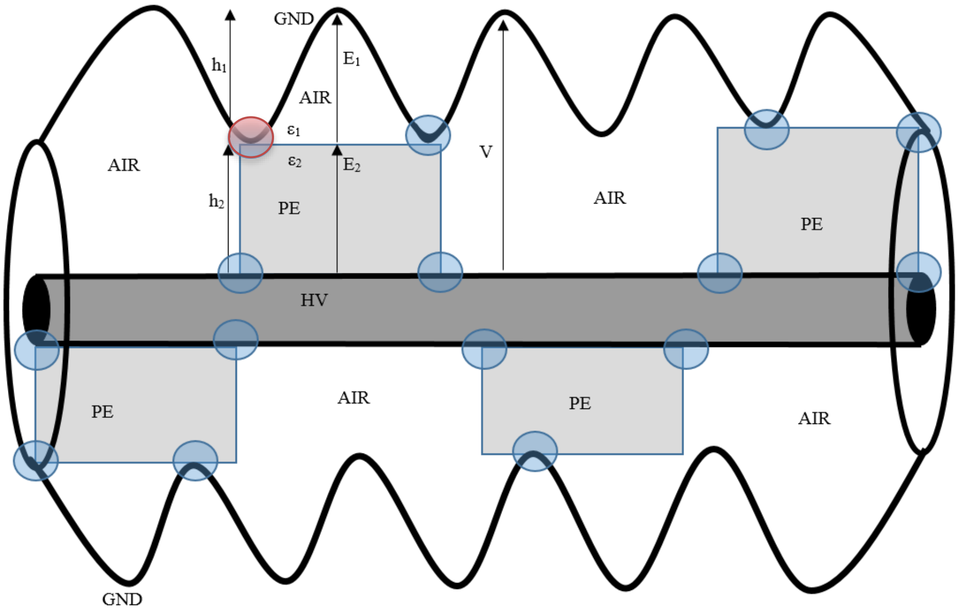

Fig. 60. Schematic diagram of the Heliflex cable, showing the weak (triple) points

In Fig. 60, in the area near the triple point (in red), as we get closer to it, h_1 goes to zero, thus E_1 acquires its higher value, which, according to our calculations is **1.505 kV/mm**, given that we apply a voltage of 16 kV (as we will later find out in the HV tests, little more than 16 kV was the BDV of the standard Heliflex). If we then add E_2, this results in a total E_{max} electric field strength for the Heliflex. Of course this is merely an approximation, because it is nearly impossible to calculate the actual E-field near the triple point, due to the complexity of the geometry of the cable. This why we will later use the simulations, to correctly calculate these values.

E_{max} = 3.667 kV/mm.

$$E1(h1) := \frac{HV}{(h1 + h2)\cdot\left(\frac{\varepsilon 1}{\varepsilon 2} + 1\right)}$$

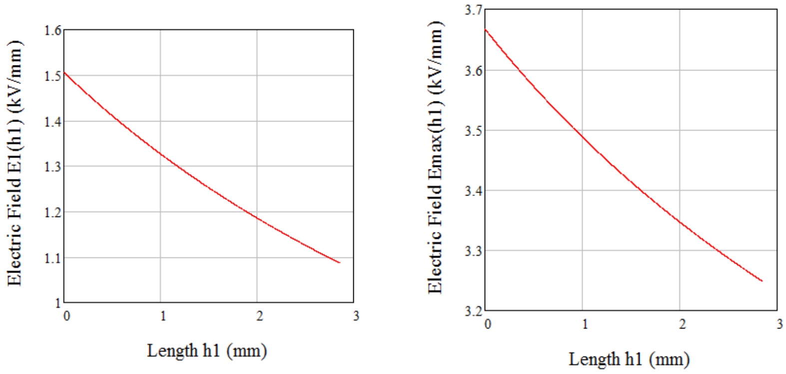

Fig. 61. E-field for the Heliflex, close to a triple point (left), total (right)

What's left now to do is to simulate the cables under the same voltages and compare the E-field values calculated here, with the results from Opera. This will be done later in the Simulations chapter (7).

5.4.3 OTHER CALCULATIONS

By using the analytical formulas from the corresponding bibliography [4], [5], we can calculate the capacitance (C_0), inductance (L_0), active resistance (R_0) and the conductivity (G_0) per unit length of the cable, plus the attenuation (α), for a frequency of 50 MHz. This was done for the standard air-dielectric cable, the modified one filled with oil (we hypothesized εr=2.7), and the 26.3 **Ω** SF_6 cable, as seen in Table IV. The attenuation and the losses are compared in Fig. 62. They are important factors for selecting the correct HV coaxial cable, since the applications that these cables are used in, are within the high frequency range, typically operating at several tens or hundreds of megahertz [24]. Other electrical specifications were drawn from the equivalent data sheet of each cable and are presented for comparison.

TABLE IV
ELECTRICAL SPECIFICATIONS OF THE CABLES FROM DATA SHEET, ANALYTICAL CALCULATIONS AND THEORETICAL PREDICTIONS (**50 MHZ**, UNLESS MENTIONED OTHERWISE)

a/a	Data Sheet				Theoretical calculations	
Type of cable	*SF_6 Cable*	*CLP50*	CLP30 @30MHz	*Standard Heliflex*		*Modified Heliflex*
ε_r	2.2	2.3	2.3	-	1.2	2.7
Zo (Ω)	26.3	50 +/- 1%	30.9	50 +/- 0.5	50.9	33.7
Co (pF/m)	189.8	100	165.2	73	73.9	162.5
Lo (μH/m)	0.129	0.26	-	0.183	0.185	0.185
Ro (Ω/km)	26.5	1.54	1.03	-	68.9	68.9
Go [1/(MΩ·km)]	$9.42 \cdot 10^3$	10^4	10^4	-	0	$5.41 \cdot 10^3$
α (dB/km)	5.5	13	9.9	6.4	6.0	9.7

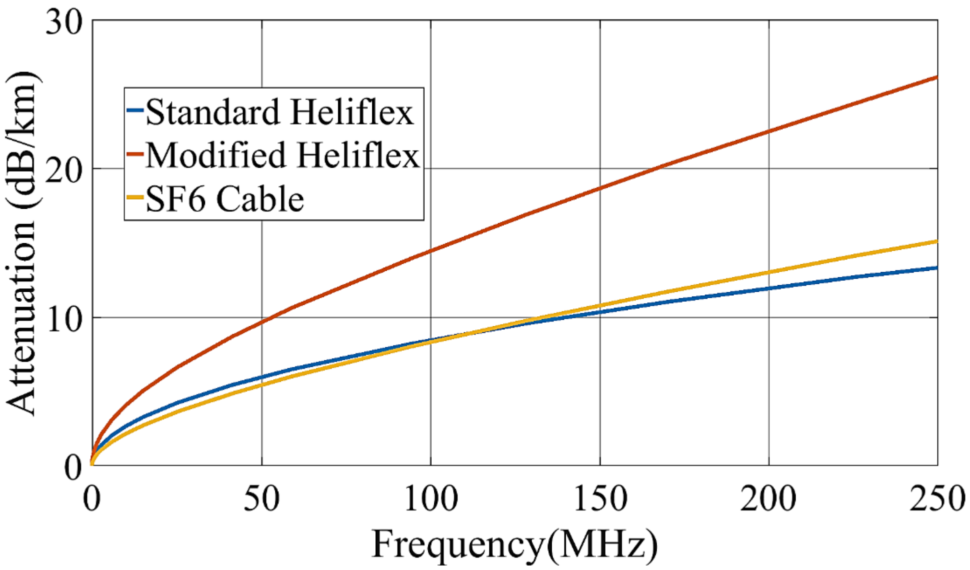

Fig. 62. Theoretical comparison of the attenuation over frequency

6. TESTS AND MEASUREMENTS

6.1 PARTIAL DISCHARGES AND BREAKDOWN VOLTAGE

The equipment available in the laboratory allowed to setup a simple, user friendly, low cost measurement system for measuring partial discharges in cables under high voltage. Also, it helped to determine the breakdown voltage (peak voltage) of the cables. The samples that went under examination were: (a) cables that are already in use at CERN in many applications; the RG-220/U and the HTC-50-5-1, (b) the standard, off-the-shelf, Heliflex cable, (c) the modified oil-filled Heliflex, along with some variations in the design in order to optimize its performance, and (d) the corresponding Spinner connector for the Heliflex. The multiple series of tests included AC and DC high voltage measurements of partial discharges, corona, and finding the inception, extinction and breakdown voltages of each cable.

6.1.1 RFS HELIFLEX STANDARD –AIR DIELECTRIC

The main interest in the project was to confirm the possibility of using an oil filled cable as a replacement for the SF_6 filled one. Various tests were conducted in the laboratory for that purpose. The first tests concerned the standard OTS Heliflex cable that uses air as dielectric. The goal was to measure its breakdown voltage in both DC and AC. It was not expected to be high enough since it’s not made for HV applications.

- DC test

Initially the tests were conducted on DC voltage, on a 3 m Heliflex cable sample, having its two ends in oil, in order to avoid any electrical arching or breakdown due to the non-usage of cable terminations. Cable terminations play a very important role in high voltage cable measurements, because they ensure due to their structure that no partial discharges or corona, originate from the cable ends.

Using the 30 kV Non-Destructive Insulation Tester we carried out the first tests in DC. The breakdown voltage (BDV) was measured at **18 kV** during the 1st test and at **20 kV** during the 2nd measurement.

- AC test

Afterwards a test was conducted on AC voltage, on the same 3 m Heliflex cable sample, having its two ends in oil. The results from the PDs are shown below.

kV peak	#PDs	total Q (nC)	highest discharge (nC)
2.114	277	19817	118.44

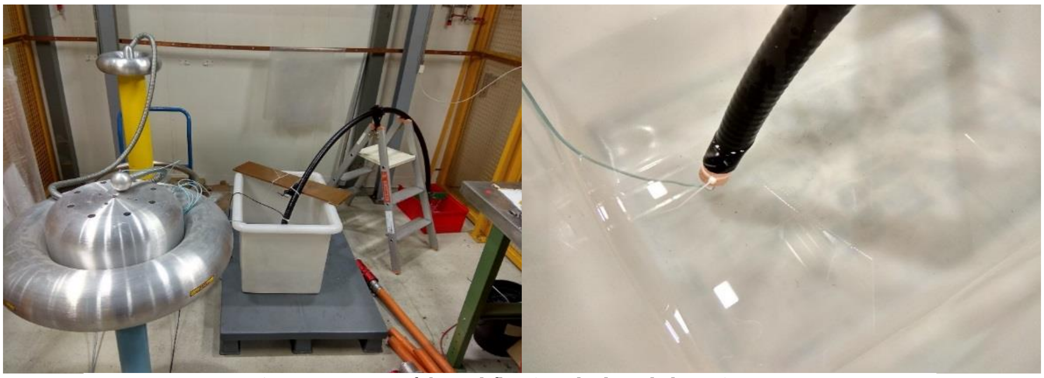

Fig. 63. First test of the Heliflex (standard air-dielectric), AC

Subsequently, a 20 cm sample was prepared and used for DC measurements, in air. The temperature inside the laboratory was 20 ^{o}C and the relative humidity was 28.2%. Because the sample had no cable terminations, the two ends of the outer conductor had plenty of sharp edges, which can be responsible for electrical arching between the conductors, flashovers and lower breakdown voltages. This is due to the fact that sharp, pointy and not smooth metallic parts, tend to accumulate strong electric fields, as the electric field lines there get really dense.

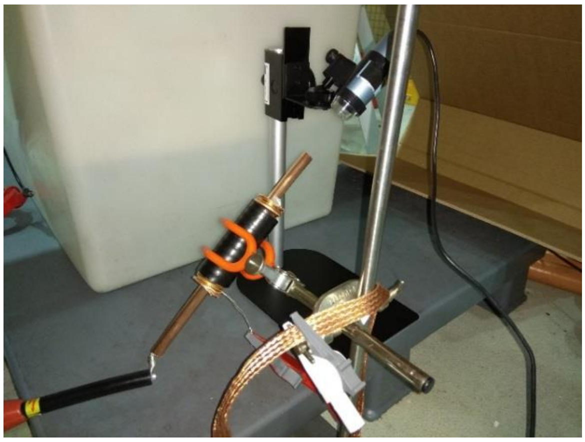

Fig. 64. **a** (upper left). **b** (upper right). **c** (bottom left): The set-up for recording breakdowns in DC

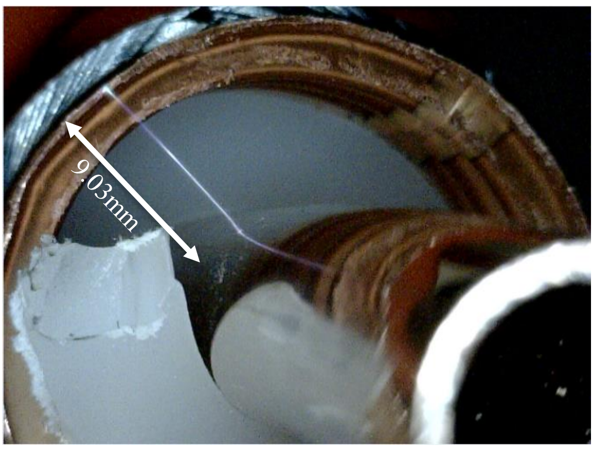

Fig. 65. An electric arc during a breakdown in air

BDV: 17.5 kV

Electric field:
17.5 kV / 9.03 mm
=1.95 kV/mm

Figure 65 depicts an electric arc during a breakdown in air. It was taken using a Dino-Lite Digital Microscope [24] connected to a laptop that was recording. If closely observed, one can see that it originates from a very sharp edge of the outer conductor, due to the fact that no cable terminations were used, and, although it was cut with a wheel and was polished and with a Dremel, it still had sharp edges that attracted such electric fields, high enough to break the air at approximately 1.95 kV/mm, much less than 3 kV/mm (BDV of air).

A way to optimize the design and thus have better results, was to try to avoid the very sharp edges and scratches at the ends of the cable. For that reason, two smooth copper rings were mounted to evenly distribute the electric field lines, in order to avoid sparks and electric arcs between the inner and the outer conductor.

6.1.2 RFS HELIFLEX MODIFIED – OIL DIELECTRIC

- DC tests

Following this, new DC tests were done, both in air and in oil. The tank was filled with the Bluesil oil, and because the 30 kV tester did not cause a breakdown, the 160 kV DC Power Supply was used.
Table V shows the initial results.

TABLE V
FIRST TESTS IN DC – IN AIR AND IN OIL

No.	Dielectric	Corona Rings	BDV [kV]
1	Air	None	17.95
2	Air	None	17.71
3	Air	None	17.28
4	Air	None	17.45
5	Air	1	17.89
6	Air	1	17.86
7	Air	1	17.47
8	Air	2	17.62
9	Air	2	18.33
10	Air	2	15.98
11	Oil	2	37
12	Oil	2	39

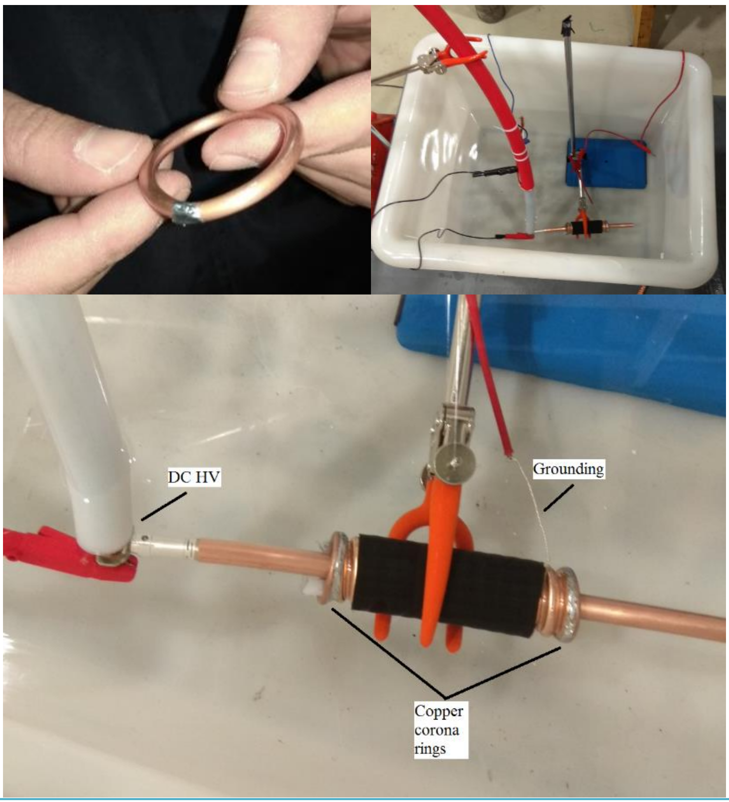

Fig. 66. HV DC tests in oil with soldered corona rings

For the tests in oil, the cable sample was fully submerged into the oil tank and all air bubbles left inside the cable were carefully removed before measurements were taken at different voltages. From these first results, one cannot say with certainty whether the small corona rings that were soldered to the two ends of the outer conductor, helped indeed to improve the breakdown voltage. What is sure though, from a first point of view is that due to the insulating oil, the BDV was increased at least by a factor of 2.

- AC tests

The next step was to conduct AC (50 Hz), HV measurements, in oil, on the same 20cm Heliflex sample, fully submerged in oil. Using the test circuit of fig. 47 we were able to measure the PD inception voltage, PD charge and count, along with the breakdown voltage. Again we had to make sure that all air bubbles were carefully removed from inside the cable. The results from the oscilloscope were processed with the help of Mathcad.

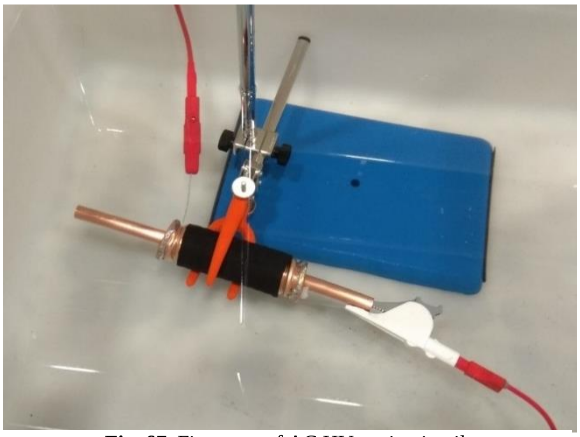

Fig. 67. First tests of AC HV testing in oil

First tests of AC HV testing in oil:

- Heliflex 20 cm
- AC, 50 Hz
- In oil dielectric
- 2 rings soldered

During these tests, no breakdown was observed.

TABLE VI
FIRST RESULTS OF AC HV TESTING IN OIL

kV (Peak)	#PDs	Total (nC)	Highest (nC)
19	0	0	0
30	7	0.469	0.125
38	3	0.157	0.058
42.9	11	31.13	26.47
43.05	6	30.61	25.47
43.03	10	24.05	18.16

More tests on the effectiveness and usefulness of the copper rings:

TABLE VII

COMPARISON OF AND EVALUATION OF SOLDERED CORONA RINGS

OIL	peak [kV]	PDs	threshold	total Q [pC]	# of PDs	highest [pC]
2 rings	17.66	YES	10 µA	78.4	106	2.841
	21.7	YES	10 µA	112.2	134	5.444
OIL	**peak [kV]**	**PDs**	**threshold**	**total Q [pC]**	**# of PDs**	**highest [pC]**
No rings	12.55	YES	10 µA	598	526	10.227
	17.7	YES	10 µA	557.132	542	10.345
	21.7	YES	10 µA	569.791	548	10.431
1 ring	17.68	YES	10 µA	606.2	654	8.483
	21.73	YES	10 µA	654	684	10.751
2 rings	17.76	YES	10 µA	91.6	116	6.461
	21.73	YES	10 µA	135.6	144	11.797

Then, what followed was the first tests for the determination of the PD inception voltage. There were two tests: one with no protection box, and the second with the spark gap and a transorb diode (both tests in oil – no rings).

TABLE VIII

MEASUREMENTS FOR INCEPTION – WITHOUT AND WITH PROTECTION BOX

Baur (kV, peak)	o/scope (kV, peak)	current (µA)	PDs	BD
0	316m	820	-	-
0.5	2.05	810	-	-
5	5.3	860	-	-
10	11.5	1080	-	-
15	16.9	1320	YES	-
20	21.8	2440	YES	-
Baur (kV, peak)	**o/scope (kV, peak)**	**current (µA)**	**PDs**	**BD**
0	37m	220	-	-
2	2.08	259	-	-
5	4.75	313	-	-
10	9.7	422	-	-
15	15.05	533	NO	-
20	20.1	720	YES	-

Because the transorb dropped the inception voltage, we kept only the spark gap.

The next series of tests included higher AC voltages to determine the possible peak voltages in oil. What was witnessed is that during the same test, while raising the voltage gradually, gas bubbles were observed. It was assumed that they originated from PDs taking place in the oil. Moreover, during each breakdown, there were enough amounts of gas formed inside the cable. The gas bubbles significantly lowered the peak voltage in the next tests.

This effect was confirmed after the first test, which went up to **66 kV (peak)**, the highest BDV we reached during all tests. Then it significantly dropped in the following test to 40 kV and then 30 kV. Moreover, the same thing happened with the PD inception voltage. The PDs appeared much sooner than the first time due to the trapped gas.

HV AC TESTS IN OIL
- 1st test: Breakdown voltage: **66 kV** (peak), (more than 3 times the BDV in air)
- 2nd test: **40 kV**
- 3rd test: **30 kV**

Table IX shows another two series of tests, with results concerning the inception voltage, the break down voltage as well as the partial discharges. Before the 1st test, air bubbles were thoroughly removed from inside the cable as to assure there are no PDs originating from them. The 2nd test was immediately done afterwards, without removing the gas that was produced from the first test. The results confirmed our initial hypothesis.

TABLE IX
PRESENCE OF PARTIAL DISCHARGES IN OIL DIELECTRIC

No rings

1st test – air bubbles thoroughly removed

kV (peak)	Presence of PDs	# PDs	total PD charge Q (pC)	highest PD charge (pC)
25	No PDs up to 25 kV	0	-	-
26.13	Yes – inception voltage	6	31	15
30.38	Yes	16	89	25
40	Yes	83	658	91
45.25	Yes	98	693	46
50.25	Yes	157	8644	837
55.38	Breakdown			

2nd test, right after the 1st breakdown - has air bubbles

kV (peak)	# PDs	total PD charge Q (pC)	highest PD charge (pC)
10	-	-	-
15.38	-	-	-
20.38	-	-	-
21.5	Yes – Inception Voltage	-	-
25.3	43	241	18

At the end of the 2nd test, breakdown occurred at approximately after 1 minute at 25.3 kV.

In the figure on the left (68), one can see the increase of the number of PDs, and their charge Q, with the increase of the voltage.
After numerous tests (as shown later below) we came to the conclusion that the major factor for the achievable peak voltage / higher inception voltage is:

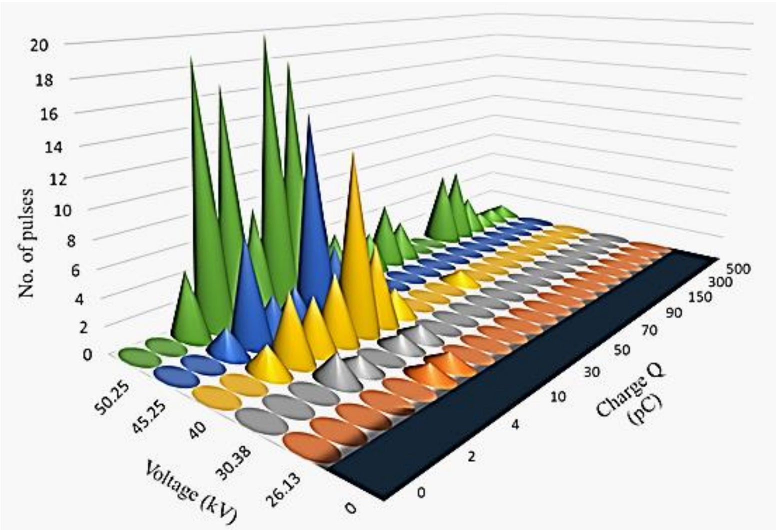

Fig. 68. Partial Discharges of the oil-filled Heliflex in AC high voltage

A. ***The voltage increase rate***

- The faster the voltage was raised, the higher peak voltage was achieved.
- When the voltage was raised slowly, the partial discharges had enough time to form gas bubbles, which led to more PDs, and ultimately breakdown.
- When the voltage was raised faster, gas bubbles did not form quickly enough, and higher voltages were achieved before break down.

B. ***Removing gas bubbles carefully after every test***

- Gas bubbles trapped in the oil inside the cable and the continuous forming of them under HV is a major drawback to the whole project.

More tests and measurements:

a) Breakdown voltages – No corona rings

No.	BDV (kV peak)
1	50 - forming of air bubbles
2	40
3	38
1	55

b) Inception voltage – BDV – PDs – No rings

1st test: Fast raise of voltage

No.	(kV) peak	PDs
1	15.44	No
2	20.88	No
3	22.13	No
4	22.88	No
5	23.63	No
6	25.56	No
7	27.63	Yes - starting PDs - Inception
8	43	Breakdown

2nd test: Slow raise of voltage – Time: 27 minutes

No.	(kV) peak	PDs	# PDs	Total Charge (pC)	Highest discharge (pC)
1	1.637	No	-	-	-
2	6.475	No	-	-	-
3	11.19	No	-	-	-
4	11.56	No	0	0	0
5	15.88	Yes - Inception	51	210	14
6	17.31	Yes	31	85	5.7
7	20.5	Yes	31	106	12
8	24.38	Yes	69	238	21
9	27.5	Breakdown	-	-	-

c) Inception / extinction voltage – BDV – PDs – 2 rings soldered – Clear of air bubbles
Raising voltage gradually and slowly, total time: 52 mins

	No.	(kV) peak	PDs	# PDs	Total Charge (pC)	Highest discharge (pC)
	1	1.74	No	-	-	-
	2	4.5	No	-	-	-
	3	10.32	No	-	-	-
	4	19.75	No	-	-	-
Inception	5	**24**	No at first, Yes after 2 mins	11	31.12	4.5
	6	24	Yes - a lot	140	1282	42
	7	3.375	No	-	-	-
	8	4.156	No	-	-	-
	9	4.172	Yes	-	-	-
Extinction	10	**3.625**	Yes at first, No after 1 min	-	-	-
	11	4.156	No	-	-	-
	12	4.344	No	-	-	-
	13	5.344	Yes	33	167	14
	14	10.63	Yes	39	228	21
	15	15.63	Yes	40	259	20.4
	16	20.19	Yes	35	355	35
	17	26.31	Yes	87	679	41.7
	18	34.25	Yes - Breakdown after 1 min	102	1187	45.4

d) Inception voltage – BDV – PDs

#1 test (2 rings soldered)
no air bubbles inside
fast raise of voltage, 7mins

No.	(kV) peak	PDs	# PDs	Total charge (pC)	Highest discharge (pC)
1	10	No	-	-	-
2	20	No	-	-	-
3	**30**	**Yes - Inception Voltage**	-	-	-
4	40	Yes	-	-	-
5	50	Yes	-	-	-
6	60	Yes	-	-	-
7	**62.5**	**1st Breakdown**	-	-	-

After 1st BD measurements - has air bubbles inside

No.	(kV) peak	PDs	# PDs	Total charge (pC)	Highest discharge (pC)
8	10	No	-	-	-
9	**15**	**Yes - Inception**	15	45.4	6
10	20	Yes	69	273.5	24
11	30	Yes	163	1369	105
12	39.13	Yes	344	6017	1755
13	**40**	**2nd Breakdown**	-	-	-

#2 test (2 rings soldered)
no air bubbles inside
raise of voltage, 11 mins

No.	(kV) peak	PDs	# PDs	Total charge (pC)	Highest discharge (pC)
1	1.5	No	-	-	-
2	23.06	**Yes - Inception Voltage**	20	71.7	11.5
3	30	Yes	35	181.4	23.5
4	40	**Breakdown**	197	1488	106.6

6.1.3 SPINNER CONNECTOR FOR HELIFLEX

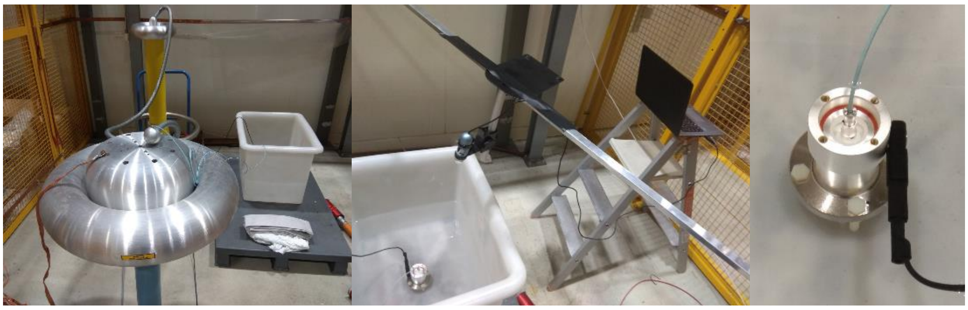

Fig. 69. The Spinner connector tests

The corresponding connector that is specially design as cable termination for the Heliflex cable, also went under testing for PDs and BDV.

Weak point inside the PE insulation of the connector.

It was light emitting during breakdowns.

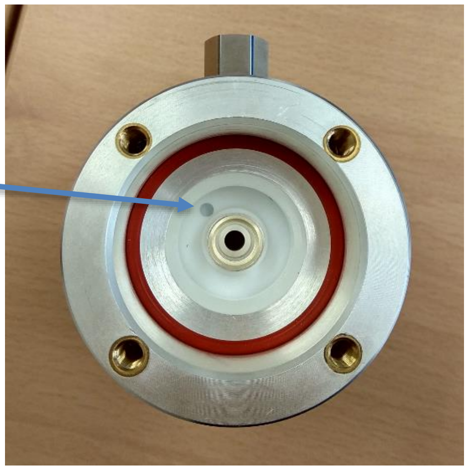

The first test for the connector was done in AC voltage, inside the oil tank. Below are the results:

No	kV peak	#PDs	total Q (nC)	highest discharge (nC)
1	20	21	13.395	1.258
2	23	48	70.139	23.889
3	25	62	127.081	56.552

The next test took place in air, under DC voltage, and the goal was to determine the BDV.

After raising the voltage gradually, the connector **broke down at 20 kV** (peak).

6.1.4 DRAKA CLP50 – PARTIAL DISCHARGE MEASUREMENTS

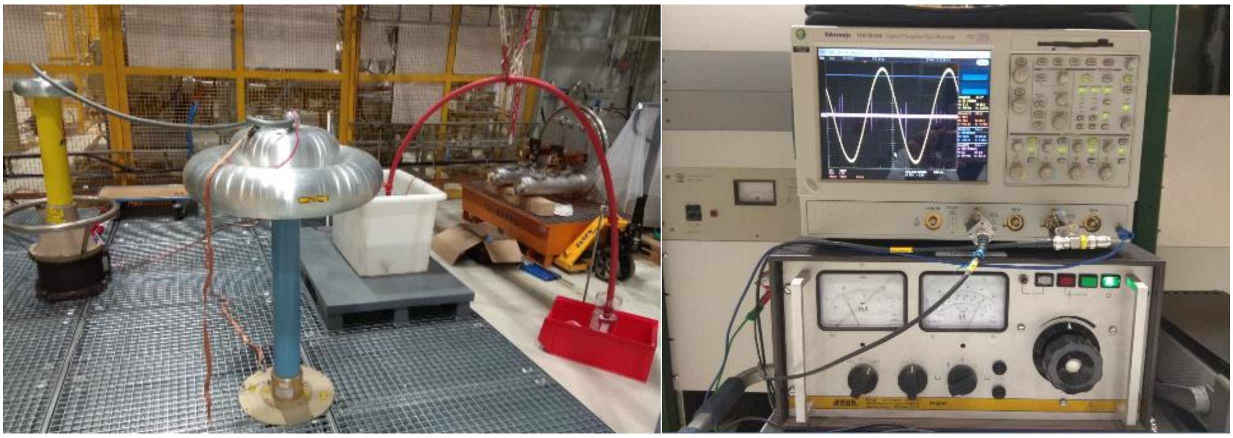

Fig. 70. The CLP50 cable HV tests

The DRAKA CLP50 cable is one of the most widely used cables at CERN. It can withstand higher voltages and went under a lot of thorough tests for PDs during this project.

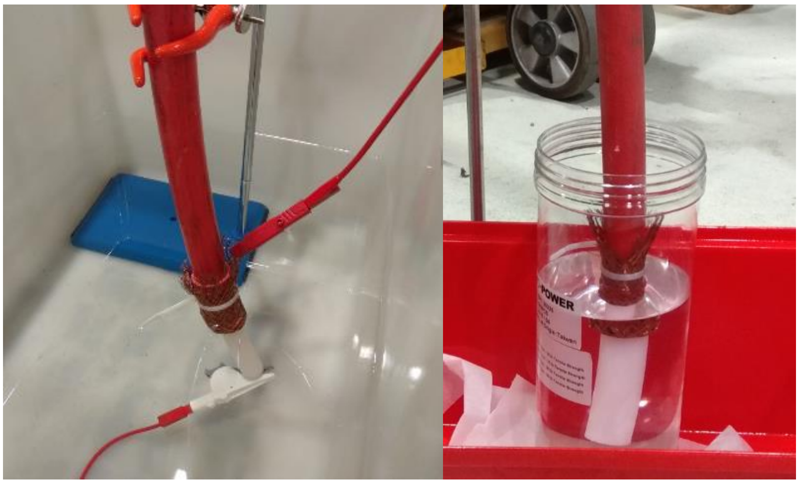

Fig. 71. Cable ends in oil

Again, the main concern was to put the ends of the cable inside insulating oil, to make sure that the partial discharges do not come from any sharp and pointy edges of the inner conductor or the outer braid, or from surface discharges on the polyethylene ends, but rather from inside the cable (PE insulation).

1) Inception voltage

No.	(V) peak	PDs
1	5	No
2	15.44	No
3	21.13	No
4	24	No
5	26.38	Yes - Inception Voltage

2) Inception / extinction voltage – BDV – PDs

No.	(kV) peak	PDs	#PDs	Total Charge Q (pC)	Highest discharge (pC)
1	1.5	No	-	-	-
2	5.2	No	-	-	-
3	10	No	-	-	-
4	15	No	-	-	-
5	20	No	-	-	-
6	25.5	No	-	-	-
7	26.13	No	-	-	-
8	26.38	No	-	-	-
9	26.5	Yes	46	129.5	10.1
10	27.38	No	-	-	-
11	28.5	No	-	-	-
12	29.38	No	-	-	-
13	30.75	No	-	-	-
14	31.5	Yes - Inception Voltage	-	-	-
15	30.75	Yes	-	-	-
16	30	Yes	-	-	-
17	28.8	Yes	-	-	-
18	26.88	Yes	32	56.75	2.7
19	25.31	Yes	47	121.7	27.8
20	24.19	Yes	-	-	-
21	23	Yes	35	59.85	3.4
22	21.81	No - Extinction Voltage	-	-	-
23	23.75	No	-	-	-
24	24.88	Yes	-	-	-
25	27.75	Yes	510	1687	44
26	30	Yes	117	438	40
27	31.75	Yes	101	988.5	214.25
28	33.63	Yes	344	2053	226.5
29	35	Yes	1060	4985	131.8

The fact that in this series of tests we have recorded PDs at 26.5 kV, does not mean that this is the inception voltage of the specific cable. Because in the next measurement, at which the voltage is raised to 27.38 kV, as well as in the few next that follow, the PDs disappear, and then they reappear at 31.5 kV. Therefore, this is the inception voltage.

The graphs based on the above measurements are about the behaviour of the PDs while raising the voltage, and the shown in the next page. What we expected, that with the increase of voltage we have increasing numbers of PDs, total charge, and higher magnitudes, is confirmed.

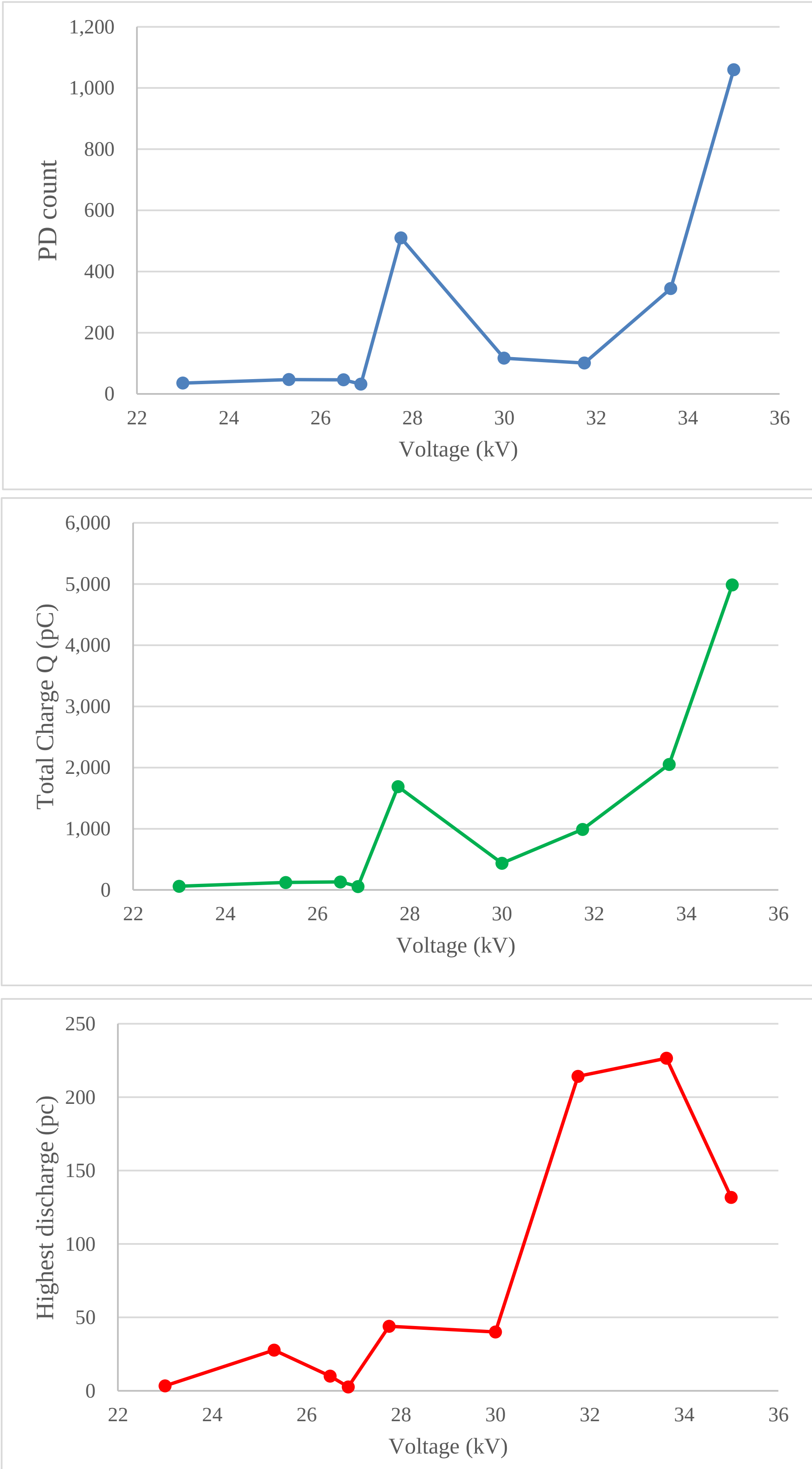

Fig. 72. Graphs of PD values over voltage, for the CLP50

6.2 IMPEDANCE AND ATTENUATION MEASUREMENTS

Fig. 74. The instrument with the measured cable

Fig. 73. Specially made connector for connecting with the VNA cable

The tests included the measurement of the impedance (Z), and the attenuation (α) of a 9 m Heliflex cable sample, with the Vector Network Analyzer.

Firstly, the standard air-dielectric model was measured and the result was 50.2 Ω, as expected.

Then, approximately 6.5 litres of the Bluesil Oil were carefully filled in between the inner and outer conductors of the Heliflex. This was a rather long procedure and it does not exclude the presence of small quantities of air left inside the cable.

Impedance measurements have been taken at different oil temperatures:

- **32.7 Ω** at 25.3 ºC and
- **32.9 Ω** at 27.5 ºC.

Finally, the attenuation measurement was **10.23 dB/km** at 50 MHz.

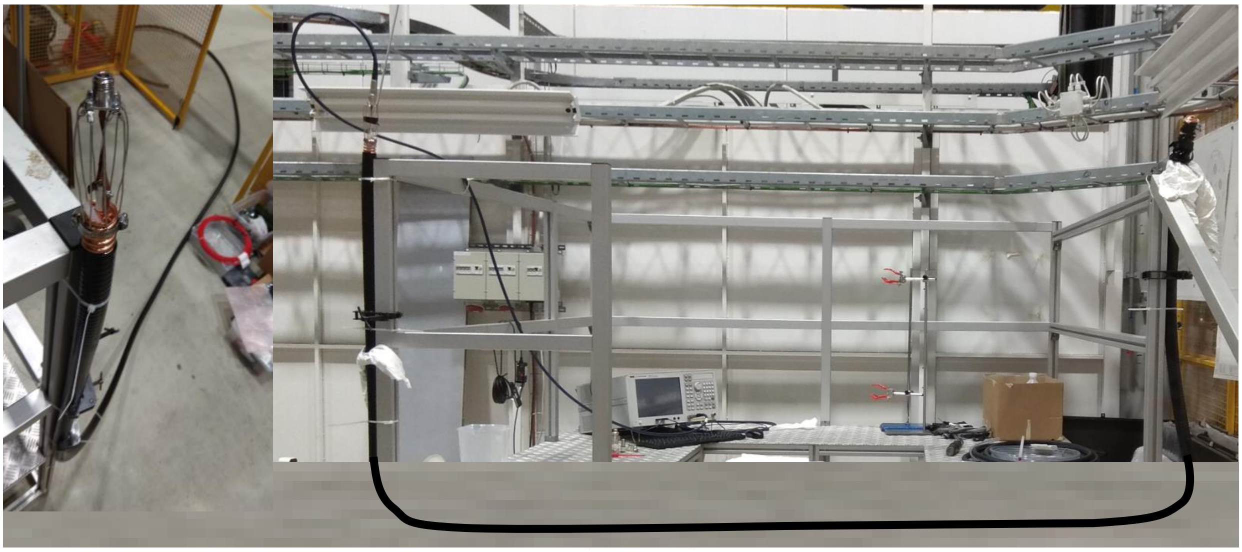

Fig. 75. The setup for the impedance measurement

6.2.1 EVALUATION OF THE IMPEDANCE / ATTENUATION MEASUREMENTS

For the impedance:

- In the case of the standard air-dielectric cable, the result of **50.2 Ω** was anticipated, as it is within the limits of the manufacturer.
- For the oil-filled cable, although we are not sure that all air inside was removed, the impedances of **32.7 Ω** and **32.9 Ω** were actually not far from the analytically calculated (with approximations) value. In fact, the theoretical expectation was 33.7 Ω, so this can be considered as a satisfactory result.

The attenuation, which was measured at **10.23 dB/km** at 50 MHz, was again close to the theoretical calculation of 9.7 dB/km. For comparison, the RG-220 (CLP50) attenuation at 50 MHz is 13 dB/km.

However, we observe that there is a significant increase in the attenuation considering the standard cable. The higher attenuation (comparing to the 6.4 dB/km of the standard 'air' Heliflex) is due to the different dielectric of the modified cable. Oil has higher ε_r (2.7) than air.

Comparing to SF_6 cable (5.5 dB/km), the Heliflex cable has a smaller inner conductor diameter, hence higher attenuation than the SF_6.

6.2.2 THOUGHTS AND CONCLUSIONS ON THE IMPEDANCE

- By means of different oils, or a mixture of them, the cable can be tuned to different impedances to match a connected magnet perfectly, which is also considered as one of the main benefits of this method.
- According to the technical information available in the data sheet of the used oil, when the temperature (T) rises, there is a drop in the viscosity of the oil, which in turn reduces the dielectric constant (ε_r), hence the impedance (Z) increases. Also, pressurizing the oil increases its viscosity and leads to a higher ε_r.
- After calculations based on the correlation between the temperature and the dielectric constant of the oil, we came to the conclusion that: **An increase by 1 ºK results in a 0.05% increase in Z.** This is not a small factor and should be definitely be taken into consideration for this kind of applications.

These results lead to the idea that temperature could be used to match the impedance, with the use of the appropriate mechanical system. But, for sure, it would also be really challenging to keep it stable.

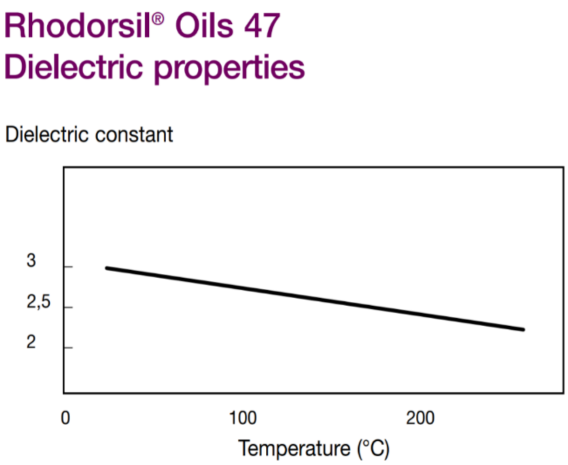

Fig. 76. Taken from the data sheet of the 'family' of oils, from which the oil we used belongs. [21]

7. SIMULATIONS

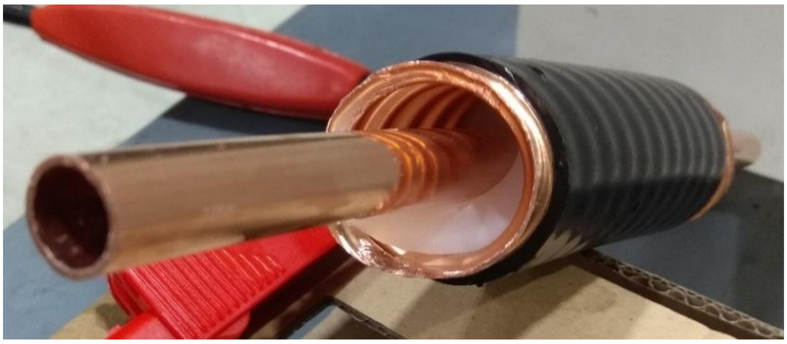

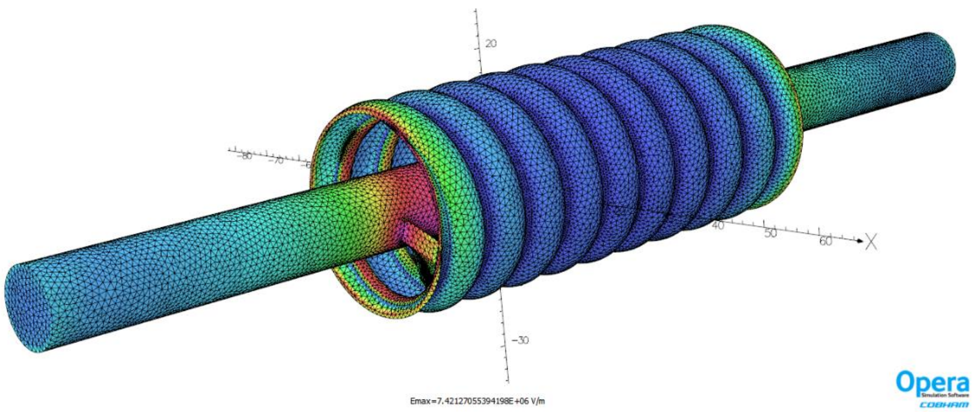

Fig. 77. The actual model to simulate (up) and the Opera simulation (down)

7.1 OPERA FEM SOFTWARE

With the help of the of finite element method software, 'OPERA Simulation Software' by Cobham, there was an attempt to simulate the performance and behaviour of the test subjects under high voltage.

Electric field simulations were conducted, in order to simulate in 3D-modelling the electric field zones and lines, as well as the performance and behaviour of existing cables and connectors and also new designs under high voltage. The goal was to determine the weak points of the cable, which means the points that are potentially capable of causing problems to the correct function of the cable and can affect its lifetime. With the help of Opera, we are able to identify these points, by finding were the electric field acquires exceptionally high values. There, we have candidate spots for partial discharges, which is the main reason for cable decaying and finally the total destruction of the insulation of the cable.

Depicted in different colors, vectors, zones or lines, the electric field strength will tell where to expect future malfunctions of the cable. These areas of high fields, are usually shown in purple or red color, whereas low or zero fields are depicted in blue. As already mentioned, the weak points of the cable are the triple points, where the electric field strength goes high around areas close to these points. The purpose of the simulation is to prove, explain and confirm the existence of such points, and also determine the magnitudes of the electric strength, with a possible divergence from the real values, due to problems while constructing and designing the model.

However, there was a high effort to be as accurate as possible, considering the design of the exact models, with persistency to precision to the geometry of the models, the properties of the materials, and finally in choosing the correct solving method of the simulation.

Another reason of why electric field simulations are important is that they are a way to confirm and validate the tests and measurements in lab, and then simulate new models in order to check the scalability of the model / optimized design, for future improvements and further studies.

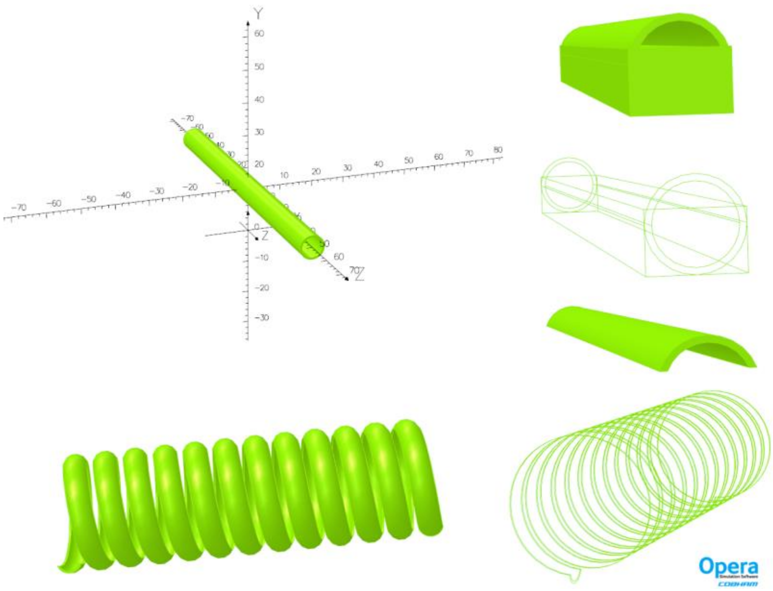

Fig. 78. Designing the outer conductor of the Heliflex

7.2 BUILDING THE GEOMETRY OF THE MODEL

The difficulties encountered in the process of building the models differ from one cable to the other. We had to simulate the exact geometry of the cables, in order to have accurate results. It was a highly demanding procedure to measure the exact dimensions of each part and try to replicate them as accurately as possible. Especially in the case of the Heliflex there were no cable dimensions in the technical data sheet, so we had to do measurements and complicated calculations.

The geometry of both the Heliflex and the SF_6 cables is quite complex, especially due to the fact that the outer conductor is corrugated in both the Heliflex and the SF_6 cables. Firstly, there was the need of very precise measurements of the cable dimensions, thicknesses of the materials and pitch, in accordance to the specifications in the data sheets (where mentioned), in order to get the exact structures.

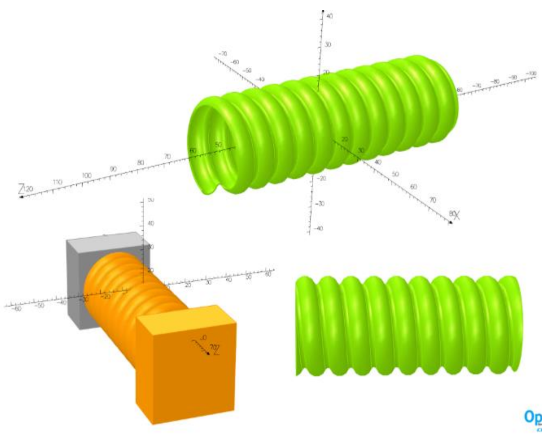

Fig. 79. Using cutting blocks to cut the edges of the outer conductor in order to be closer to the reality (sharp edges)

In the case of the SF_6 cable, the corrugation could be described as parallel big and small toroidals cut

Fig. 81. The actual spirally corrugated OC and the helical spacer

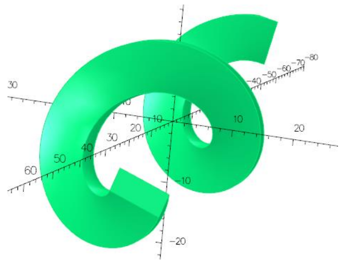

Fig. 80. Producing the spiral shape of the PE helical spacer

almost in half and joined together. The outcome seemed like a tube of rings in parallel, something that proves useful for bending the cables, but not for the voltage holding.

On the other hand, the corrugation of the Heliflex was different in the sense that it was in the form of a spiral, following the helical spacer that was inside, and thus excluding any symmetry. For this, a different approach was made in modelling it: two long cylinders were cut and formed using a mathematical function in order to bend into a spiral with the correct pitch, and finally form the model which was close to the real one with great accuracy. Afterwards, the problems of the volume and the surface meshing, which was very irregular, had to be dealt, and in return the appliance of the material properties and boundary conditions was made.

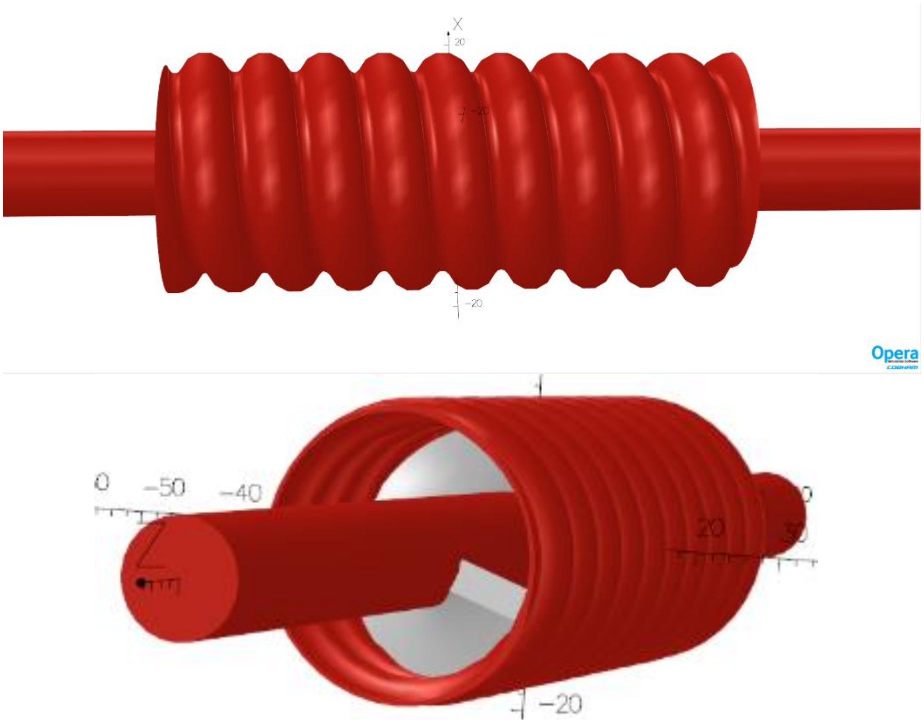

Fig. 82. The RFS Heliflex model

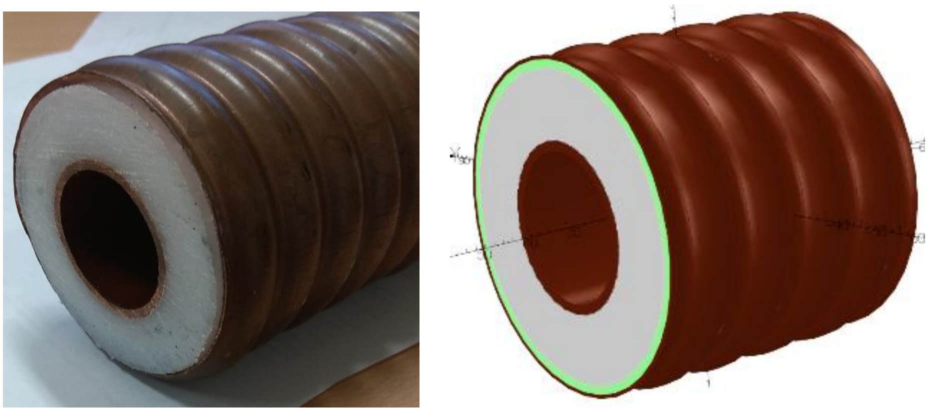

Fig. 83. The SF_6 cable and its simulation model

7.3 CONDUCTING ELECTRIC FIELD SIMULATIONS

The main issue in reassuring that the simulations are correct, in terms being close to the reality, was the size of the mesh. In other words, the finer the mesh, the more accurate results and more precise values we get from the simulations, with the price of longer time to analyze them.

The small scale Heliflex (20cm) was simulated at 16 kV (17.89 kV was the lowest breakdown voltage that was measured during the tests in air dielectric). Also, the SF_6 cable was simulated at the operational voltage of 80 kV. For the all the simulations, voltage independent characteristics were assumed for the permittivity.

7.3.1 SIMULATION OF STANDARD HELIFLEX IN AIR AT 16 kV

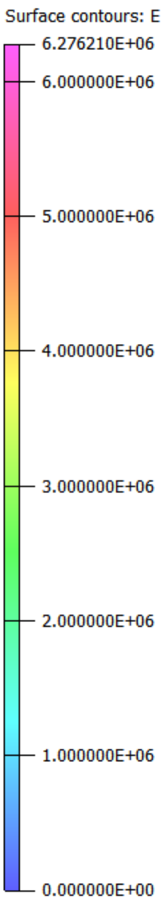

Simulation #1

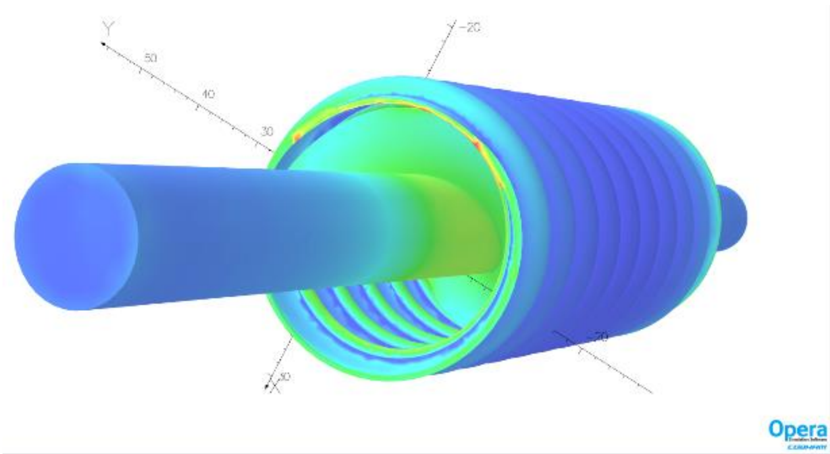

The highest value of electric field is observed on the sharp edges of the outer conductor, because we did not use any cable terminations.

The maximum value of the electric field strength E_{max} is 6.276 MV/m.

$$\mathbf{E_{max} = 6.276\ MV/m}$$

Simulation #2

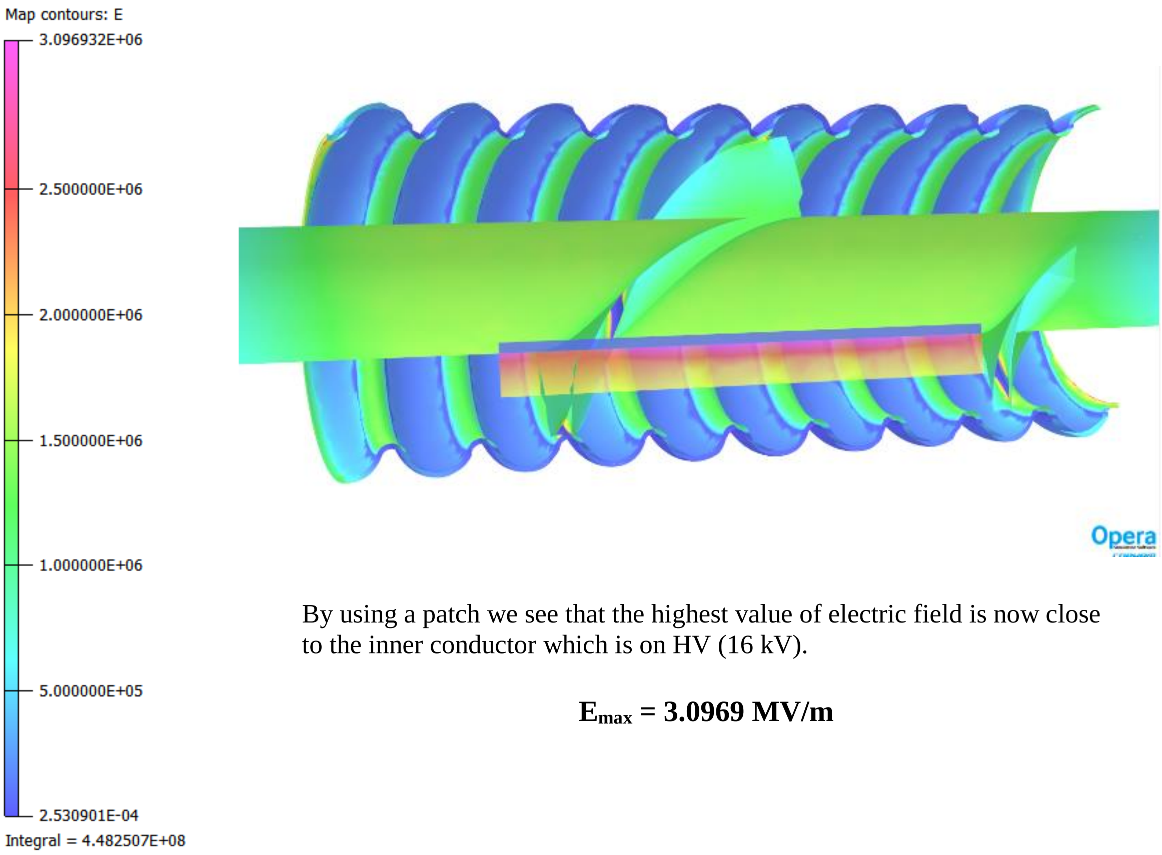

By using a patch we see that the highest value of electric field is now close to the inner conductor which is on HV (16 kV).

E_{max} = 3.0969 MV/m

Simulation #3

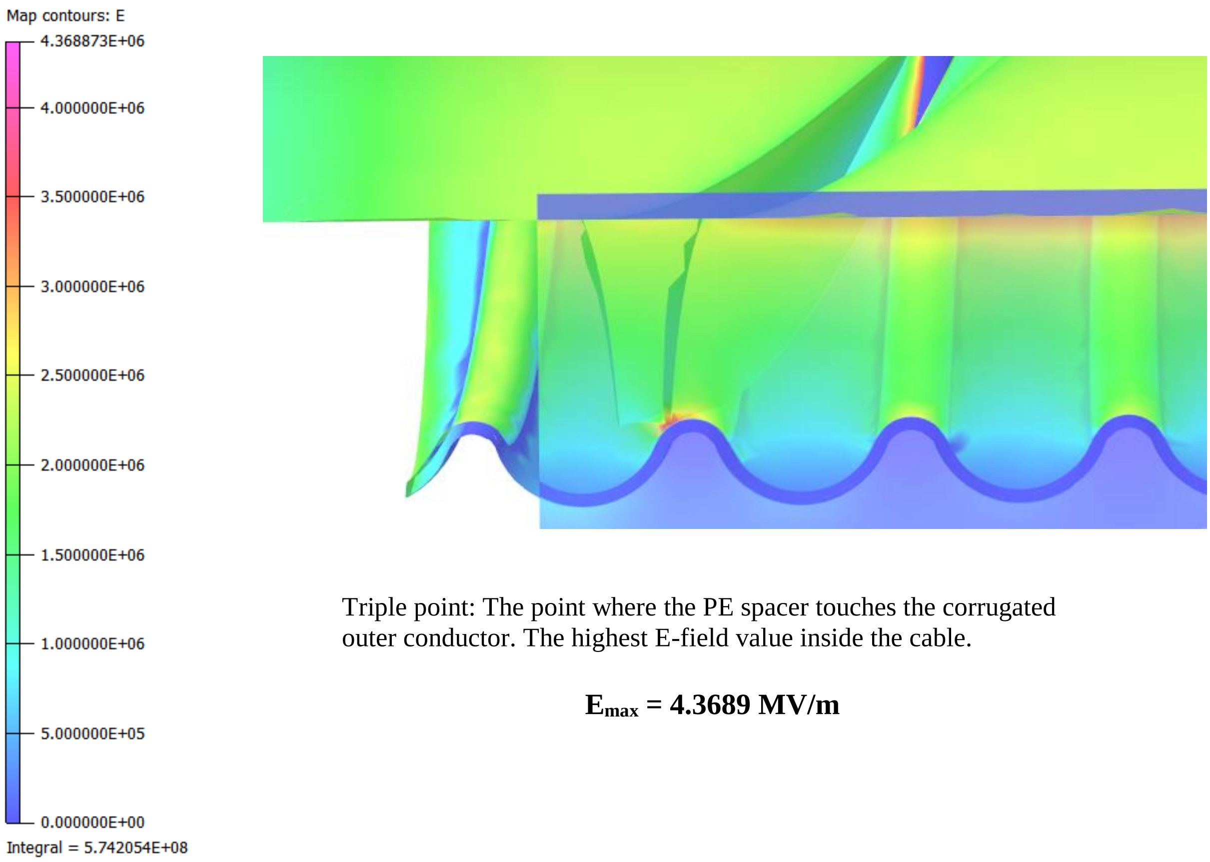

Triple point: The point where the PE spacer touches the corrugated outer conductor. The highest E-field value inside the cable.

E_{max} = 4.3689 MV/m

7.3.2 SIMULATION OF HELIFLEX IN OIL

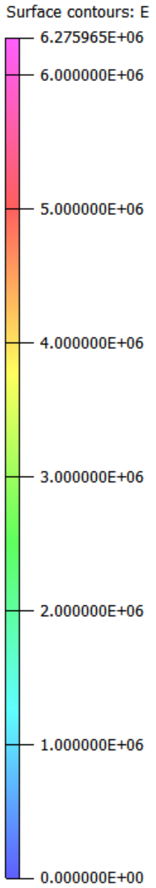

Simulation #1

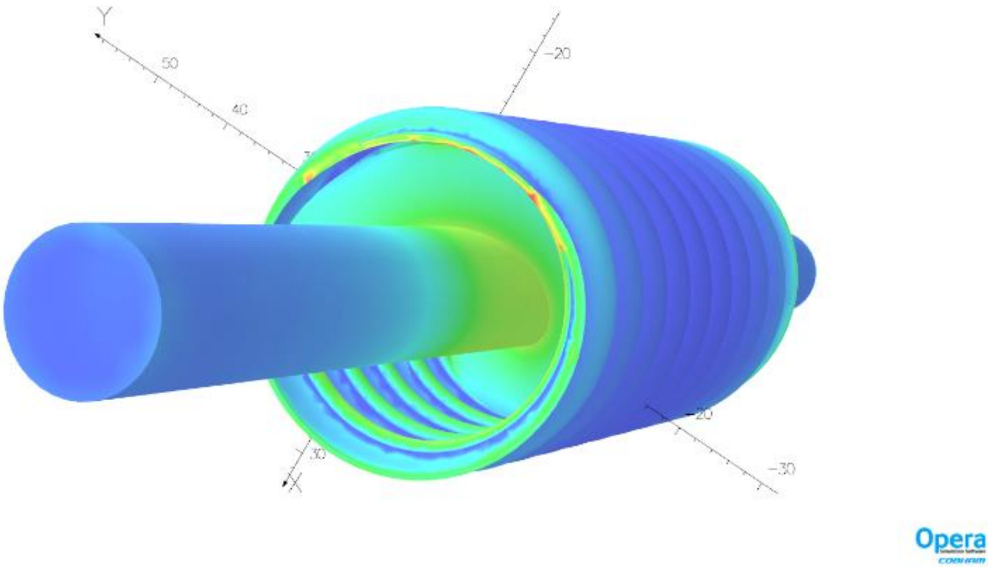

Again, the highest value of electric field is observed on the sharp edges of the outer conductor. It is almost the same value.

$$E_{max} = 6.27596 \text{ MV/m}$$

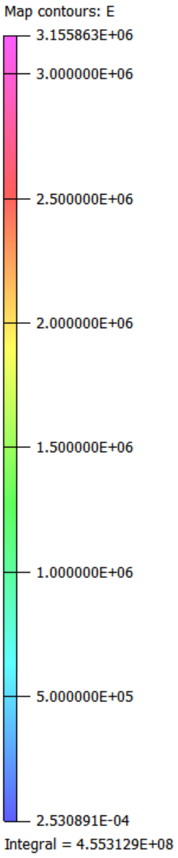

Simulation #2

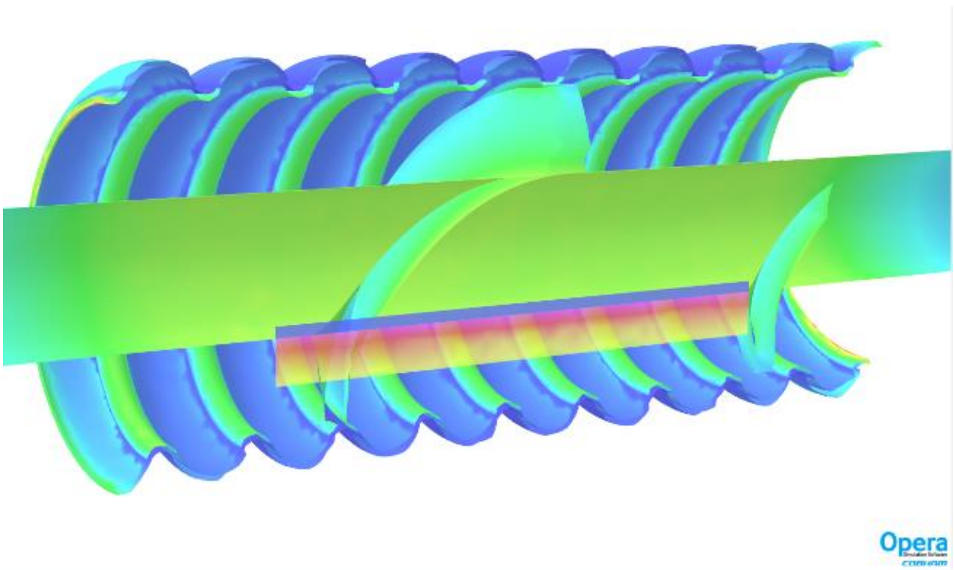

Again, using the same patch. The highest value of E-field, is close to the inner conductor.

$$E_{max} = 3.1558 \text{ MV/m}$$

Simulation #3

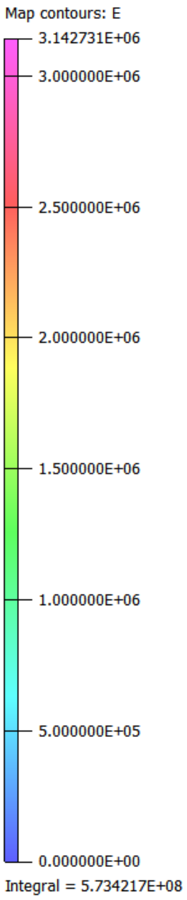

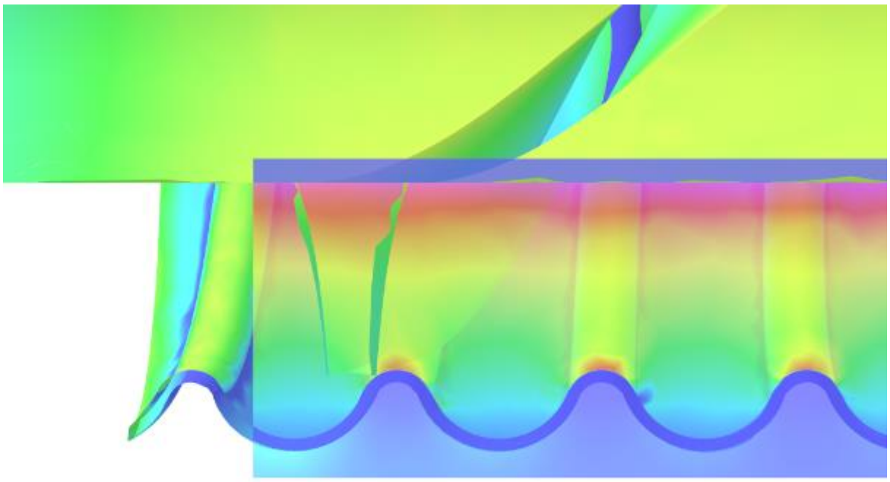

No high field close to the triple point, due to the presence of the oil. The highest E-field is still on the inner conductor.

$$E_{max} = 3.1427 \text{ MV/m}$$

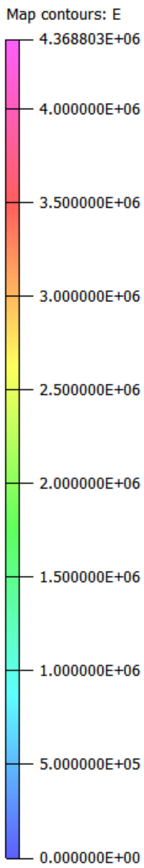

Comparison of the same triple point in air (up) and in oil (down)

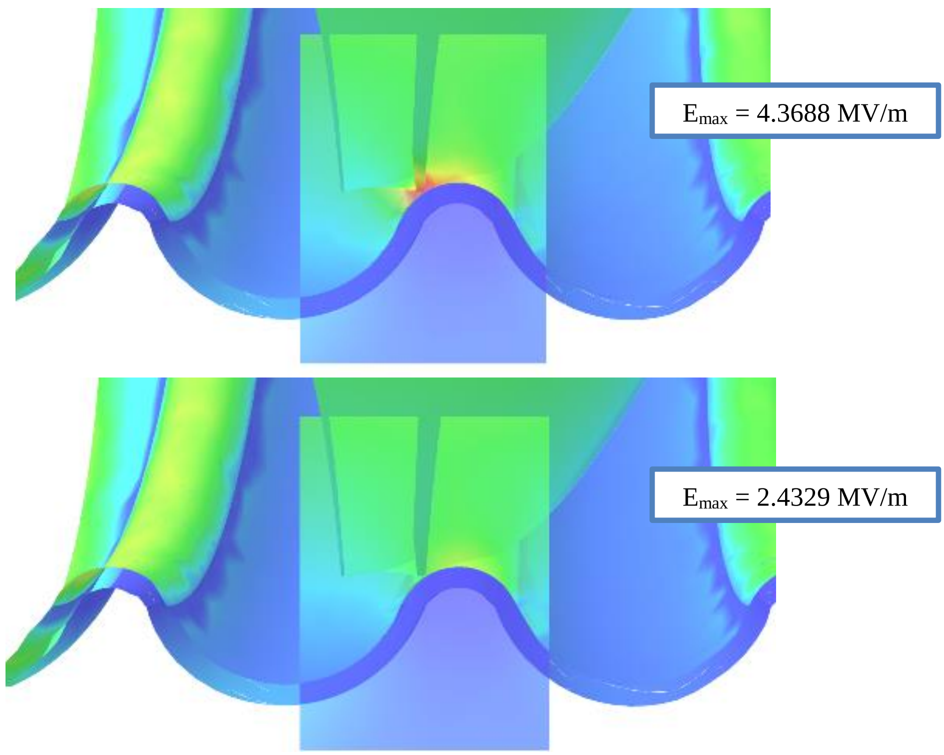

Fig. 84. The same triple point in air (up) and oil (down)

As it clearly shows from the previous comparison, using the same chromatic scale, one can see the impact of the oil on the triple point. So, there now, there is a much less E-field, 2.4329 MV/m, compared to the same point in air 4.3688 MV/m.

Which means that we have a significant decrease of the E-field, near this area of the triple point, equal with **44.31%.**

7.3.3 SIMULATION OF THE SF_6 CABLE at 80 kV

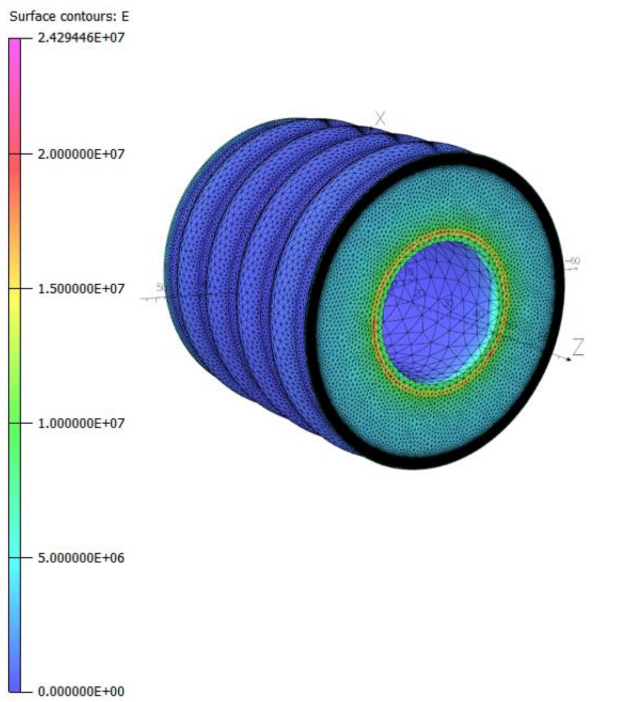

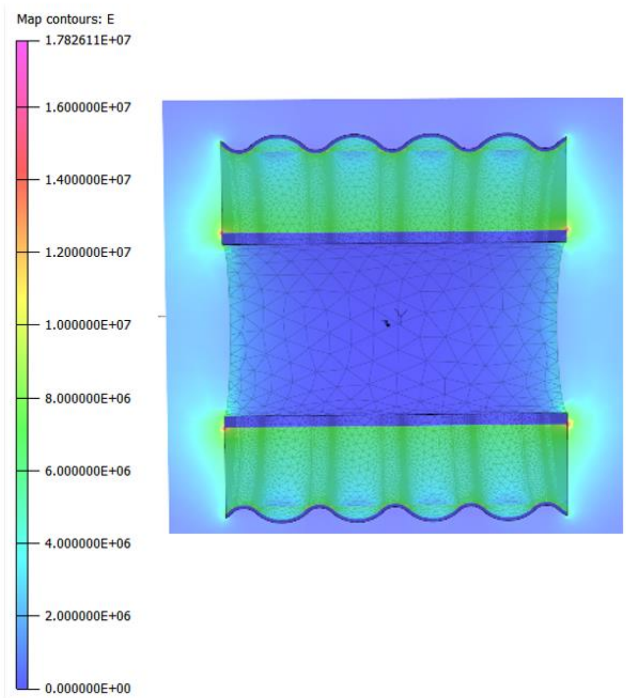

Of course the E-field will be high at the edges of the cable, but this is not of our concern. What we care for, is inside the cable, since it will never be used without cable terminations. But inside the SF_6 cable, as we have already seen, there are voids filled with SF_6 gas.

The same geometry we tried to simulate, by using a really fine mesh, in order to be sure that the results are correct. And we were able to confirm the accuracy by exploiting the fact that the program can integrate the voltage over a very small length, giving us quite accurate values of the E-field, close to the triple point.

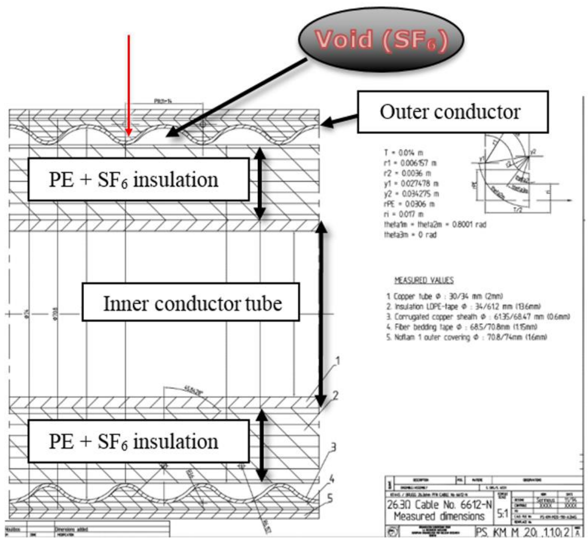

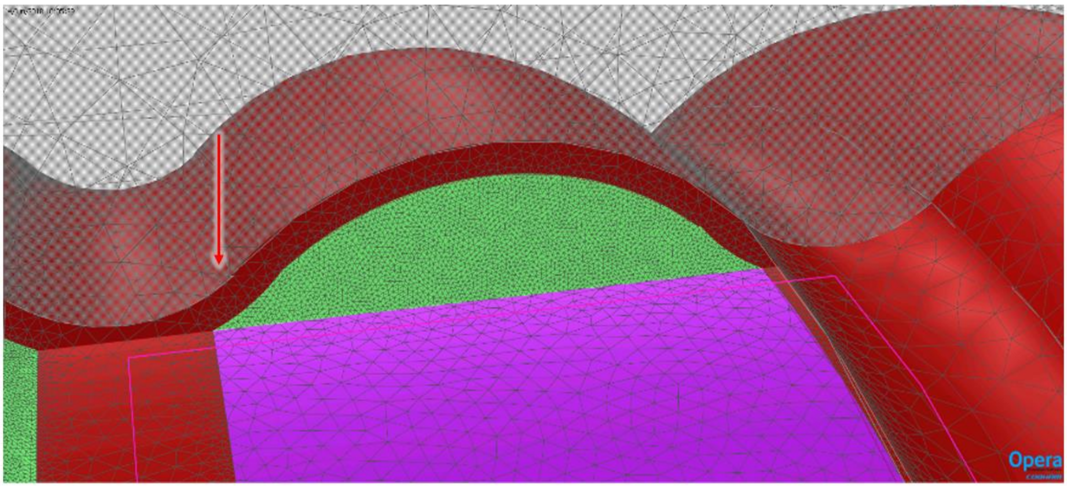

Fig. 85. Triple point inside the SF_6 gas cable

As suspected, the triple point that the red arrow shows in Fig. 85, is definitely a candidate for extra high E-field values. The simulation below confirms our suspicions.

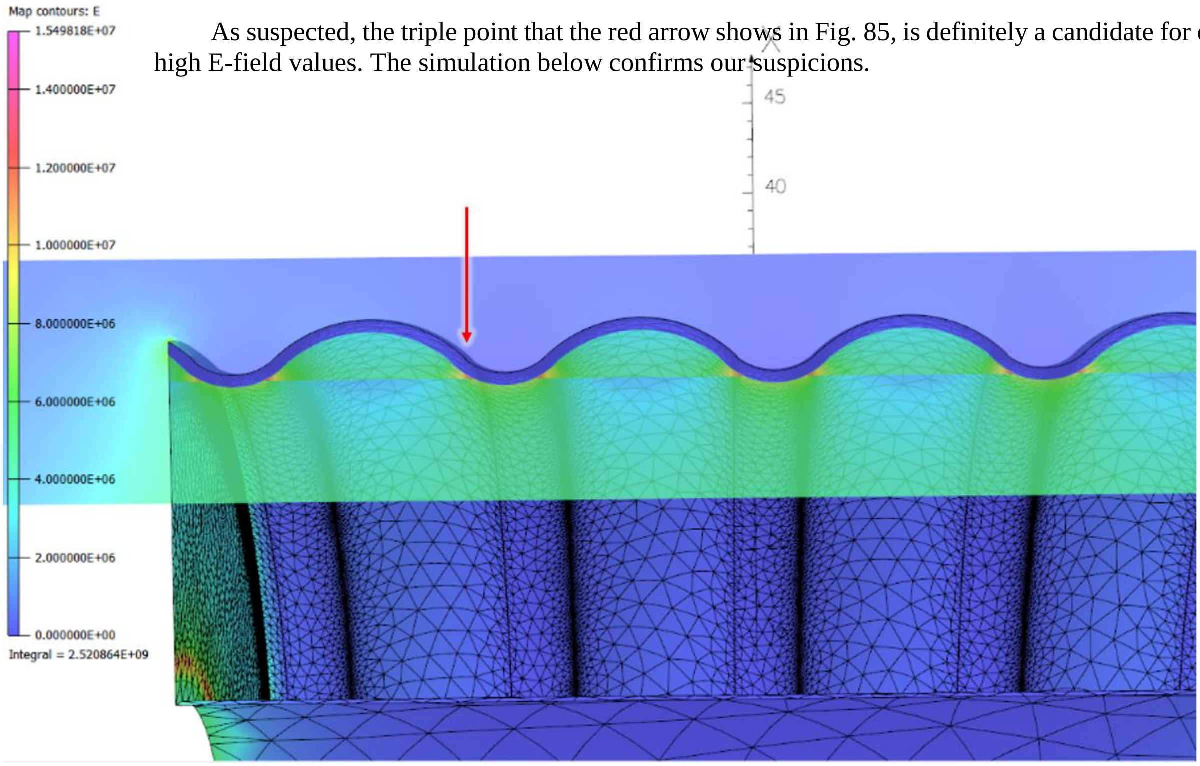

A closer look to the particular spot reveals the magnitude of the electric field, close to the triple point.

E_{max} = 15.927 MV/m

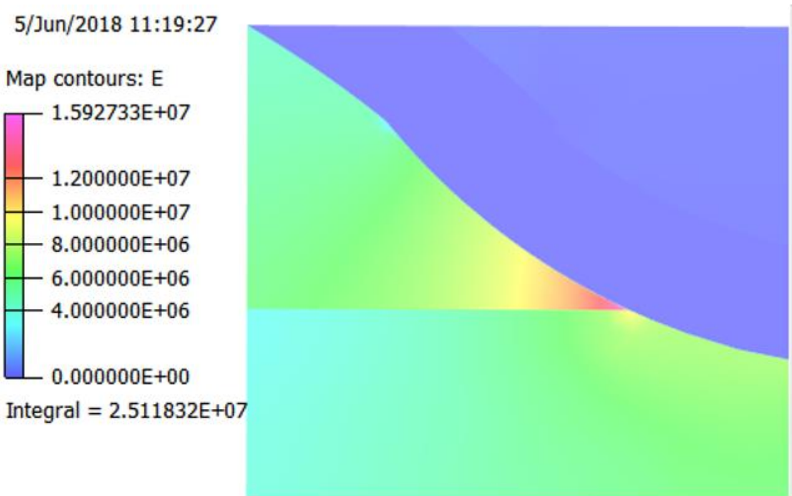

7.4 SIMULATION RESULTS

- The corrugation (although needed for such bulky structures) is useful for the flexibility of the cables, but not for the voltage holding.
- Because of the corrugated outer conductor, the PE does not fit smoothly to the copper in both cables.
- It creates triple points and areas with excessive high fields.
- Thus, is responsible for weak points of the cables, which subsequently show PDs and lower BDV.

Opera FEA Simulation Software proved to be a very useful and powerful tool which helped to confirm the predictions we had made during the tests in lab, concerning the shape and strength of the electric field, and how this is distributed around the inner and the outer conductor, on the surfaces of them and the spacer but mostly close to the areas surrounding the so-called 'triple points'

7.5 OTHER SIMULATIONS: CLP50

The more simple coaxial geometry of this cable, allowed us to simulate and analyze only a quarter of the structure, due to cylindrical symmetry.

It was simulated at 40, 60, and 96 kV. Also, some variations in the structure like small voids of the cable, in the form of an air bubble, were added, to check the behaviour of a real cable with imperfections. The air bubble was placed at the inner conductor and in the middle of the PE, to show the difference in E-field caused by the bubble.

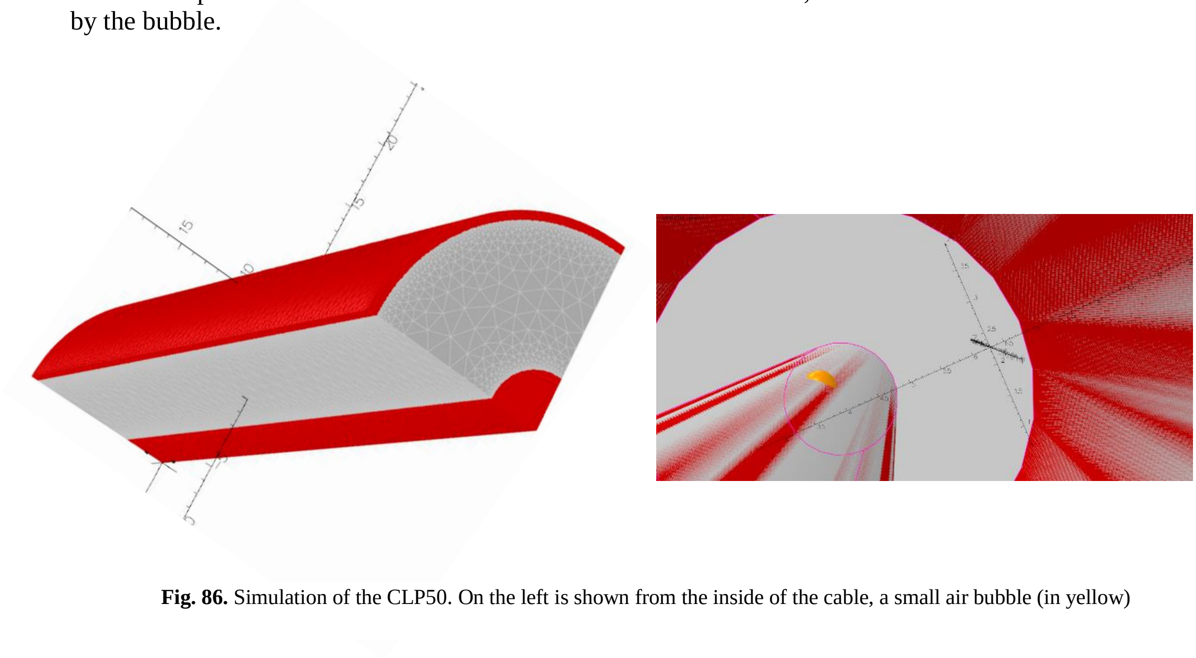

Fig. 86. Simulation of the CLP50. On the left is shown from the inside of the cable, a small air bubble (in yellow)

The simulation results near the bubble (for 40 kV) were:

E_{max} = 15.4 MV/m

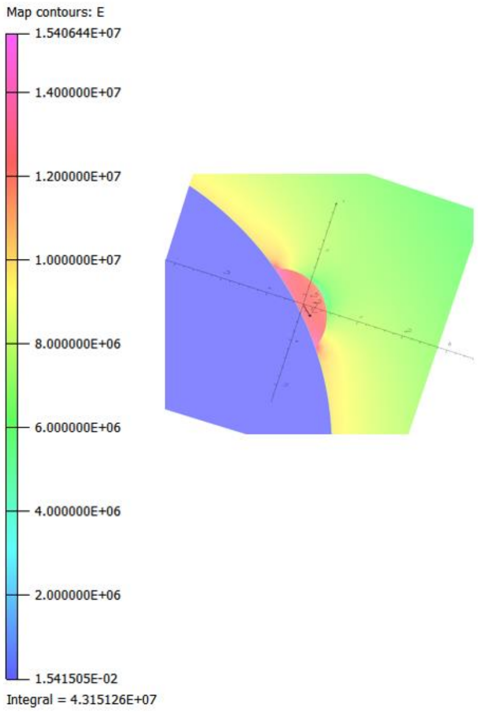

The standard cable without imperfections, was also simulated at 40 kV. For confirming the simulation result, we performed as well analytical calculations.

- at 40 kV, **9.6 MV/m**

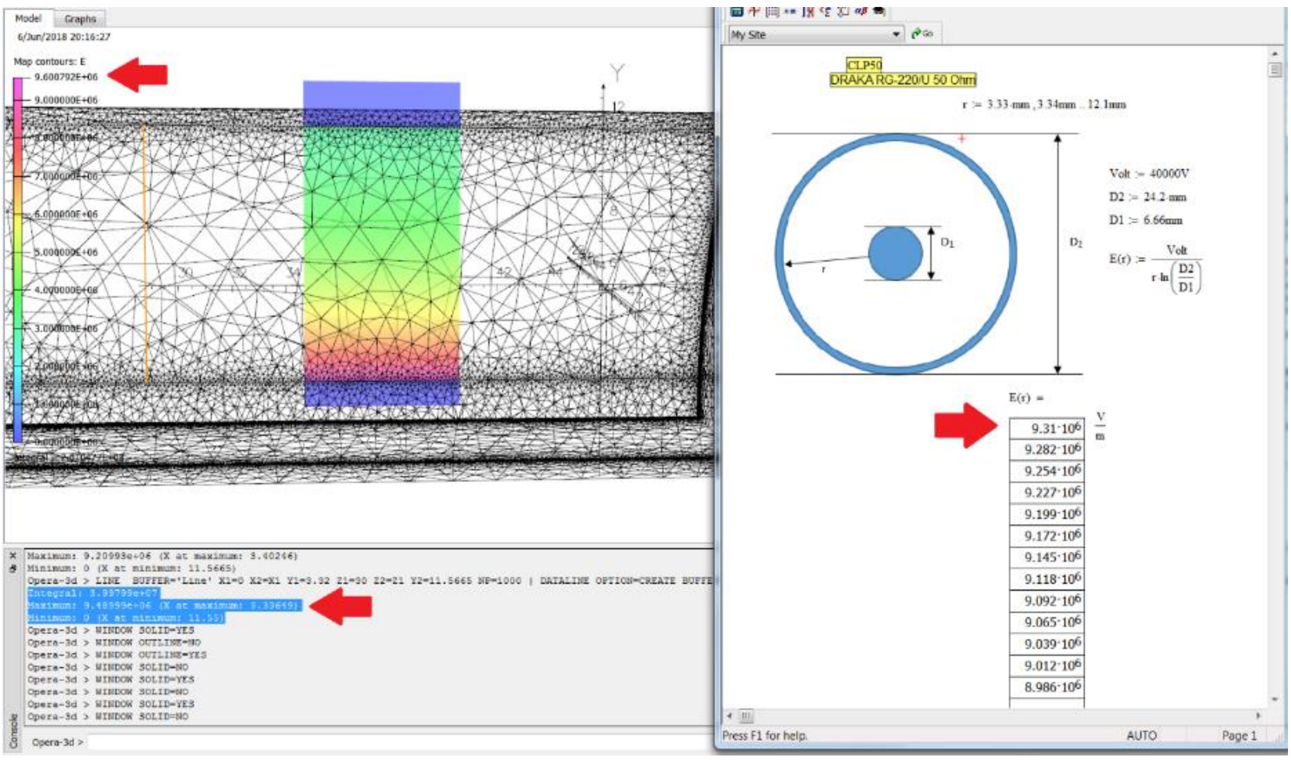

- With an air bubble in the middle: **9.656 MV/m**

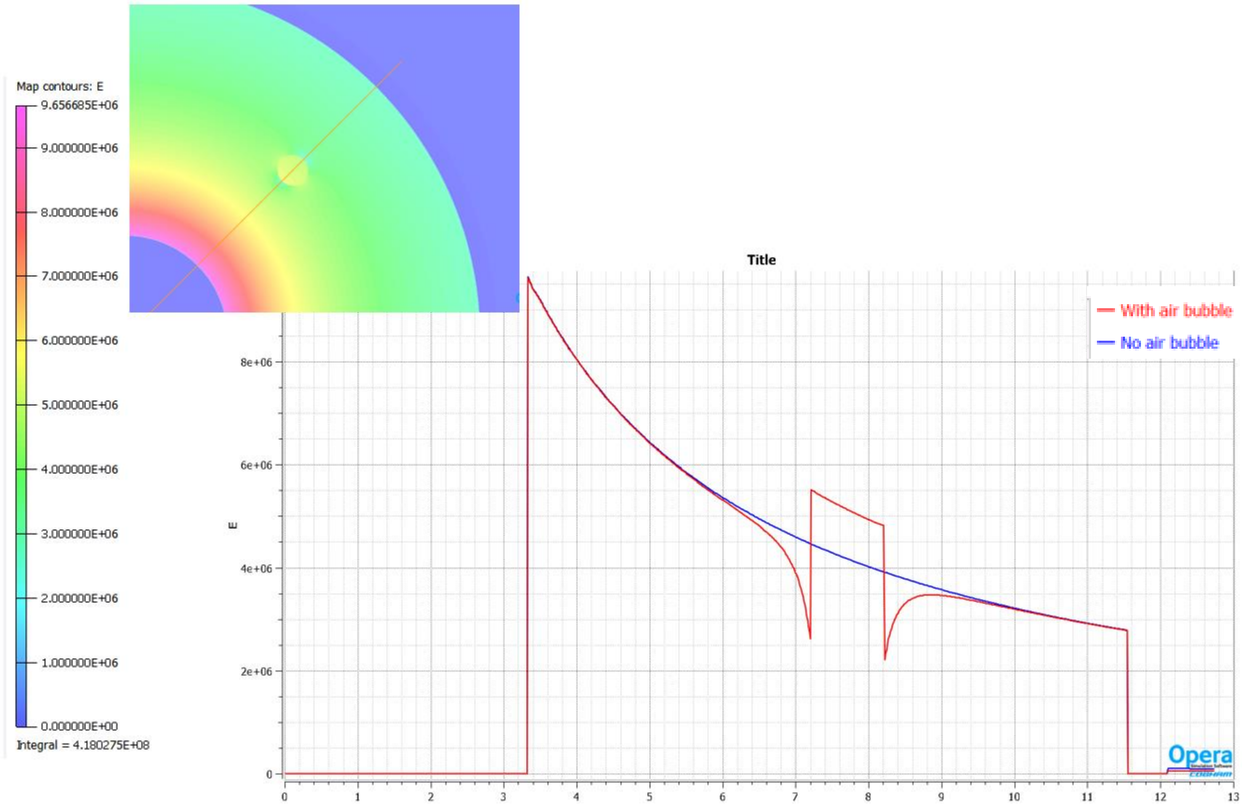

- With an air bubble right in the middle of the surface of the inner conductor: **14.98 MV/m**

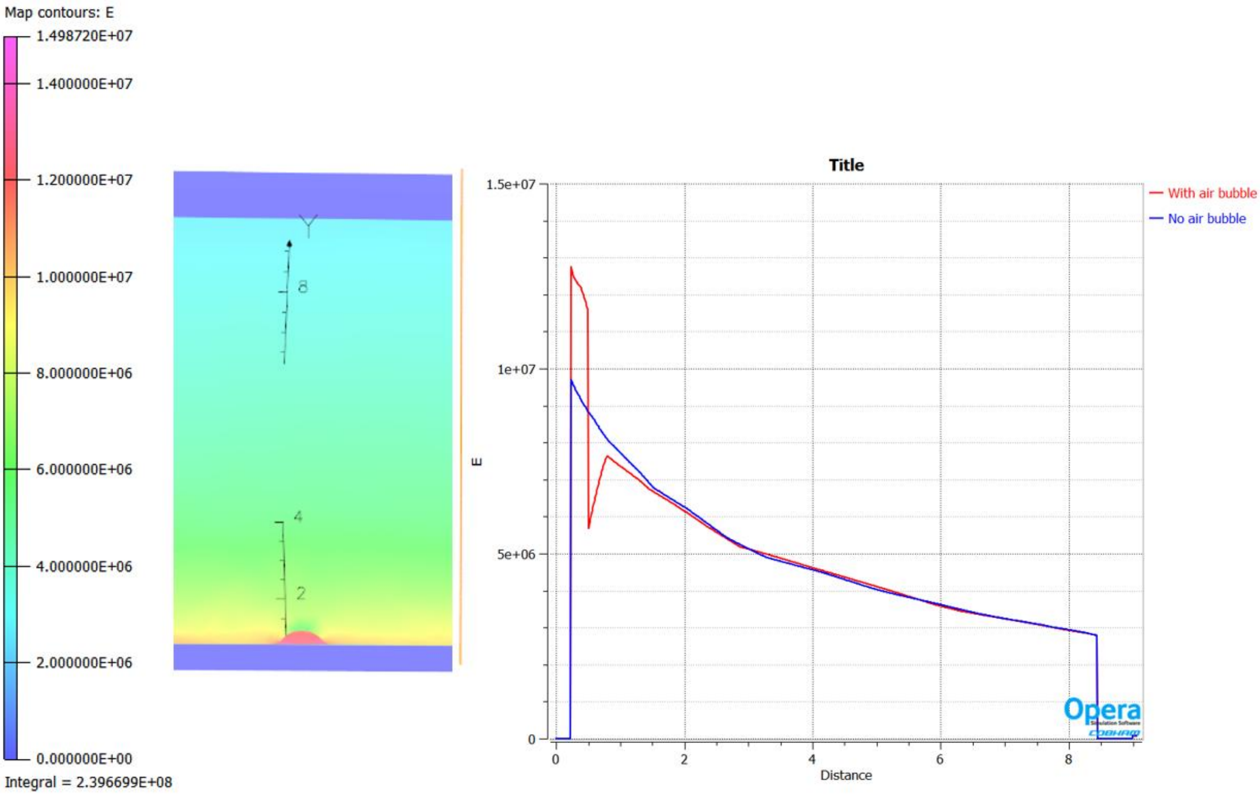

- At 96 kV, $\mathbf{E_{max}}$ **= 23.04 MV/m**

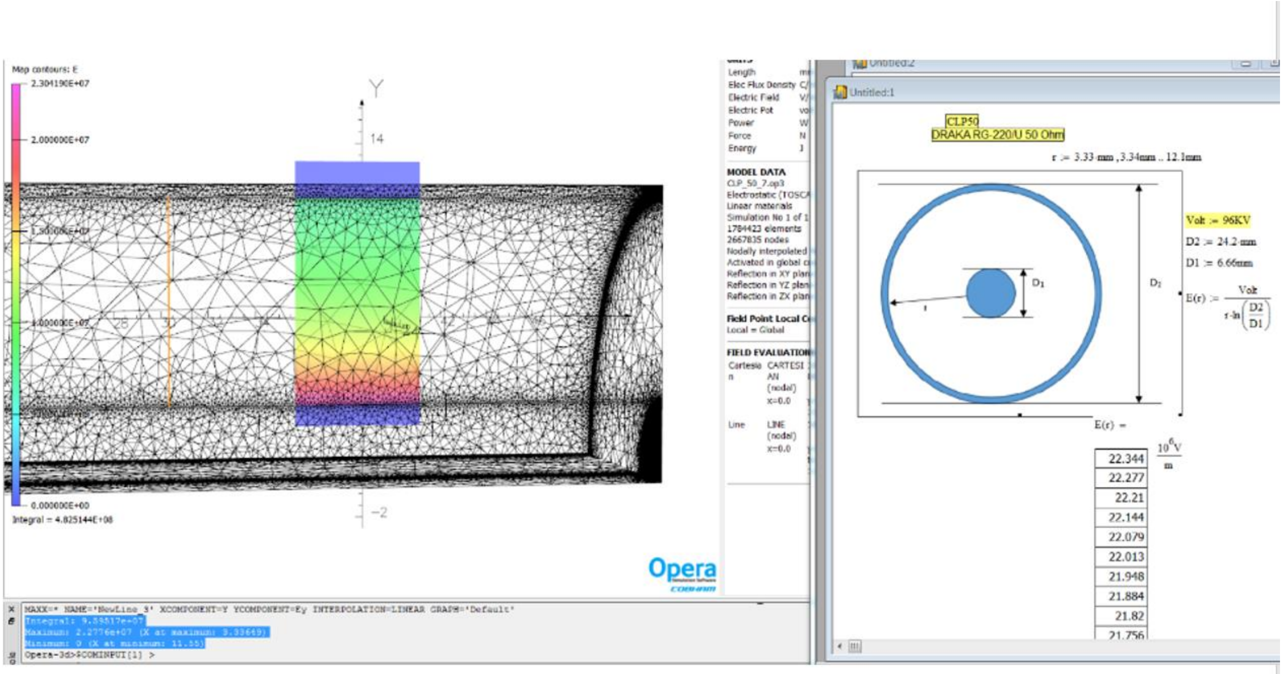

7.6 SCALABILITY – FUTURE DEVELOPMENTS

The question arising from the whole project was whether there is the possibility to scale up the oil – filled Heliflex to a full-scale prototype that could withstand higher voltages and show fewer or no PDs, according to our needs. The idea was very simple: The small scale oil-filled did not BD at 20 kV, nor did it have PDs.

The maximum E-field at this voltage was simulated by Opera and was:

- 8.3637 MV/m (at cable ends)
- **3.96803 MV/m** (inside, inner conductor)

Since we wanted to go to 80 kV, we decided to scale our model, to four times bigger the dimensions of it, and then run the simulation for 80 kV.

The maximum E-field now was:

- 9.699 MV/m (at cable ends)
- **3.992 MV/m** (inside, inner conductor)

Which means that the maximum electric field inside the cable stayed almost the same, and that it could potentially work, in case there is such a cable available in the market.

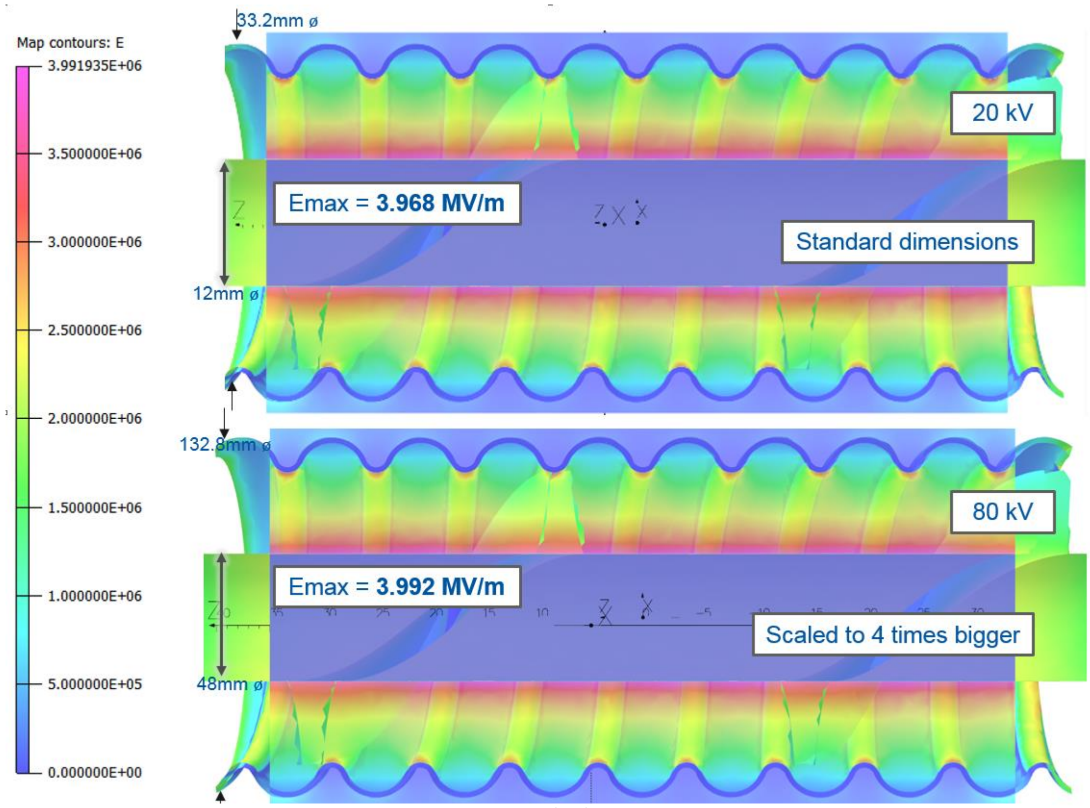

Fig. 87. Scalability for future improvements

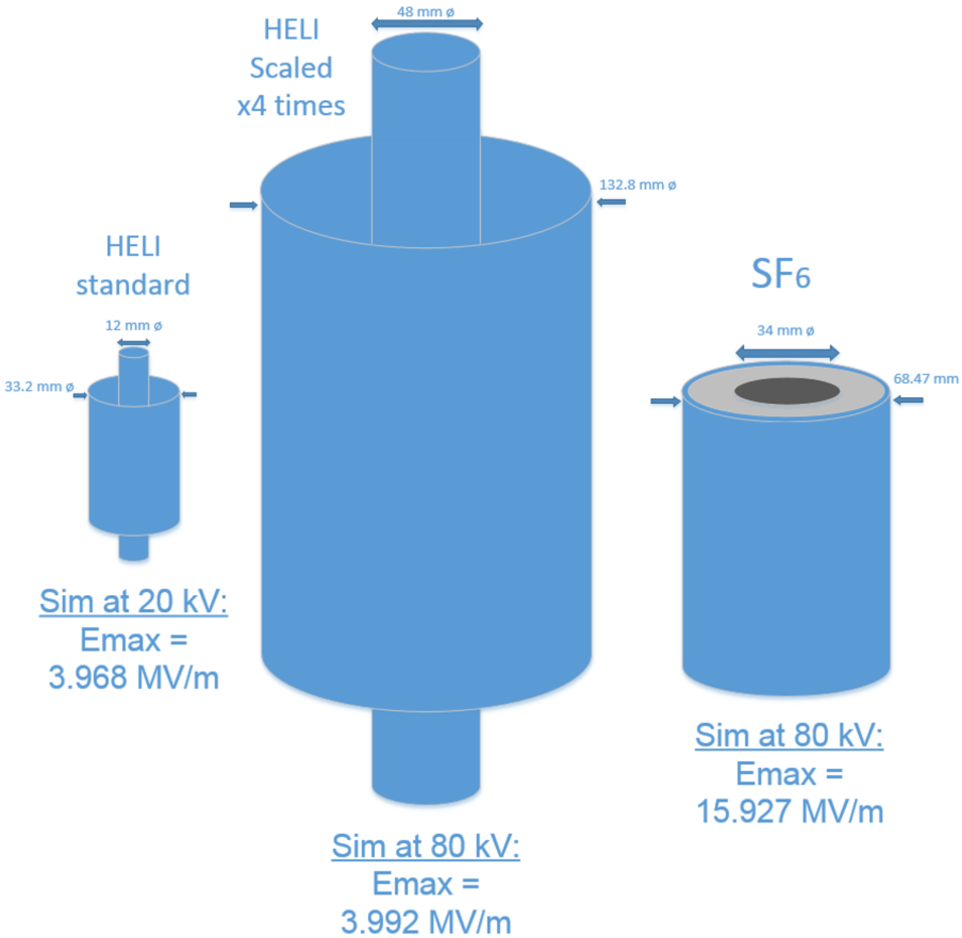

Fig. 88. Comparison of the different models

Apparently, there is, such an off-the-shelf cable that meets these dimensions shown in Fig. 88, above. A suggestion for future investigation would be the **5-1/2" HCA550-50J Heliflex air-dielectric**, 50 Ω, 1.5 dB/km at 50 MHz, with the undermentioned specifications:

Inner Conductor	mm (in)	58 (2.28) Corrugated Copper Tube
Dielectric	mm (in)	127 (5) Helical Polyethylene Spacer
Outer Conductor	mm (in)	140.5 (5.53) Corrugated Copper

8. CONCLUSIONS

As a summary, we could include some specific main points:

- It has been shown that an OTS cable can be easily modified to achieve higher **breakdown voltages** for use in high voltage applications (ratio ~3:1).
- The modified cable shows significantly higher **attenuation** compared to the SF_6 gas filled cable.
- Formation of gases inside the oil-filled cable was observed after PD inception voltage was reached, subsequently leading to a decrease of the PD inception voltage. The same was observed during breakdowns, which led to a constantly lower **BDV**.
- Each time the gas bubbles were removed, the inception and the BDV went back to the initial level.

Some thoughts on further improvements and the difficulties that may arise:

- ✓ Attenuation: It will need further studies to optimize this important parameter for a full-scale prototype. (Bigger inner diameter = less attenuation)
- ✓ Complexity: A constant circulation of the oil in the cable could reduce or avoid the observed degradation effects, provided that care is taken to avoid creation of air bubbles by the circulation.
- ✓ Filling a long cable with oil might be only achieved by vacuum pumping before filling with oil, in order to avoid trapped air.
- ✓ Impedance: The possibility to change the dielectric constant is considered a beneficial feature to perfectly match the cable to an existing system impedance.
- ✓ Furthermore one mechanical design could serve the complete "impedance zoo." For this purpose, different oil types and nanomaterials would need to be studied in detail.
- ✓ A major drawback will be the needed hydraulic system featuring a precise control and stabilization for temperature and dielectric constant.

9. ANNEX

MATHCAD: Code developed for PD calculations

Function to detect, measure, count, and integrate over the waveform of the current in order to calculate the magnitude of partial discharges

Set input data

Input := "45.61-p-p-voltage.Wfm.csv"

Import of waveforms in the form of data (arrays), collected from the oscilloscope, in a .csv file.

Read input data:

$$t := \mathrm{READFILE}\left[\mathrm{Input}, \text{"delimited"}, 1, \begin{pmatrix}1\\1\end{pmatrix}\right]\cdot s$$

Time (s)

$$I := \frac{\mathrm{READFILE}\left[\mathrm{Input}, \text{"delimited"}, 1, \begin{pmatrix}2\\2\end{pmatrix}\right]}{6}\cdot A$$

Current (A), 1st probe channel

Number of loops of the cable of the CT: 6

$$U := \mathrm{READFILE}\left[\mathrm{Input}, \text{"delimited"}, 1, \begin{pmatrix}3\\3\end{pmatrix}\right]\cdot 1000\cdot V$$

Voltage (V), 2nd probe channel

Scale of voltage division: 1000:1

Voltage and Current waveforms

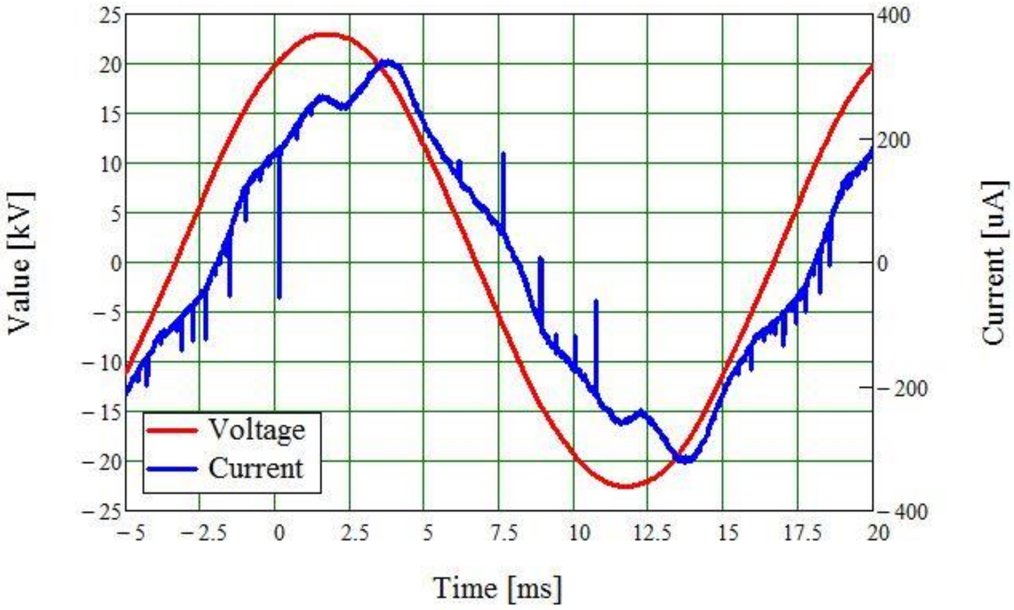

Use of smoothing function
to cutoff the peaks
in the waveform of the current

$I_{Smoothed} := \text{medsmooth}(I, 59)$

Overlay of the smoothed current (green line)
over the initial signal (blue line)

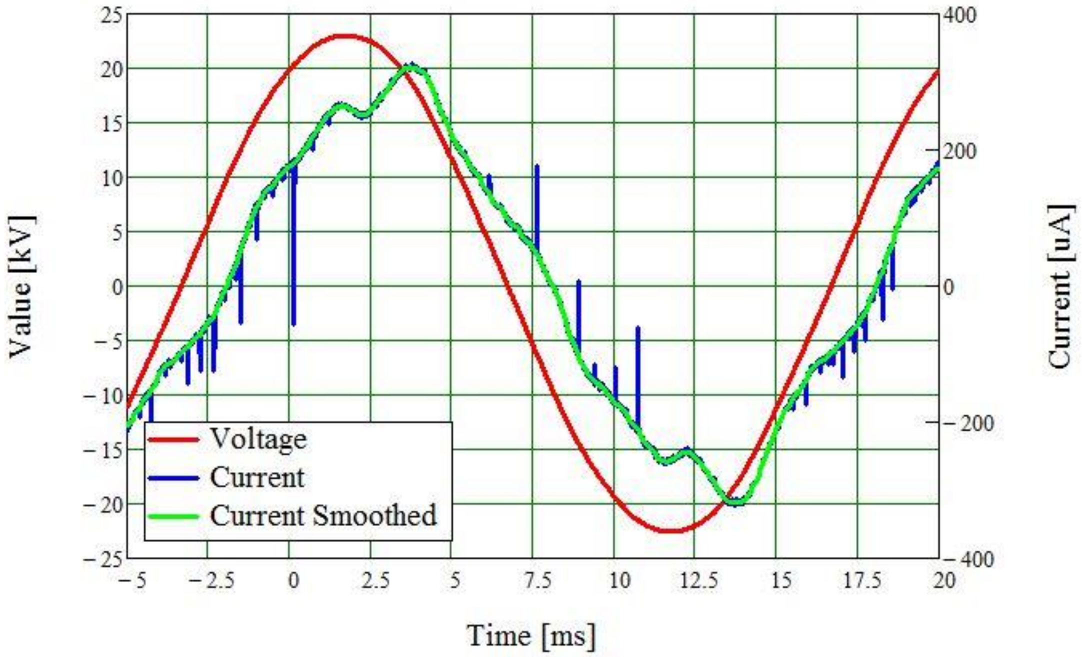

$Current_x := I_x - I_{Smoothed_x}$

Substraction of the smoothed current
from the initial signal leaves only the peaks
(=partial discharches)

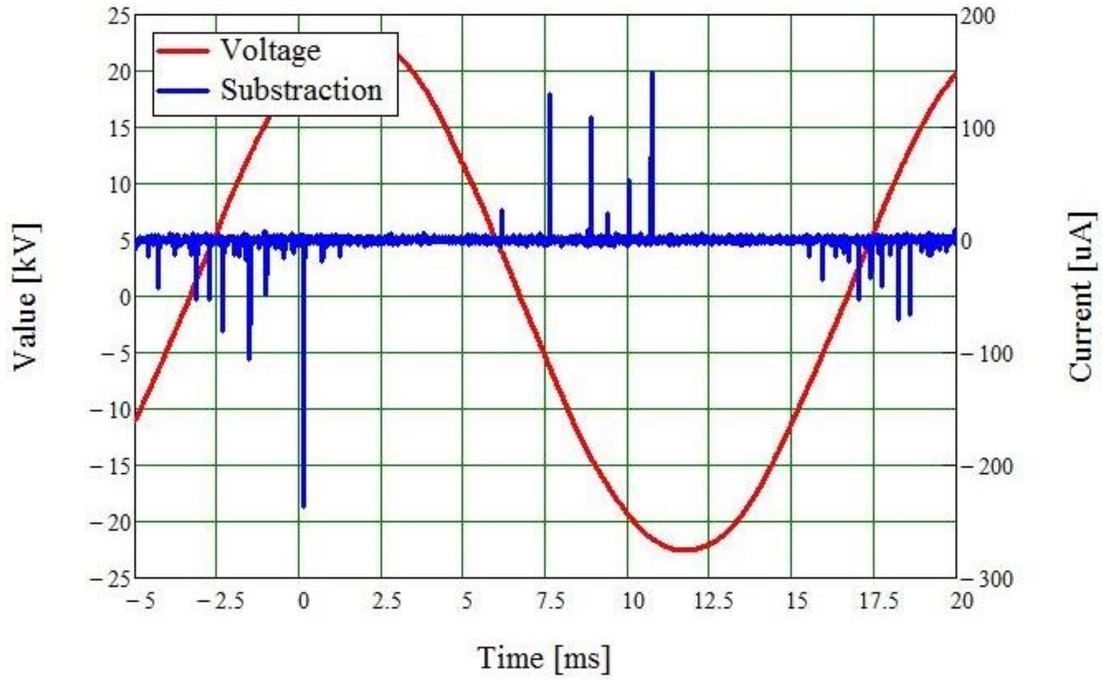

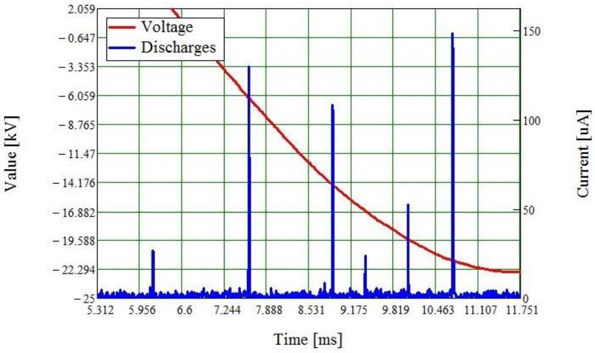

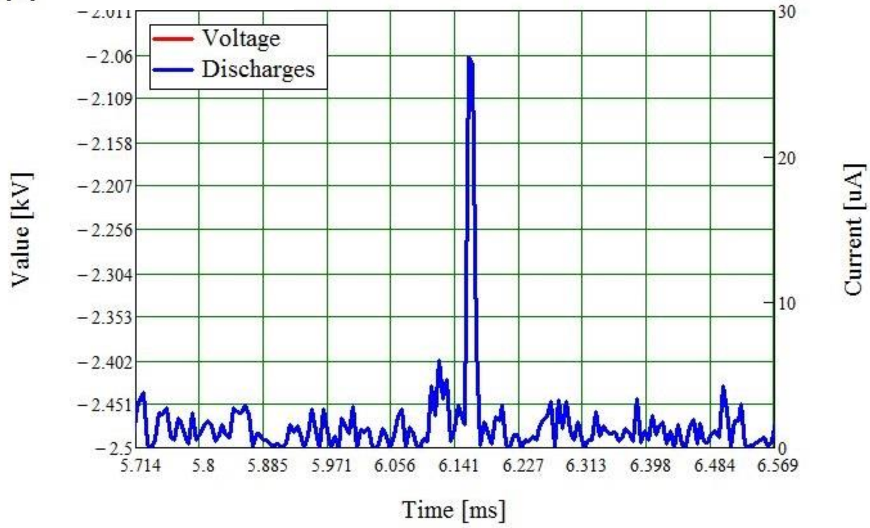

$$
\begin{aligned}
PD_{count} := \ & \text{for } i \in 1 .. \text{length}\left(Current_{Absolute}\right) - 1 \\
& \quad \text{if } \left(Current_{Absolute_i} > PD_{threshold}\right) \\
& \quad\quad \text{if } Current_{Absolute_{i-1}} < PD_{threshold} \\
& \quad\quad\quad PD_{count} \leftarrow PD_{count} + 1 \\
& \quad\quad\quad start \leftarrow i - 1 \\
& \quad\quad 1 \\
& \quad \text{otherwise} \\
& \quad\quad \text{if } Current_{Absolute_{i-1}} > PD_{threshold} \\
& \quad\quad\quad stop \leftarrow i \\
& \quad\quad\quad Q_{PD_{count}} \leftarrow \sum_{i = start}^{stop} \left[\frac{Current_{Absolute_i} + Current_{Absolute_{i+1}}}{2} \cdot \left(t_{i+1} - t_i\right)\right] \\
& \quad\quad 1 \\
& \quad PD_{count}
\end{aligned}
$$

Number of discharges: $PD_{count} = 90$

Total charge Q: $Qtotal := \sum_{i=0}^{length(I)-2} \left[Current_{Absolute_i} \cdot (t_{i+1} - t_i) \right] = 49.896 \cdot nC$

$start := 0$ $stop := 0$ $PD_{count} := 0$ $PD_{threshold} := 5 \cdot 10^{-6} A$

```
Q := for i ∈ 1 .. length(Current_Absolute) − 1
       if (Current_Absolute_i > PD_threshold)
         if Current_Absolute_(i−1) < PD_threshold
           PD_count ← PD_count + 1
           start ← i − 1
         1
       otherwise
         if Current_Absolute_(i−1) > PD_threshold
           stop ← i
           Q_PD_count ← Σ_(i = start)^(stop) [ (Current_Absolute_i + Current_Absolute_(i+1)) / 2 · (t_(i+1) − t_i) ]
         1
       Q
```

Total charge of the PDs: $Qpartialdischarges := \sum_{i=0}^{length(Q)-1} Q_i = 18.259 \cdot nC$

$Q =$ (pC)

	0
0	118.532
1	57.03
2	167.071
3	316.9
4	63.946
5	136.127
6	45.805
7	100.616
8	47.155
9	517.231
10	49.664
11	390.496
12	66.648
13	730.556
14	124.869
15	79.129
16	178.586
17	...

$TOL := 10^{-20}$

$Highest\_Discharge := \max(Q)$

$Highest\_Discharge = 2.221 \cdot nC$

$At\_position\_number := match(\max(Q), Q)$

$At\_position\_number = (33)$

$number := 0 .. PD_{count}$

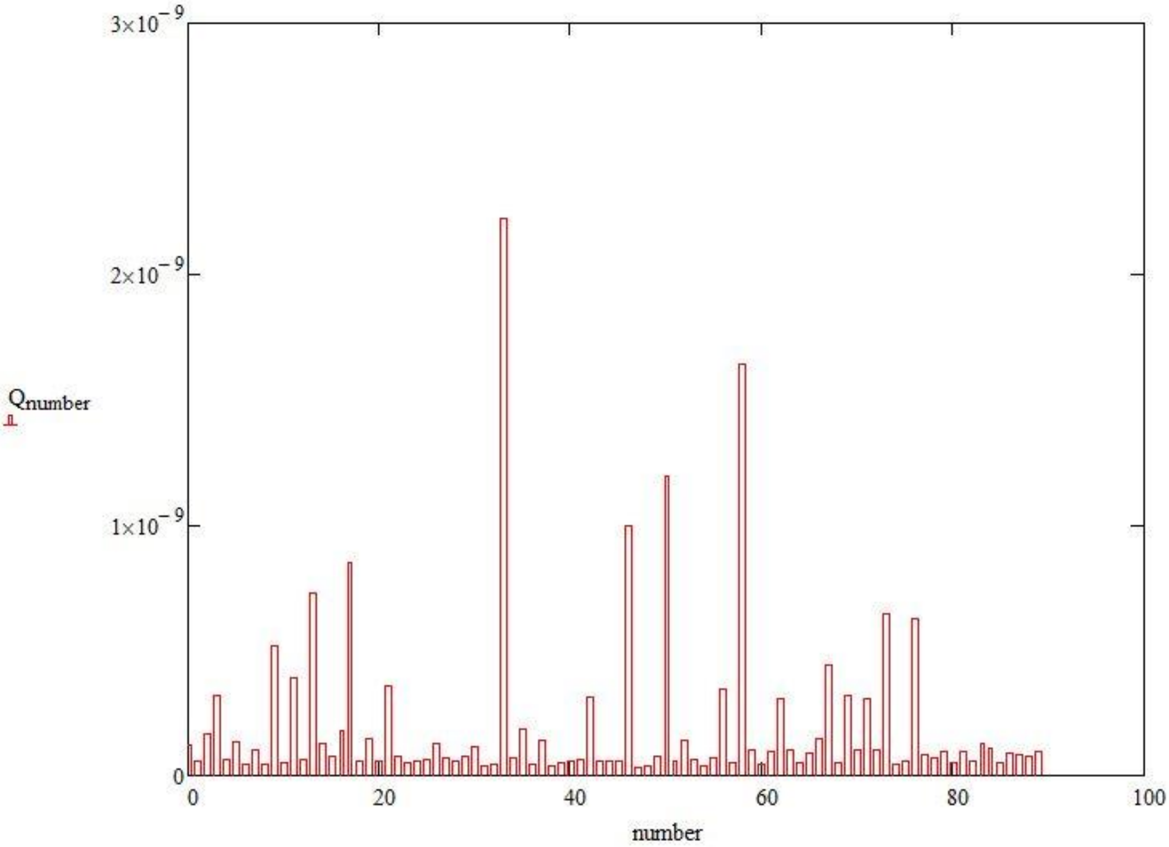

10. TABLE OF FIGURES

11. REFERENCES

[1] CERN, "About CERN," 2012. [Online]. Available: http://home.cern/about.

[2] CERN, "CERN Brochure 2017," 2017. [Online]. Available: https://cds.cern.ch/record/2255762/files/CERN-Brochure-2017-002-Eng.pdf.

[3] Barnes, M J; Ducimetière, L; Fowler, T; Senaj, V; Sermeus, L, "Injection and extraction magnets: kicker magnets," CERN Document Server, 2011. [Online]. Available: https://cds.cern.ch/record/1334789?ln=en.

[4] Mesyats, G. A., Pulsed Power, New York: Kluwer Academic / Plenum Publishers, 2005.

[5] D. Pozar, Microwave Engineering, 4th Edition, Wiley, 2011 .

[6] Shugg, W.T. and IEEE Dielectrics and Electrical Insulation, Handbook of electrical and electronic insulating materials, New York: IEEE Press, 1995.

[7] Brandt, D., "Proceedings of the CAS–CERN Accelerator School: Magnets," in *CERN-2010-004*, Bruges, Belgium, 16 – 25 June 2009.

[8] D. Kontelis, A. Ferrero Colomo, I. Gonos, T. Kramer, T. Stadlbauer, "Evaluation, Optimization and Test of a Standard Air-Dielectric Coaxial Cable Filled with Oil for Possible use in HV Kicker Systems at CERN," in *2018 IEEE International Conference on High Voltage Engineering and Application*, Athens, Greece, 2018.

[9] R. Van Brunt, "Present and future environmental "problems" with SF_6 and other fluorinated gases," in *IEEE International Conference on Plasma Science*, Boston, MA, 96CH35939, p.145, 1996.

[10] D. Woog, J. Holma, "Inductive Adders for CLIC DR Kickers and FCC Injection Kicker Systems," in *PULse POwer for Kicker Systems (PULPOKS) Workshop 2018 CERN*, Geneva, 13.Mar.2018.

[11] L. M. Redondo, A. Kandratsyeu and M. J. Barnes, "Marx Generator Prototype for Kicker Magnets Based on SiC MOSFETs," *IEEE Transactions on Plasma Science,* vol. PP, no. 99, 2018.

[12] *1-1/8" HELIFLEX® Air-Dielectric Coaxial Cable, HCA118-50J,* Radio Frequency Systems, RFS, 11.Feb.2012.

[13] Mayer M., Schröder G., "Coaxial 30 kV Connectors for the RG220/U Cable - 20 Years of Operational Experience," in *High Voltage Workshop, Dielectric and Electric Insulation Society of the IEEE*, Newport Beach, CA, May 6-8,1997.

[14] International Electrotechnical Commission , IEC 60270 - International Standard - High-voltage test techniques - Partial discharge measurements, GENEVA, SWITZERLAND: IEC Central Office, 2000.

[15] Stadlbauer, Tobias, "Partial discharge measurements, ABTEF," Tuesday 14 Aug 2018. [Online]. Available: https://indico.cern.ch/event/739636/contributions/3053164/attachments/1700433/2738318/20180814_PD_Measurements_TST.PPTX.

[16] Omicron Academy Training Material, Rene Hummel, Stephan Korber, Daniel Gebhardt, Ulrike Broniecki, "Coupling Methods for PD Measurement," Omicron Academy Training Material.

[17] Omicron Academy Training Material, Rene Hummel, Stephan Korber, Daniel Gebhardt, Ulrike Broniecki, "Interpretation of PRPD Pattern," Omicron Academy Training Material.

[18] Parametric Technology Corporation, *Mathcad 15.0,* 2010.

[19] Kramer, Thomas, "Overview of HV Cables and Connectors, Cable Procurement and Future Work," in *PULse POwer for Kicker Systems (PULPOKS) workshop 2018*, Geneva, 2018.

[20] L. Sermeus, "KFA45 / BRUGG 26.3ohm PFN CABLE No 6612-N," 1994. [Online]. Available: \\cern.ch\dfs\Departments\TE\Groups\ABT\BT\Sections\KPS\KPS_MACHINES_&_EXP-AREAS\Cables_general\BRUGG\PS-KM-M20-110-A.pdf .

[21] Cobham Software, *OPERA Simulation Software, Opera 18R2 x64,* Cobham Software.

[22] Bluestar Silicones, *Rhodorsil® Oils 47 Technical information,* Bluestar Silicones.

[23] les cables de Lyon, "Cables Coaxiaux 26,3 Ω et 52,6 Ω sous pression de SF6," les cables de Lyon, Lyon, 1978.

[24] A. Ferrero Colomo, L. Ducimetière, T. Kramer, L. Sermeus, "Measurement and Characterization of Cable Losses for High Voltage Coaxial Cables Used in Kicker Systems," in *IPAC2017*, Copenhagen, Denmark, 2017.

[25] A. E. Corporation, *Dino-Lite Digital Microscope,* Dino-Lite Edge.

[26] McCauley, Thomas, "CMS Higgs Search in 2011 and 2012 data: candidate tau-tau event (8 TeV)," CERN Document Server, 2013. [Online]. Available: https://cds.cern.ch/record/1633370.

[27] Laurent Guiraud, "One of the 'kicker magnets' used to kick an injected beam into SPS," CERN Document Server, 2000. [Online]. Available: https://cds.cern.ch/record/41264.

[28] Mobs, Esma Anais, "The CERN accelerator complex," CERN Document Server, 2016. [Online]. Available: https://cds.cern.ch/record/2225847.

[29] DFS, CERN, "G:\Departments\TE\Groups\ABT\BT\BT-FPNEW\Systems\Components\Cables\20 & 40 & 50 Ohm connectors," [Online]. Available: cern.ch.

[30] Draka Multimedia Cable, "HF-Pulse Cable RG220/U FRNC-C," 02.09.03.

[31] "1 5/8" EIA connector HCA118-50 air dielectric cable 1 1/8"-50," SPINNER, [Online]. Available: https://products.spinner-group.com/1-5-8-eia-connector-hca118-50-air-dielectric-cable-1-1-8-50-bn858210.

[32] CERN, "CERN DFS," 2002. [Online]. Available: G:\Departments\TE\Groups\ABT\BT\BT-FPNEW\Systems\Components\Cables\20 & 40 & 50 Ohm connectors\40 Ohm connector.

[33] A. Küchler, Hochspannungstechnik, Springer-Verlag Berlin Heidelberg, 2009.

[34] Omicron Academy Training Material, Rene Hummel, Stephan Korber, Daniel Gebhardt, Ulrike Broniecki, "Introduction, History and Theory of Partial Discharge Measurement," Omicron Academy Training Material.

[35] Electronics Tutorials, "Electronics Tutorials - Home / Transformers / The Current Transformer," [Online]. Available: https://www.electronics-tutorials.ws/transformer/current-transformer.html.

[36] Lemke, E., "Analysis of the partial discharge charge transfer in extruded power cables," *IEEE Electrical Insulation Magazine*, vol. vol. 29, no. no. 1, pp. pp. 24-28, January-February 2013.

[37] Borburgh, J., "An introduction to HV cables," CERN.

[38] GIMENEZ, PIERRE, "CERN Drawing Number: PSBRKPFL0015, HELICOIDAL CABLE CONNECTOR - ASSEMBLY, CERN Drawings Directory," [Online]. Available: https://edms5.cern.ch/cdd/plsql/c4w.display_details?cookie=2161502&p_drob_id=893953&p_version=**.

12. BIBLIOGRAPHY

Mesyats, G. A., Pulsed Power, New York: Kluwer Academic / Plenum Publishers, 2005.

D. Pozar, Microwave Engineering, 4th Edition, Wiley, 2011 .

Shugg, W.T. and IEEE Dielectrics and Electrical Insulation, Handbook of electrical and electronic insulating materials, New York: IEEE Press, 1995.

International Electrotechnical Commission , IEC 60270 - International Standard - High-voltage test techniques - Partial discharge measurements, GENEVA, SWITZERLAND: IEC Central Office, 2000.